UNIVERSITÀ DEGLI STUDI DI MILANO

COURSE OF PhD IN:

AGRICULTURE, ENVIRONMENT AND BIOENERGY

DEPARTMENT OF AGRICULTURAL AND ENVIRONMENTAL SCIENCES

PhD THESES:

MODELLING THE INTERACTION BETWEEN WILD AND CULTIVATED SPECIES.

AGR/02

FULL NAME OF THE CANDIDATE:

ERMES MOVEDI

FULL NAME OF THE TUTOR:

Prof. ROBERTO CONFALONIERI

FULL NAME OF THE COORDINATOR:

Prof. PIERO ATTILIO BIANCO

A.Y.: 2021/2022

Contents

Contents 2

Abstract 8

1. Background 10

1.1. Models for the interaction among plant species 11

1.1.1. Crop-weed interactions 11

1.1.2. Grassland models 12

1.1.2.1. Grassland quality estimation 13

1.2. Modelling crop-insect interactions: a case study for olive trees, olive fruit fly and fly predators 14

1.3. Aim of the thesis 15

1.4. Outline of the thesis 15

Notes 18

2. A new approach for modelling crop-weed interaction targeting management support in operational contexts: a case study on the rice weeds barnyardgrass and red rice 19

2.1. Abstract 19

2.2. Introduction 20

2.3. Materials and methods 23

2.3.1. A new approach for simulating rice-weed interaction 23

2.3.1.1. Principle 23

2.3.1.2. The WARM model 24

2.3.1.3. WeedyCoSMo 24

2.3.2. Experimental data, model calibration and evaluation 29

2.3.3. Evaluating weed management scenarios 32

2.4. Results 33

2.4.1. Model calibration 33

2.4.2. Model evaluation 35

2.4.3. Evaluating weed management scenarios 39

2.5. Discussion 40

2.5.1. Novelty of the proposed approach 40

2.5.2. Reliability, domain of validity and limits 41

2.5.3. Application and implications for weed management support 43

2.5.4. Perspectives 44

2.6. Conclusions 44

3. Adaptation strategies to alleviate climate change impacts on grasslands productivity and forage quality. A case study in northern Apennines. 47

3.1. Abstract 47

3.2. Introduction 48

3.3. Materials and methods 50

3.3.1. The modelling approach 50

3.3.2. Model parameterization 52

3.3.3. Evaluation of climate change impacts on grasslands productivity 54

3.3.4. Definition of adaptation strategies based on management practices 56

3.4. Results 56
3.4.1. Model evaluation 56
3.4.2. Climate change impact on forage production and quality 58
3.4.3. Testing of management adaptation strategy 65
3.5. Discussion 67
3.5.1. Model performance 67
3.5.2. Climate change impacts and adaptation strategies 67
3.6. Conclusions 68
4. Assessment of climate change impacts on alpine pastures productivity and floristic composition 73
4.1 Abstract 73
4.2. Introduction 74
4.3. Materials and methods 76
4.3.1. Experimental data 76
4.3.2 The modelling approach 77
4.3.2.1. Model initialization and parameterization 80
4.3.2.2. Evaluation of climate change impacts 81
4.4. Results 82
4.4.1. Floristic composition, growth dynamics and grazing value 82
4.4.2. Model evaluation 86
4.4.3. Climate change impacts 88
4.5 Discussion 92

4.6. Conclusions 94

4.7. Electronic Supplementary Material 96

5. Development of a new model for simulating the interaction between olive trees, olive fly and fly predators 100

5.1. Abstract 100

5.2. Introduction 101

5.3. Materials and methods 102

5.3.1. Model description 102

5.3.1.1. Olive plant sub-model (biophysical model) 103

5.3.1.2. Olive fruit fly sub-model (population model) 105

5.3.1.3. Olive fruit fly predator sub-model (population model) 106

5.3.2. Reference data 107

5.3.2.1. Olive tree data 107

5.3.2.2. Olive phenology and fly data 108

5.3.3. Sub-models sensitivity analysis and calibration 109

5.3.3.1. Olive trees sub-model SA and calibration 109

5.3.3.2. Olive fruit fly and their predator sub-models SA and calibration 110

5.3.4. Model evaluation 111

5.3.5. Model test 111

5.4. Results 111

5.4.1. Sensitivity analysis 111

5.4.1. Model calibration 113
5.4.3. Model test 116
5.5. Discussion 118
5.5.1. Olive trees sub-model 118
5.5.2. Olive fruit fly and their predator sub-models 119
5.6. Summary and concluding remarks 119
5.7. Supplementary material 121
Olive fruit fly sub-model 133
Thermal time 133
Dormancy 134
Phenological phases 135
Reproduction 136
Impacts on olive 139
Mortality 140
Migration / Immigration 143
Olive sub-model 144
Phenology 144
Vernalization 145
Plant growth 147
Limitation on photosynthesis 148
Partitioning 149

Olive demand 150
Reserve remobilization 151
Olive drop 153
LAI accumulation and senescence 154
Twigs accumulation and buds 155
Canopy growth 156
Pruning 158
Abiotic damages 160
Predators of the olive fruit fly submodel 165
6. Conclusions and remarks 168
7. References 169

Modelling The Interaction Between Wild And Cultivated Species.

Abstract

Yield losses due to wild species are relevant for a variety of cropping systems worldwide, e.g., in the case of rice weeds they can reach 60%. However, in the broader sense, wild species may also have positive effects on cropping systems for their capability to provide environmental benefits. In fact, they are fundamental to maintain high levels of biodiversity and, in the context of grassland communities, they are crucial for the provision of ecosystem services like those involved with pollination and recreational experiences. A quantitative understanding of the complex and dynamic interactions among species within agro-environmental systems is thus crucial to better analyze, for instance, the possible effects of climate change on community dynamics and to timely define effective adaptation strategies. In this context, the aim of this thesis was the development of new models for the simulation of the interaction between cultivated and wild species.

Biophysical models are powerful tools to analyze the interactions between plants and environmental variables as well as to optimize crop management. However, one of their main weakness is the lack of algorithms for simulating the interactions between cultivated and wild species. The few examples available that consider these interactions are mainly related to fungal pathogens, whereas approaches considering weeds, insects and multi-species plant communities are extremely rare and insufficiently validated.

To fill this gap, this PhD Thesis focused on the modelling of three categories of communities of increasing complexity: crop-weed (two plant species), grasslands (multi-species plant communities) and crop-insect-insect predators (different kingdoms). For the three categories, agroecosystems of worldwide importance were identified as case studies: paddy rice (chapter 2), grasslands (chapter 3 and 4) and olive trees (chapter 5). In particular, in chapter 2 a new model was developed for simulating the interaction between rice and two weeds (barnyardgrass and red rice); chapter 3 and 4 are focused on the extension of a model for the simulation of plant community dynamics in the context of mountain grassland systems, with case studies in temporary grasslands in the Apennine and in natural pastures in the Alps. The third chapter, in particular, focuses on the definition of strategies for adapting

grasslands management to climate change by explicitly considering their floristic composition, whereas the fourth chapter presents initial results on the effects of grazing and climate change on the productivity and floristic composition of pasture communities. Chapter 5 shows a new model of interactions among olive trees, the olive fruit fly (*Bactrocera oleae* (Rossi, 1790)) and its predators, whereas chapter 6 refers to the general conclusions of the researches carried out in this PhD Thesis.

Although the new models developed in this work are process-based to reflect the complexity of interactions occurring in agroecosystems, they assume simplified descriptions of biophysical processes through a limited number of parameters to make them usable in operational contexts.

Keywords

Simulation models, Interactions, Crops, Management, Wild species, Agroecosystems, Ecosystem services.

1. Background

Wild species have a deep impact on qualitative and quantitative aspects of crop production as well as on the ecosystem services provided by agroecosystems. Interactions between cultivated and wild species play indeed a major role in the reduction of crop productivity (Oerke and Dehne, 2004). Conversely, in specific cropping systems, such as those involved with forage production, wild plant species may positively affect the quality and quantity of forage (Argenti et al., 2021; Daget and Poissonet, 1971) and the provision of other ecosystem services (Oliver et al., 2015). For example, when alfalfa (*Medicago sativa* L.) is sown in monoculture, *Lolium multiflorum* Lam. and *Dactylis glomerata* L. often naturally enrich the community as weeds, and – during the life of the temporary grassland – they can support the production of forage earlier in the spring and later in the autumn.

Wild species represent most of the biodiversity in agroecosystems and this biodiversity can be threatened by climate change, which may deeply modify the spatial distribution and behavior of plants (Mooney and Hobbs, 2010) and insects (Gutierrez et al., 2009), both for the way they interact with the physical environment and for their capability to compete for resources with other species. It is thus crucial to better understand in quantitative terms the complex interactions between wild and cultivated species. Farmers' experience may be not enough to avoid reductions in the quantity and quality of yields while minimizing the use of chemicals to preserve biodiversity and environment in a context increasingly characterized by global challenges like those dealing with climate change.

Crop simulation models are powerful tools to support agroecosystems management at different spatial and temporal scales. However, when multi-species communities need to be simulated, they are often too complex, empirical or insufficiently tested under operational conditions to provide effective support. For this reason, this PhD Thesis focused on the development of new models for the interaction among plant species and between plants and insects. Fungal pathogens and other microorganisms like virus were not explicitly considered given some examples suitable for operational contexts are already available for the former (e.g., Bregaglio and Donatelli, 2015), whereas viruses are considered as less relevant in affecting crop productivity (Oerke and Dehne, 2004).

1.1. Models for the interaction among plant species

1.1.1. Crop-weed interactions

Different models for the simulation of crop-weed interactions are available in the literature (e.g., Graf et al., 1990, Kropff et al., 1992; Debaeke et al., 1997; Caton et al., 1999). However, they are often insufficiently evaluated using experimental data and, in some cases, they incorporate empirical factors that, to some extent, make them site- or context-specific (Holst et al., 2007). In other cases, crop-weed interaction models are too complex to be successfully transferred to operational farming conditions (Caton et al., 1999; Colbach et al., 2014), or are limited to simulating the interaction between a crop and a single weed species.

Eco-physiological models for the simulation of crop-weed interactions can be classified according to different criteria, e.g., the level of abstraction in the representation of plants (individual, species or field level models), the degree of empiricism (empirical, process-based or mixed approaches), the spatial resolution (virtual field, large-area or spatially explicit) and the temporal resolution (seasonal or multi-annual). Despite these major differences, there is no one-model category that is better than another. Colbach (2010) underlined that it is impossible to identify *a priori* best categories of models, the choice of a model depending on the specific objectives and the context of application.

To improve these interaction models, some authors (e.g., Renton, 2013) suggested moving from field-level to individual-based models. Despite the theoretical reasons for the shift towards more detailed approaches, increased complexity has often limited the usability of models (e.g., Park et al., 2003), due to the increasing effort required for model parameterization and the uncertainty associated with it (Colbach, 2010). For this reason, some of the models potentially available for their use within decision support systems are in fact often too complex to be calibrated or initialized, or are too sensitive to uncertainty in parameter values (Freckleton et al., 2008; Colbach et al., 2014). This makes many of these models unsuitable for being implemented in decision support systems (DSS), which are increasingly needed for tactical weed management and for the strategic comparison of management scenarios to identify medium- to long-term weed management strategies (Beltran et al., 2011). Other approaches are potentially suitable for being used as simulation

engines within operational DSSs but they are not yet sufficiently evaluated (Freckleton and Stephens, 2009).

To fill this gap, a new model suitable for the tactical and strategic support to weed management was developed and evaluated (chapter 2), with a case study on rice and two of its most relevant weeds.

1.1.2. Grassland models

Available approaches for the simulation of multi-species plant communities can be classified into two categories depending on how plants are modelled: (i) generic crop-like models and (ii) interspecific competition models.

The first category of models estimates the grassland community as a monoculture. In other words, this category of models (e.g., LINGRA, Rodriguez et al., 1999; STICS grassland, Brisson et al., 2008) does not explicitly consider interactions among herbaceous species. The pros of these solutions are the limited effort during model parameterisation and the parsimony in terms of hardware resources needed. However, changes in botanical composition during the season or in the medium term cannot be simulated. For this reason, this solution cannot offer any guarantee of robustness when environmental conditions change. This makes these approaches unsuitable for, e.g., climate change or management support studies.

The second category of models such as INTERCOM (Kropff and Van Laar, 1993), GEMINI (Soussana et al., 2012) and DynaGraM (Moulin et al., 2018), explicitly accounts for inter- and intra-specific competition, thus considering the various types of interaction among herbaceous species and also among individual plants, through multi-instance simulation systems, one per species or individual plant present in the community. This allows the growth and development of each entity (species or individual) of the plant community to be simulated by means of a detailed parameterisation. This category of models is potentially able to dynamically estimate botanical composition and its changes during the season. However, their complexity makes them very demanding in terms of computational power and inputs. In addition, the difficulties of initialisation and parameterisation make these models unsuitable for operational contexts, especially for regional analyses (Röhrig and Stützel, 2001). In fact, examples of application and evaluation are limited to a few species growing in controlled environments (Susanna at al., 2012).

Before starting this PhD, a compromise solution between the two categories just mentioned was developed (CoSMo; Confalonieri, 2014). CoSMo uses a single instance of a generic crop simulator to reproduce the growth and development of plant communities, with the parameters of a generic crop simulator dynamically changing depending on the simulated relative abundance of the different species in the community. This is possible thanks to hierarchically-arranged suitability functions that allow estimating the interactions and the suitability of each species to the environmental and management conditions explored at each time step. Suitability factors mimic changes in the ability to compete in case of perturbing events (e.g., mowing, grazing), and according to plant status (phenology) and environmental conditions (temperature, solar radiation, water and nitrogen availability).

In chapters 3 and 4, the CoSMo model was improved and extended to allows accounting for new drivers, and it was evaluated – including the quality of forages – for temporary grasslands in the Apennine and natural pastures in the Alps, in this case accounting also for grazing animals.

1.1.2.1. Grassland quality estimation

The forage quality is very complex to simulate: approach as PaSim (Ben Touhami et al., 2013, Ma et al., 2015) has parameter to describe the percentage of legume to fix at the beginning of simulation, a better approach is ModVege (Calanca, 2016; Jouven et al., 2006) that dynamically estimate the digeriblity of the forage tanks the plant aging. But both models do not dynamically estimate the florisc composition. Thanks CoSMo model and its dynamic floristic composition it is possible to estimate dynamically the forage quality (in term of crude protein content or grazing vale) easily appling the Argenti et al. (2021) equation or the Daget and Poissonet (1971) equation. A possile application will be using a mixed approach ModVege – CoSMo.

1.2. Modelling crop-insect interactions: a case study for olive trees, olive fruit fly and fly predators

Examples of models for olive tree growth are available (Morales et al., 2016; Villalobos et al., 2006; Abdel-Razik, 1989, Moriondo et al., 2019), as well as for olive fruit fly population dynamics (Gutierrez et al., 2009). However, the formers are either too simplified or too complex for being effectively used within applied researches, whereas the latter is not well documented. In particular, according to Moriondo et al. (2019), the model from López-Bernal et al. (2018) is too complex and needs specific inputs that are hardly available outside experimental conditions. On the contrary, the models proposed by Moriondo et al. (2019), Morales et al. (2016), Villalobos et al. (2006) and Abdel-Razik (1989) are oversimplified, missing specific algorithms for key processes deeply influencing the underlying system. As an example, the approach proposed by Moriondo et al. (2019) does not consider tree reserves. Moreover, all these models do not consider the interaction with the olive fruit fly, which can severely affect olive tree productivity. The dynamics of olive fruit fly populations are instead considered by the model proposed by Gutierrez et al. (2009), which however does not consider water stress (crucial for the simulated system) and is not well documented.

For these reasons, a new model for the simulation of the interaction between olive trees, olive fruit fly and fly predators was developed and evaluated during this PhD Thesis (chapter 5).

1.3. Aim of the thesis

The aim of this PhD Thesis was to develop new models for the simulation of the interaction between cultivated and wild species. Attention was paid to agroecosystems productivity (including quality and quantity of products) and to ecosystem services dealing with biodiversity, as well as to the interactions between simulated communities and the physical environment (including climate change) and management.

In particular, the specific objectives addressed in this PhD Thesis were:

- developing and evaluating a new model to estimate crop-weed interactions;
- demonstrating its suitability to support management;
- improving the CoSMo model to quantify climate change impact on temporary grasslands in the Apennines (central Italy) and to identify adaptation strategies;
- developing approaches to dynamically derive forage quality from species characteristics and botanical composition of the community
- quantifying climate change impact on high altitude, actively grazed natural pastures in the Alps;
- developing and evaluating a new model for the simulation of the interaction of olive trees, olive fruit flies and fly predators.

1.4. Outline of the thesis

Chapters 2 to 4 deal with the modelling of the interaction within plant communities. In particular, chapter 2 deals with simple 2-species communities, where the interactions between rice and weeds are simulated. Chapters 3 and 4 refer to the development of new approaches for the simulation of multi-species plant communities in different environments (including climate change scenarios), with and without the presence of grazing animals. Chapter 5 refers to the development of a new model for the simulation of the interactions between olive trees, olive fruit fly and fly predators. Chapter 6 derive general conclusions on the activities carried out during this PhD Thesis.

In particular:

- The second chapter presents a new crop-weed interaction model, namely WeedyCoSMo, derived from the generic plant community model CoSMo. The interaction is daily estimated based on various suitability functions (e.g., to temperature, water availability, light) aggregated hierarchically. The model, unlike the original CoSMo, considers the states of coexisting plant species distinctly. The new model was linked to WARM, a rice growth model able to estimate the interactions of the crop with fungal pathogens. The model was calibrated and evaluated using data from the literature on rice in interaction with two major rice weeds: red rice and barnyardgrass. The performance of WeedyCoSMo was satisfactory for all variables assessed (aboveground biomass, leaf area index, yield and plant height) and regardless of the simulated species, with R^2 values always above 0.80.
- The third chapter presents the results of an assessment of CoSMo in alfalfa grasslands grown in the Tuscan-Emilian Apennines (northern Italy). Dedicated measured data were used to extend CoSMo by including an existing model that uses the simulated percentage of legumes in the grassland as input to derive forage quality (CP: crude protein content). The assessment of the possible effects of climate change was conducted by using two general circulation models (GISS-ES and HadGEM2) and two representative concentration pathways (RCP4.5 and RCP8.5). Model indicated that CP could increase (+0.9/+2.6%), accompanied by a projected decrease in forage production (-3.6/-14.3%). Using the model, we derived adaptation strategies to optimize the system in the coming decades, based on the postponing of the last cut and on the sowing of a specific mixture of herbaceous species.
- The fourth chapter presents the first test of CoSMo on natural, grazed pastures. The model was extended with new suitability functions and calibrated using field data collected during the 2019 growing season in Alpine sites at 2200 m a.s.l. First, the model was calibrated and evaluated to properly simulate observed aboveground biomass and floristic composition (R^2>0.9). Then, the impact of climate change was estimated using two general circulation models (GISS-ES and HadGEM2) and two representative concentration pathways (RCP4.5 and RCP8.5). It resulted an increase in forage production (+10.7% on

average) but a decrease in forage quality (grazing value -11.1% on average).

- The fifth chapter presents a new daily time-step model for simulating the interactions among olive trees, olive fruit flies and fly predators. The model estimates:
    - for the olive trees: plant phenology, yield alternation, photosynthesis, partitioning among organs, growth in canopy diameter and height, senescence, fruit drop, evapotranspiration, lignification, winter hardening, self-shading and abiotic damages;
    - for olive fruit fly: the interaction between the fly and olive trees, fly phenology, predators, oviposition, mortality, immigration and emigration and the main limitations to oviposition.

  The model error was low (MAE<1 t in fruit dry biomass; and ~5% in the percentage of olive fruits infected by the olive fruit fly).

The last chapter (#6) presents the general conclusions of the Thesis.

Notes

The researches presented in this PhD Thesis were carried also thanks to national and international projects: MODIPRAS (Modelling relationships between species diversity, the functioning of grassland systems and their ability to deliver ecosystem services) of the ex-INRA meta-programme ECOSERV (Ecosystem services); AGER Interdisciplinary Project for assessing current and expected Climate Change Impact on MOUntain Pasture (IPCC MOUPA), Grant number 2017-1176; Generali Assicurazioni Italia, which co-founded the development of the olive tree-olive fruit fly-fly predators model; FEASR PSR Emilia-Romagna, FOCUS AREA 3A, Operazione 16.2.01.

The PhD thesis was partially co-funded by Cassandra lab and Cassandra tech s.r.l.

The second chapters has been published in the journals Ecological Modelling; the fourth chapter has been submitted to the journal Climatic Change; the third and fifth chapters will be submitted in the coming weeks. I would like to acknowledge the Editors of Ecological Modelling and Climatic Change for the permission to include the papers in this PhD Thesis.

The numbering of tables, figures, equations and appendices resumes to one at the beginning of each chapter and in the supplementary material.

2. A new approach for modelling crop-weed interaction targeting management support in operational contexts: a case study on the rice weeds barnyardgrass and red rice

Ermes Movedi, Daniele Valiante, Alessandro Colosio, Luca Corengia, Stefano Cossa, Roberto Confalonieri,

Submitted: 7 September 2021; Accepted: 25 October 2021; Published: 8 November 2021

Journal: Ecological Modelling

2.1. Abstract

Despite their potential to support the optimization of weed management, available ecophysiological models for the simulation of crop-weed interaction are still not adopted in operational contexts. For some of them the reasons deal with the insufficient validation in farming conditions, whereas others are either too complex for being used in operational contexts or too empiric for being free from site- or context-specific effects. Here we present a new approach (WeedyCoSMo) to support strategic decisions on weed management, derived from the CoSMo process-based model for the simulation of phytocoenosis dynamics. The model dynamically reproduces on a yearly basis the interaction between crop and weeds at canopy level through the daily quantification of the suitability of each species to weather conditions and management practices, as well as to the simulated system state variables. Dynamically predicted outputs are the relative abundance of crop and weeds and state variables for each species like, e.g., aboveground biomass, biomass of different plant organs, grain yield, leaf area index, plant height. WeedyCoSMo was calibrated and validated using data from different sites (in the Jiangsu province, China, and in Arkansas, USA) and years (from 1982 to 2014), where different rice varieties and two major rice weeds – i.e.,

red rice (*Oryza sativa* L., var. *sylvatica*) and barnyardgrass (*Echinocloa crus-galli* L.) – were grown in monoculture or mixture. Model performances were satisfying: for rice crops grown in interaction with weeds, relative root mean square error never exceeded 25.2%, regardless of the variable considered, and Nash-Sutcliffe modelling efficiency was always higher than 0.63. Despite the low number of inputs and parameters needed to run the simulations, the degree of accuracy was similar to the ones achieved with other models for crop-weed interaction. This allows considering WeedyCoSMo as a promising approach in light of the possible integration in decision support systems targeting operational farming conditions.

Keywords

Echinochloa crus-galli, inter-specific competition, *Oryza sativa* var. *sylvatica*, WARM, WeedyCoSMo.

2.2. Introduction

Optimizing the use of pesticides is a priority in agricultural management because of their impact on the environment, on biodiversity (Fletcher et al., 1988; Freemark and Boutin, 1995), on the health of farmers (Lopez et al. 2007) and consumers (Ascherio et al. 2006; Stillerman et al. 2008), as well as on farmers' income. However, since it is hard imagining to satisfy global food demand without using pesticides (Seufert et al., 2012; Leifeld, 2016), the optimization of pesticide management largely relies on limiting unnecessary applications.

Despite differences due to the crops and contexts considered, weeds are worldwide responsible for about 32% of yield losses, thus representing one of the most severe biotic factors limiting global food production (Oerke and Dehne, 2004). In the case of important staple food like rice, incorrect management of weeds can lead to yield losses that can exceed 60%, with even higher values in case of direct sowing under aerobic conditions (Dass et al., 2017).

Farmers' experience may be not enough to avoid yield losses while minimizing the use of herbicides because of the complex dynamics that characterize the interactions between crops, weeds, environmental conditions and other management practices. For this reason, tools for optimizing herbicides application were developed. They range from simple rule-based

systems to equations relating the number of weed individuals or damaged area to the treatment timing, up to complex systems based on mathematical simulation models (Park et al., 2003). Ecophysiological models for the simulation of crop-weed interaction (e.g., Graf et al 1990, Kropff et al., 1992; Debaeke et al., 1997; Caton et al., 1999) can be classified according to different criteria, e.g., the degree of empiricism, leading in this case to the identification of empiric, mechanistic and mixed approaches. Other classifications are based on the level of abstraction in the way plants are represented (individual level, species level or field level models), or on the spatial (virtual field, large-area, spatially explicit) and temporal (seasonal, multi-annual) extent of the simulation. Despite such large differences, many authors underlined that it is impossible to identify a priori a category of models that is better than the others, the choice of a model depending on the specific objectives and conditions of application (Colbach, 2010). As an example, some authors (e.g., Renton, 2013) suggested to shift from field level models to individual-based ones in case the objective is the analysis of the effects of tillage on weed populations in the medium-long term, or in case the effects of pesticides on resistance phenomena need to be investigated. Despite the theoretical reasons behind shifting towards modelling approaches more detailed in the way underlying processes are represented, the increase in complexity has often limited the use of models for decision-making (e.g., Park et al., 2003), given increasing the detail in process representation often translates into huge effort and uncertainty during model parameterization (Colbach, 2010). Some of the models potentially available to support decision-making, indeed, are often too complex (i.e., too many parameters and input variables) to be calibrated or initialized, and too sensitive to uncertainty in parameter values (Freckleton et al., 2008) for being successfully transferred to operational farming conditions (Colbach et al., 2014). Other models for the simulation of crop-weed interaction are not suitable for being implemented in decision support systems (DSS) targeting the tactical (in-season) management of weeds, although they can be successfully used to compare management scenarios to identify strategies for weed management in the medium-long term (Beltran et al., 2011). Other approaches are instead potentially suitable to be used as simulation engines within operational DSS but are still insufficiently validated (Freckleton and Stephens 2009). Moreover, one of the factors that often limit the adoption of models within decision support systems is their insufficient capability to reproduce long-term effects of weed management strategies (Park et al., 2003).

One of the solutions to overcome these limitations is extending cropping system models already used within operational or pre-operational DSS (e.g., Thorp et al., 2008; Kadiyala et al., 2015; Busetto et al., 2017; Bonfante et al., 2019) by providing them with algorithms for the simulation of key dynamics of crop-weed interaction. Some of these models have indeed been used for years in a variety of contexts and they have been validated under operational conditions for a variety of purposes. Moreover, their functioning and outputs are often simple enough to be understood by farmers directly (Thorp et al., 2008) or after their implementation in dedicated software platforms (e.g., Busetto et al., 2017). The main strength of this kind of models is the favourable relationship between the effort needed to run simulations (parsimony for inputs) and the capability to capture key aspects of the system of interest. This allows obtaining outputs at canopy scale (clearly understandable and suitable for decision making) by relying – at least partially – on existing spatially-distributed sources of weather, soil and management data. Another advantage of extending existing operational crop models is the possibility to reuse the parameterizations available to estimate growth and development of cultivars and hybrids for the crops of interest, thus limiting the calibration effort to weed parameters.

The objectives of this study were: (i) developing a new model – annual in the current configuration – for crop-weed interaction suitable for operational contexts, i.e., a simulation engine for DSS targeting strategic decisions, and (ii) evaluating the model for rice and two of the most important rice weeds worldwide, i.e., barnyardgrass (*Echinocloa crus-galli* L.) and red rice (*Oryza sativa* L. var. *sylvatica)*. The approach we propose extends the CoSMo (Confalonieri, 2014; Movedi et al., 2019) algorithms for the simulation of the interaction among different species in phytocoenosis, and it uses the WARM model (Confalonieri et al., 2009) for the simulation of growth and development of rice and weeds. WARM has been used since it was demonstrated to be suitable for being used in operational contexts. Indeed, after being extensively evaluated under a variety of conditions, it is already adopted for large area applications dealing with yield forecasts (Pagani et al., 2019) and with supporting the distribution of fertilizers (Busetto et al., 2017) and fungicides (Nettleton et al., 2019). The reason for starting from the CoSMo principles for inter-specific dynamics derives from its capability of extending cropping system models already used within operational DSS.

2.3. Materials and methods

2.3.1. A new approach for simulating rice-weed interaction

2.3.1.1. Principle

The proposed approach for rice-weed interaction (WeedyCoSMo) derives from the generic plant community model CoSMo (Confalonieri, 2014; Movedi et al., 2019). CoSMo is a process-based, virtual field model that simulates at a daily time step annual dynamics of phytocoenosis in terms of productivity of the community and relative abundance of the different species, by using weather data, physical and chemical soil properties and management information. It simulates community dynamics based on two assumptions: (i) inter-specific competition and changes in species relative abundance are derived from species-specific responses (by means of sets of suitability functions) to hierarchically-arranged environmental and management drivers; (ii) parameter values of the community as a whole are daily derived from the relative abundance of each species and from the parameter values of the different species when grown in monoculture. In practice, the suitability of each species to the conditions explored each day is used to drive changes in the characteristics of the community (changes in the relative abundance of the different species reflect in changes in the parameter values of the community), which are daily used to estimate the rate variables (i.e., changes in the values of state variables within the time step) of the phytocoenosis as a whole using a single instance of a crop model. Using this approach, the traits of the plant community – codified in the parameters of the generic crop model – dynamically change at each time step as a function of the suitability of each species in the community to environmental and management conditions, and the only state variables that are daily integrated are those referring to the community.

In the case of crop-weed interaction, rate and state variables of crop and weeds need to be explicitly simulated to allow, e.g., quantifying the impact of weeds on crop yields and identifying infestation thresholds to trigger herbicide distribution. Moreover, keeping track of rate and state variables of crop and weeds allows the explicit simulation of the competition for resources between the different species. For this reason, contrarily to the original CoSMo approach, in WeedyCoSMo one instance of crop model is used for simulating growth and development of each of the crop and weed species present in the field.

2.3.1.2. The WARM model

The crop model used in this study is the daily time step version of WARM (Confalonieri et al., 2009). This model was used for estimating rice and weeds rate and state variables at each time step. In particular, two instances of the model were run, given only rice and one weed species (either barnyardgrass or red rice) were simultaneously available in the datasets used for model evaluation (Table 1). Plant emergence is estimated when a species-specific thermal time threshold is reached, with thermal time being cumulated between base and maximum temperatures starting from the sowing day. WARM simulates species development as a function of the thermal time accumulated between base and maximum temperatures, with an option to account for the effect of photoperiod. Biomass accumulation is reproduced using a canopy-level net photosynthesis approach (Monteith, 1977), with radiation use efficiency (g dry biomass MJ-1) modulated by temperature, senescence, diseases, light saturation of enzymatic chains, and atmospheric CO_2 concentration. Daily cumulated aboveground biomass (AGB; kg ha-1) is partitioned to the different plant organs as a function of development stage, with differences among genotypes reproduced by modulating the value of a parameter that represents the fraction of photosynthates that are daily partitioned to leaves at early phenological stages. Grain yield (kg ha-1) is the cumulated biomass partitioned to reproductive organs at physiological maturity. Plant height is estimated as a function of biomass partitioned to stems (Confalonieri et al., 2011), whereas green leaf area expansion (m2 m-2 day-1) is simulated as a function of the biomass daily partitioned to leaves and of a development-dependent specific leaf area. Daily-emitted leaf area index units are considered senescent once they reach a thermal time threshold. The amount of intercepted radiation is derived from green leaf area index (LAI; m2 m-2) and canopy extinction coefficient for solar radiation using the Beer's law (Monsi and Saeki, 1953). Concerning agro-management practices, the model simulates the effect of fertilization, fungicide distribution, and water management (in terms of water availability due to irrigation and effect on the vertical thermal profile in case of flooding). Details on WARM algorithms are available in reference papers (e.g., Confalonieri et al., 2009; Pagani et al., 2014).

2.3.1.3. WeedyCoSMo

In order to explicitly simulate the state variables of each crop and weed species, the CoSMo approach has been modified to allow using an instance

of a generic crop model (in this study WARM) for each of the species in the simulated field. This allowed keeping track of species state variables separately without preventing WeedyCoSMo from simulating the state variables of the community, which are derived as the average of the species state variables weighted by their relative abundance (Fig. 1).

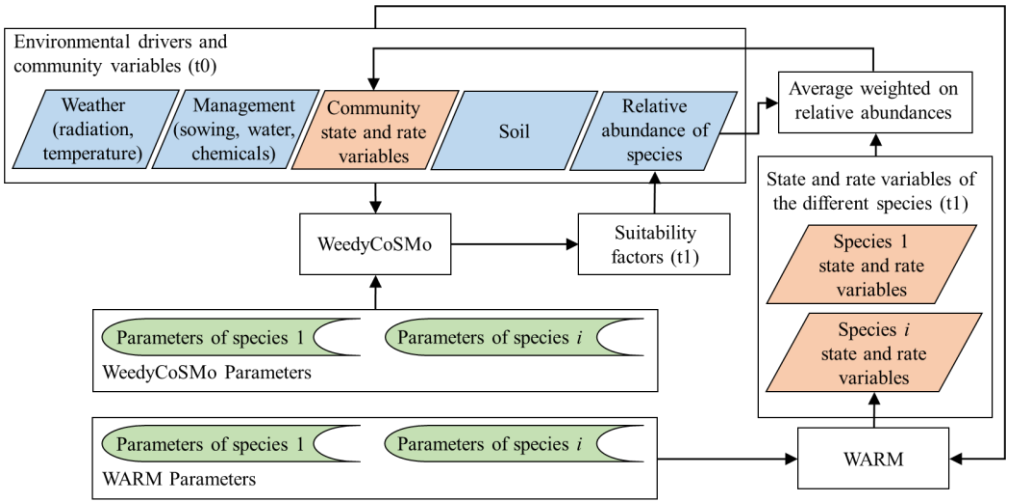

Figure 1: *WeedyCoSMo flowchart; i represents the i*th *species in the field; t is the time step (daily), with t0 and t1 representing two consecutive time steps. Blue, green and red shapes refer to drivers, parameters and state/rate variables, respectively; white shapes indicate models. WeedyCoSMo estimates crop and weeds suitability (to be used at t1 for estimating changes in the relative abundance of the different species) based on environmental drivers and on the state and rate variables of the community at t0. Rate and state variables of the different species are updated using the WARM model.*

Similarly to the original CoSMo approach, WeedyCoSMo estimates at each time step changes in the relative abundance of each crop and weed species using a set of hierarchically-arranged unitless suitability functions. This allows reproducing the response of each species to environmental (e.g., temperature, flood tolerance and nitrogen contents) and management (e.g., chemical treatments) factors by accounting for the state variable of the community and for the features of the different species (Fig. 1).

The relative abundance of the ith species (SCP_i, 0-1, AGB AGB-1) in the community is derived at each time step (t) according to Eq. 1, whose meaning is changing the relative abundance of each of the species in the community according to its suitability to the conditions explored during the time step compared to the suitability of the community as a whole during the same time step:

$$SCP_{i(t)} = SCP_{i\,(t-1)} + \left(\frac{Sfs_i - \frac{CSf}{n}}{I \cdot z}\right) \quad (1)$$

where $SCP_{i\,(t-1)}$ (0-1, unitless) is the relative abundance at time step t-1, Sfs_i (unitless; Eq. 2) is the overall suitability of the species i, I (parameter, unitless; set here to 40 according to the experience in previous studies) is an inertial replacement coefficient (used to implicitly represent the system resilience to changes in environmental conditions), z is the number of drivers, n is the number of species in the community, and CSf (unitless) is the community suitability (Eq. 3).

$$Sfs_i = \sum_{q=1}^{z} HSf_{i\,q} \quad (2)$$

$$CSf = \sum_{i=1}^{n} Sfs_i \quad (3)$$

In practice, Eq. 2 is used to derive the overall suitability for the species i as the sum of the hierarchy-corrected suitability factors (Eq. 4) obtained for the z drivers, whereas Eq. 3 is used to derive the suitability of the community as a whole as the sum of the suitability of the different species in the community.

In Eq. 2, q is the position of a driver in the drivers' hierarchy and $HSf_{i\,q}$ (unitless) is the hierarchy-corrected suitability of the ith species to the qth driver, estimated as:

$$HSf_{i\,q} = \begin{cases} Sf_{i\,q} & q = 1 \\ \sqrt{Sf_{i\,(q-1)}} \cdot Sf_{i\,q} & q = 2 \\ \sqrt{HSf_{i\,(q-1)}} \cdot \sqrt{Sf_{i\,(q-1)}} \cdot Sf_{i\,q} & elsewhere\ (q > 2) \end{cases} \quad (4)$$

where $Sf_{i\,q}$ (unitless) is the suitability of the ith species to the driver in the qth position in the hierarchy. In this study, according to the knowledge on plant responses to different categories of drivers and to the studies from Lindquist and Kropff (1997) and Hattori et al. (2009), the drivers were arranged in the following hierarchy: herbicide treatments, global solar radiation (competition for light), floodwater level (tolerance to submergence), and mean air temperature (different response to thermal regimes of the different species). Other drivers available in WeedyCoSMo (e.g., soil water and nitrogen contents) were switched off for this study since the datasets used for model evaluation referred to experiments where fields were fully irrigated and fertilized (no competition for water and nutrients).

For solar radiation, the original CoSMo suitability function (Confalonieri, 2014) was slightly modified to increase the relative importance of plant height compared to leaf area index (LAI). The new function (f_r; 0-1, unitless) is calculated for each species in the rice-weeds community according to Eq. 5:

$$f_r = 0.5 + \frac{\left(\frac{LAImax - LAIcomm}{LAImax + LAIcomm} + 2 \cdot \frac{Hmax - Hcomm}{Hmax + Hcomm}\right)}{6} \quad (5)$$

where LAI_{comm} ($m^2\ m^{-2}$) and H_{comm} (cm) are the LAI and height of the community as a whole at time step t, whereas LAI_{max} ($m^2\ m^{-2}$) and H_{max} (cm) are parameters defining the maximum LAI and height that the species (or cultivar or population in case of weeds) can reach under unlimiting conditions. In practice, Eq. 5 is used to compare the community state variables at a certain time step and the potential of each of the species in the community for the same variables. LAI_{comm} and H_{comm} are estimated as an average of the corresponding rice and weeds state variables at time step t weighted by the relative abundance of the different species at the same time step. The hypothesis behind Eq. 5 is that – at each time step – the higher the maximum height (or maximum LAI) of a species compared to the current height (or LAI) of the community, the higher the suitability of that species for competing for radiation.

For the water suitability function, the CoSMo approach for the species capability to uptake water from soil is used for unflooded conditions, whereas a new function (f_{sb}, 0-1, unitless; Eq. 6) was developed to consider species tolerance to floodwater (Hattori et al., 2009) as a function of water depth and plant height.

$$f_{sb} = H_{sub} \cdot \sqrt{T} \quad (6)$$

H_{sub} (0-1, unitless) is calculated according to Eq. 7, whereas T (Eq. 8) is a species-specific tolerance factor (0-1, unitless).

$$H_{sub} = 0.5 + 0.5 \cdot \frac{H_{act} - W_{act}}{H_{act} + W_{act}} \quad (7)$$

$$T = 1 + 0.5 \cdot \frac{W_{crit} - 1}{W_{crit} + 1} \quad (8)$$

where W_{act} (cm) is the actual floodwater level; H_{act} (cm) is the actual plant height; W_{crit} (parameter, unitless, 0 to 1) represents the percentage of H_{max} corresponding to the floodwater level at which gas exchanges are arrested. In practice, according to Eq. 7, the larger the actual plant height compared to the floodwater level, the higher the tolerance to floodwater; Eq. 8 modulates the tolerance according to species-specific factors such as the presence and development of aerenchyma.

A triangular approach is used for the suitability to temperature (f_T, 0-1, unitless, Eq. 10):

$$f_T = \begin{cases} \frac{T_a - T_b}{T_{opt} - T_b} & T_a > T_b \cap T_a \leq T_{opt} \\ 1 - \left(\frac{T_a - T_{opt}}{T_{coff} - T_{opt}} \right) & T_a > T_{opt} \cap T_a \leq T_{coff} \\ 0 & elsewhere \end{cases} \quad (10)$$

where T_a (°C) is the mean air temperature, T_b, T_{opt} and T_{coff} (°C) are parameters representing minimum, optimum and cutoff temperatures for photosynthesis and development, respectively, which are set to the same values of the corresponding parameters of the crop model WARM.

The impact of weed chemical treatments is reproduced by using a coefficient that quantifies the efficiency of specific chemicals in reducing the presence of the different weed species. In practice, in case of a single weed species, weed and crop relative abundance after the treatment are calculated according to Eqs. 11 and 12:

$$SCP_{w(at)} = SCP_{w(bt)} \cdot (1 - Eff_T) \quad (11)$$

$$SCP_{c(at)} = SCP_{c(bt)} + \left(SCP_{w(bt)} - SCP_{w(at)}\right) \quad (12)$$

where $SCP_{w(at)}$ and $SCP_{w(bt)}$ (0-1, unitless) are the relative abundance of the weed before and after the treatment, respectively; $SCP_{c(at)}$ and $SCP_{c(bt)}$ (0-1, unitless) are the corresponding values for the crop (which, for the sake of simplicity, is assumed to be not affected by treatments); Eff_T (parameter, 0-1, unitless) is the chemical treatment efficiency. The same approach is applied in case of more weed species.

State variables of the weeds (e.g., AGB, LAI) and of the community are then reduced accordingly.

2.3.2. Experimental data, model calibration and evaluation

WeedyCoSMo was evaluated for rice crops including two major rice weeds (Kraehmer et al., 2016), i.e., barnyardgrass (*Echinocloa crus-galli*) and red rice (*Oryza sativa* var. *sylvatica*), using datasets published by Zeng et al. (2011) and Zhang et al. (2017) for barnyardgrass, and datasets from Diarra et al. (1985) and Kwon et al. (1992) for red rice (Table 1). In these datasets, rice and weeds were grown both individually and in mixture, in this case with rice and a single weed species at a time (Table 1).

For all the datasets, rice and weeds were grown under unlimiting conditions for water and nutrients. Fields were continuously flooded (2-5 cm water level) in the datasets from Zeng et al. (2011) and Zhang et al. (2017), whereas irrigation or temporary flooding were applied in the other datasets. Simulations were performed from 13 June to 11 October for dataset with ID 1, from 10 May to 7 October for ID 2-5 and 13-16, from 28 May to 25 October for ID 6-11 and 17-18, from 8 June to 5 November for ID 19-22, and from 18 May to 15 September for ID 12 and 23. Further details on the management of experimental fields are provided in the reference literature (Table 1).

Weather data were derived from the European Center for Medium-Range Weather Forecasts (ECMWF) Era-Interim database (Dee et al., 2011). Given nutrients were unlimiting in all the datasets, the model suitability functions for nitrogen and water limitation were switched off during the simulations. The relative abundance of weed and rice was initialized at sowing according to the information made available with the datasets.

Table 1: *Datasets used for model calibration and evaluation. ID 1 refers to dataset collected in Yangzhou (119°42′ E, 32°35′ N; Jiangsu, China), ID 2-5 and 13-16 to datasets collected in Nanjing (32°18′ N, 118°52′ E; Jiangsu, China), ID 6-12 and 17-23 to datasets collected in Stuttgart (34°29’ N, 91°33’ W; Arkansas, USA). Dataset name is composed of an acronym for rice varieties (J: Japonica 9915; Lo: Liangy-oupeijiu; N: Nanjing 9108; L: Lebonnet; M: Mars), sowing year, percentage of weed species at sowing, and weed acronym (E: barnyardgrass; R: red rice). AGB: aboveground biomass; LAI: leaf area index.*

Dataset name	ID	Rice			Weed				Reference	Symbol used in Figs. 2 and 3 [a]
		AGB	LAI	Yield	AGB	LAI	Height	Yield		
Calibration										
J 2006 25% E	1	✓	✓	✓	✓	✓	✓	✓	Zeng et al. (2011)	● (3)
Lo 2013	2	✓	✓	✓					Zhang et al. (2017)	○ (2)
N 2013	3	✓	✓	✓						■ (2)
Lo 2013 20% E	4	✓	✓	✓			✓			○ (3)
N 2013 20% E	5	✓	✓	✓			✓			■ (3)
L 1982	6			✓					Diarra et al. (1985)	△ (2)
1982	7			✓						◆ (2)
L 1982 4% R	8			✓						△ (3)
L 1982 45% R	9			✓						◆ (3)
M 1982 4% R	10			✓						◇ (3)
M 1982 45% R	11			✓						+ (3)
1987 100% R	12				✓				Kwon et al. (1999)	× (2)
Evaluation										
Lo 2014	13	✓	✓	✓					Zhang et al. (2017)	□ (2)
N 2014	14	✓	✓	✓						▲ (2)
Lo 2014 20% E	15	✓	✓	✓			✓			□ (3)
N 2014 20% E	16	✓	✓	✓			✓			▲ (3)
L 1983	17			✓					Diarra et al. (1985)	◇ (2)
M 1983	18			✓						+ (2)
L 1983 4% R	19			✓						✱ (3)
L 1983 45% R	20			✓						− (3)
M 1983 4% R	21			✓						× (3)
M 1983 45% R	22			✓						✚ (3)
1988 100% R	23				✓	✓			Kwon et al. (1999)	– (2)

[a] Numbers in brackets (i.e., 1 and 2) refer to Fig. 2 and Fig. 3.

Calibration and evaluation were carried out using different datasets (Table 1) and in two steps, focusing first on the parameters of the WARM model for the rice varieties and the two weeds, and then on the WeedyCoSMo parameters involved with inter-specific dynamics (Appendix A). Model parameters were calibrated using the trial and error approach, with trials carried out after analysing time trends of different state variables with respect to available observations from the calibration datasets (Table 1). The procedure is considered as complete when satisfying values of agreement metrics are reached. The trial and error approach has been preferred to the use of automatic optimization algorithms because of the presence of some inconsistencies in data pattern over time, which can be better interpreted by expert users rather than by automatic algorithms, to the benefit of the robustness of parameterization (Confalonieri et al., 2016). The values of maximum height and maximum LAI were instead set to the values published by Zeng et al. (2011), Zhang et al. (2017), Diarra et al. (1985), and Kwon et al. (1992). Then, model evaluation was performed on the remaining datasets (Table 1).

Model performance was evaluated using the dataset presented in Table 1 with the following metrics: mean absolute error (MAE; Eq. 13; minimum and optimum 0, maximum +∞), relative root mean square error (RRMSE; Eq. 14; %; minimum and optimum 0, maximum +∞), modelling efficiency (EF; Eq. 15; from -∞ to +1, optimum +1; Nash and Sutcliffe, 1970), coefficient of residual mass (CRM; Eq. 16; if positive it indicates underestimation and vice versa; Loague and Green, 1991), and the R^2 and the slope of the linear regression equation between observations and simulated data.

$$MAE = \frac{\sum_{i=1}^{n}|S_i - O_i|}{n} \quad (13)$$

$$RRMSE = \frac{\sqrt{\frac{\sum_{i=1}^{n}(S_i - O_i)^2}{n}}}{\bar{O}} \cdot 100 \quad (14)$$

$$EF = 1 - \frac{\sum_{i=1}^{n}(S_i - O_i)^2}{\sum_{i=1}^{n}(O_i - \bar{O})^2} \quad (15)$$

$$CRM = 1 - \frac{\sum_{i=1}^{n} S_i}{\sum_{i=1}^{n} O_i} \quad (16)$$

where n is the number of observations, O_i and S_i are the ith observation and simulated value, respectively.

2.3.3. Evaluating weed management scenarios

In order to evaluate the potential use of the model as a management support tool, a scenario analysis was run to evaluate the model sensitivity to changes in management practices and in the characteristics of the rice cultivar.

Rice (cultivar Liangy-oupeijiu) and barnyardgrass parameters were those calibrated and evaluated (Table 1), the only exception being the growing degree days to flowering and from flowering to maturity for rice, which were decreased by 30% because of the lower temperatures and higher latitude in Milan compared to those that characterize the Jiangsu area where the Zhang et al. (2017) experiments were carried out.

A base scenario was defined where growth and development of rice and barnyardgrass were simulated in a paddy field close to Milan (45°22' N, 9°12' E; Lombardy, northern Italy) under unlimiting conditions for water (continuous flooding) and nutrients. Simulations were run using 20 years of weather data (1986 - 2005) to account for differences in weather among seasons. Weather data were retrieved from the European Center for Medium-Range Weather Forecasts (ECMWF) Era-Interim database (Dee et al., 2011). Each year was considered as independent, simulations being re-initialized with barnyardgrass at 30% relative abundance (initial infestation) at the beginning of each season. Sowing for the management strategy in the base scenario was on 30 May, with the field kept flooded (5 cm water level) throughout the season. Two broad-spectrum herbicide (penoxsulam; 40 g a.i. ha-1, 92% efficiency against *Echinochloa* spp.; Cavanna et al., 2004) treatments were applied 15 and 35 days after sowing.

The base scenario was compared with four alternative scenarios that differed from the base one for: (i) the first herbicide treatment was applied when rice was at the 2nd-leaf stage and the second was not fixed but triggered by the model when barnyardgrass relative abundance exceeded 6.5% (scenario 1), (ii) floodwater level at 10 cm instead of 5 cm (scenario 2), (iii) higher thermal requirements for rice to emerge (+50 growing degree days) (scenario 3), (iv) taller rice plants (135 cm instead of 125 cm) (scenario 4). Analysis of variance (followed by the Tukey test) was run to evaluate the significance of the

differences among scenarios. For each scenario, the 20 yields simulated using the 20 years of weather data were used as replicates.

2.4. Results

2.4.1. Model calibration

Calibrated values for all parameters are available in Appendix A. For all rice cultivars, parameter values of the WARM model are in the range of those used by Confalonieri et al. (2009) and Pagani et al. (2014) for rice cultivars grown in Chinese and Italian rice districts. Cardinal temperatures are consistent with the values used by Casanova et al. (1998) for modelling rice growth and development in Spain, whereas calibrated values for maximum radiation use efficiency and extinction coefficient for solar radiation fall in the range of the values estimated by Campbell et al. (2001) and Dingkuhn et al. (1999), respectively. Specific leaf area at emergence and at mid tillering are close to the values measured by Dingkuhn et al. (1998) for different rice genotypes in Cote d'Ivoire. Main differences among rice cultivars deal with radiation use efficiency, which is lower for the US cultivars, and with the growing degree days needed to reach emergence, flowering and maturity, with the cultivars grown in the experiments performed in China presenting higher thermal requirements. Other differences deal with canopy development, with the Chinese cultivars being characterized by higher values for maximum leaf area index and maximum plant height, and by lower specific leaf area at emergence.

Model results were overall satisfactory, R^2 being always higher than 0.81 and the slope of the linear regression between simulated and observed data ranging from 0.77 to 1.37. Time dynamics of the different state variables were reliably reproduced for all rice varieties and for both weeds, regardless they were grown in monoculture or in mixture (Figs. 2 and 3, Table 2).

Concerning the simulation of rice and red rice in monoculture (Fig. 2, Table 2), the model accurately estimated aboveground biomass (AGB). In particular, the values achieved by the agreement metrics for the simulation of rice (○ and ■ in Fig. 2a) and red rice (✖ in Fig. 2b) AGB, and rice LAI (○ and ■ in Fig. 2c) were always in ranges considered as full y satisfactory, i.e., < 20%, > 0.5, < |0.2| for RRMSE, EF and CRM, respectively (Chung et al., 1999; Bellocchi et al., 2002; Moriasi et al., 2007). The good performances achieved for red rice were – to a certain extent – expected, given the

similarities between red rice and cultivated rice in terms of morphological and physiological features and the known suitability of the WARM model for rice.

The accuracy in simulating time trends of rice AGB and LAI reflected in reliable yield estimates (○, ■, △ and ◆ in Fig. 2e), regardless of the cultivar and of the experimental site and year.

Observations referring to rice grown with barnyardgrass and red rice (Fig. 3) were accurately reproduced by the model, which showed performances very similar to those achieved for the datasets where rice was grown in monoculture. In particular, agreement metrics for AGB (○ and ■ in Fig. 3a) were consistent with monoculture ones, whereas those calculated for LAI (○ and ■ in Fig. 3c) were slightly better, with EF equal to 0.87. Results were satisfactory (EF = 0.87) also for yield simulation, although in this case model performances were lightly poorer compared to what achieved for rice in monoculture (○, ■, △, ◆, ◇ and + in Fig. 3e). The model capability to reproduce rice growth in monoculture and in interaction with barnyardgrass and red rice led to a good simulation of the yield losses due to the competition from the two grass weeds, with EF equal to 0.79, respectively, and CRM close to 0, indicating the absence of systematic under- or over-estimations (Table 2).

The low number of observations available for calibrating barnyardgrass parameters affected the values of some of the performance metrics (Table 2), although the agreement between observed and simulated variables was overall satisfactory. LAI values (Fig. 3.d) were accurately reproduced by the model, with MAE and RRMSE very close to their optima, whereas the negative value for EF is due to the low variability in measured data (Criss and Winston, 2008). Concerning AGB (Fig. 3b), barnyardgrass simulations presented a marked overestimation for the first sampling event, whereas good agreement was achieved for the others. The accuracy in the simulation of barnyardgrass height is demonstrated by the good values achieved for all the metrics (Table 2).

2.4.2. Model evaluation

No relevant worsening in model performance were noticed while moving from calibration to evaluation datasets (Table 2), regardless of the simulated species and of the growing conditions (monoculture vs mixtures).

The only exception was for LAI of rice grown in monoculture (□ and ▲ in Fig. 2c), for which the values of the agreement metrics were less satisfying compared to those achieved for the same variable during calibration and, in general, for the other variables. For LAI values higher than 3, the model overestimated LAI of rice (Fig. 2c) and underestimated the one of red rice (Fig. 2d), with overall CRM values of -0.33 and 0.21, respectively (Table 2). The underestimation of LAI values in the second part of the red rice cycle is due to the fact that the model does not simulate new leaf emergence after the flowering stage, contrarily to what happens in reality.

Compared to what achieved during calibration, rice AGB was simulated with the same degree of accuracy when the crop was grown in monoculture (□ and ▲ in Fig. 2a), whereas better values for all the metrics were obtained for the same variable when rice was competing with weeds (□ and ▲ in Fig. 3a). Good results were achieved also for rice yield simulations, with the crop grown in monoculture (□, ▲, ◇, + in Fig. 2e) and in mixture with weeds (□, ▲, ✱, −, ×, ✚ in Fig. 3e).

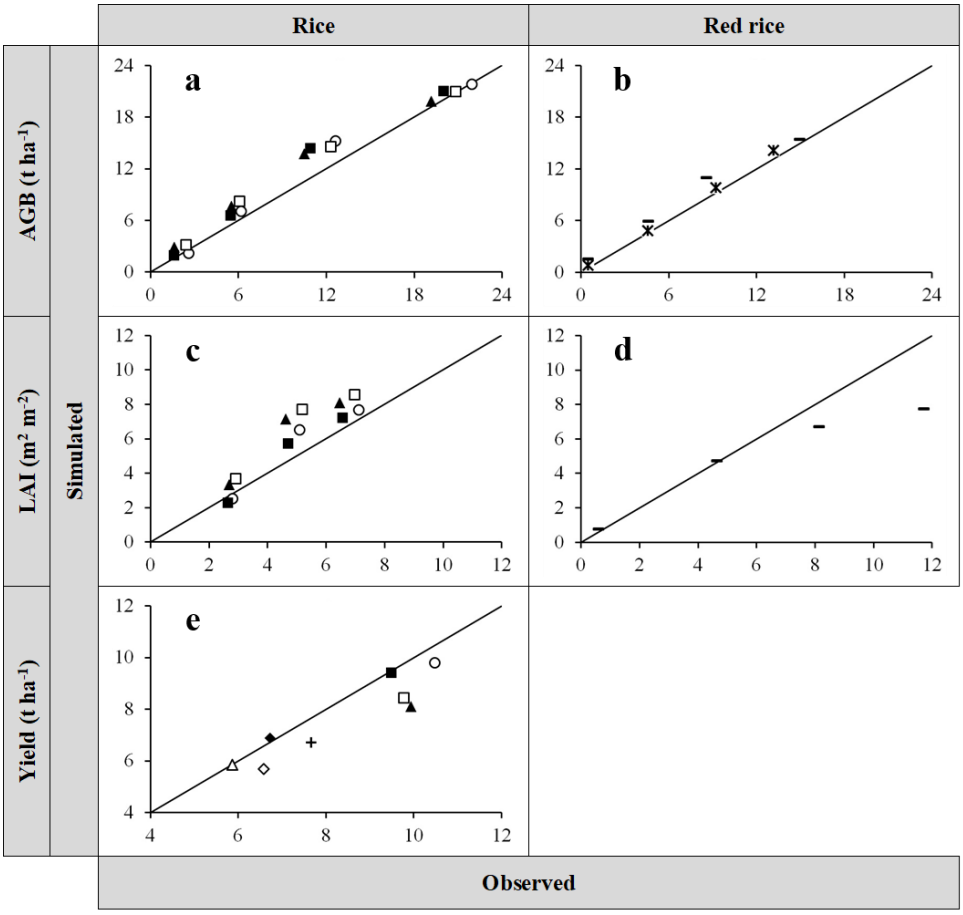

Figure 2: *Comparison between observed and simulated aboveground biomass (AGB), leaf area index (LAI) and yield data for rice and red rice in monoculture. Symbols refer to the datasets presented in Table 1, where information on calibration and evaluation datasets is also provided; black line is the y=x line, indicating the theoretical perfect agreement between observations and model outputs.*

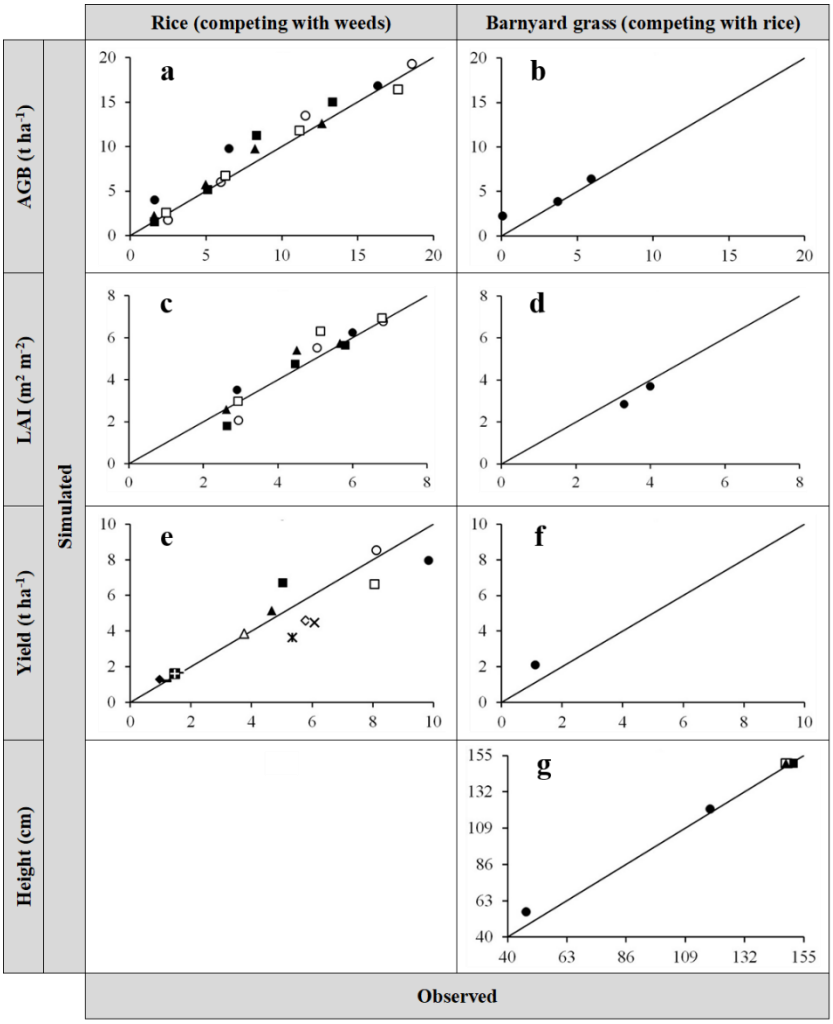

Figure 3: *Comparison between observed and simulated aboveground biomass (AGB), leaf area index (LAI) and yield data for rice (competing with weeds) and barnyardgrass (competing with rice) in mixture. For the latter, plant height data are also compared. Symbols refer to the datasets presented in Table 1, where information on calibration and evaluation datasets is also provided; black line is the y=x line, indicating the theoretical perfect agreement between observations and model outputs.*

Table 2: *Agreement metrics (Eqs. 11-14) calculated on observed and simulated yield, yield losses due to weeds (Yield-W), aboveground biomass (AGB), leaf area index (LAI), plant height (H).*

Species	Variable	Conditions	MAE	RRMSE (%)	EF	CRM	R^2	Slope
Calibration								
Rice	AGB	Monoculture	1.23 t ha^{-1}	16.10	0.95	-0.10	0.97	0.95
		Mixture	1.29 t ha^{-1}	20.50	0.91	-0.14	0.95	0.93
	LAI	Monoculture	0.70 m^2 m^{-2}	16.50	0.78	-0.10	0.95	0.77
		Mixture	0.45 m^2 m^{-2}	11.70	0.87	0.01	0.92	0.82
	Yield	Monoculture	0.24 t ha^{-1}	4.40	0.96	0.02	0.99	1.14
		Mixture	0.80 t ha^{-1}	21.20	0.87	0.01	0.88	1.05
	Yield-W	Mixture	9.10%	25.30	0.79	0.06	0.81	0.95
Red rice	AGB	Monoculture	0.94 t ha^{-1}	9.20	0.98	-0.08	1.00	0.94
Barnyard grass	AGB	Mixture	1.37 t ha^{-1}	39.30	0.72	-0.28	0.93	1.37
	LAI		0.39 m^2 m^{-2}	4.40	-0.30	0.11	-a	-a
	Yield		1.00 t ha^{-1}	90.10	-a	-0.90	-a	-a
	H		3.0 cm	3.80	0.99	-0.02	1.00	1.10
Evaluation								
Rice	AGB	Monoculture	1.55 t ha^{-1}	18.70	0.93	-0.16	0.98	1.03
		Mixture	0.69 t ha^{-1}	10.40	0.97	-0.04	0.98	1.08
	LAI	Monoculture	1.60 m^2 m^{-2}	36.70	-0.19	-0.33	0.91	0.73
		Mixture	0.39 m^2 m^{-2}	13.00	0.83	-0.08	0.92	0.86
	Yield	Monoculture	1.25 t ha^{-1}	15.40	0.16	0.15	0.98	1.28
		Mixture	0.90 t ha^{-1}	25.50	0.78	0.16	0.89	1.21
	Yield-W	Mixture	9.63%	25.10	0.84	-0.04	0.86	1.17
Red rice	AGB	Monoculture	1.27 t ha^{-1}	20.20	0.93	-0.18	0.98	1.01
	LAI		1.40 m^2 m^{-2}	33.70	0.74	0.21	0.94	1.49
Barnyard grass	H	Mixture	2.0 cm	0.70	-	0.01	-a	-a

[-a] Not enough data to calculate the metric.

2.4.3. Evaluating weed management scenarios

Means and standard deviations of the outputs from the 20 annual simulations run for the scenario analysis are shown in Fig. 4. Compared to the base one, scenario 1 led to a light increase in rice yield (+3.1%) that resulted non-significant. However, considering the 20 seasons, it was characterized by a lower number of herbicide treatments per year (1.55 treatments year-1 versus 2.00 treatments year-1). This means that, one the one hand, differences in the weather conditions among seasons allowed avoiding the second treatment in nine years out of 20, given the weed relative abundance never exceeded the threshold triggering the second treatment (maximum relative abundance after the first treatment in those nine years was 6.4%). On the other hand, the higher mean yield demonstrates that triggering the second treatment based on the weed relative abundance instead of applying it a constant number of days after sowing allowed increasing the treatment efficiency in the years when the second treatment was applied.

Results from scenario 2 demonstrate the model sensitivity to floodwater level: increasing floodwater level from 5 cm to 10 cm allowed penalizing the weeds, which are less tolerant than rice to partial submergence of culm tissues (Hattori et al., 2009). Indeed, the mean of the daily floodwater level suitability factors for rice decreased by 5.3% because of the increase in floodwater level, whereas it decreased by 36.0% for the weed. This translated into higher competitiveness of rice, with a 11.8% increase in mean yield compared to the base scenario. However, the large variability among seasons made the increase non-significant.

Scenarios 3 and 4 are instead based on changes to the values of two of the traits of the simulated rice cultivar: increased thermal requirements for emergence (scenario 3) led the weed establishing faster than rice, thus making more pressure on the crop, with an effect that was only partially mitigated by the two herbicide treatments (the weed relative abundance before the second treatment was 25% higher compared to the base scenario). This led to a mean rice yield that was 21.2% lower ($p < 0.05$) compared to the value simulated for the base scenario. On the contrary, the 10 cm taller rice plants that characterized the scenarios 4 allowed achieving slightly higher – although the difference was not significant – yields compared to the base scenario (+2.7%) because of a higher capability to compete for radiation. The mean of the weed daily suitability factors for radiation was indeed 2% less compared the base scenario.

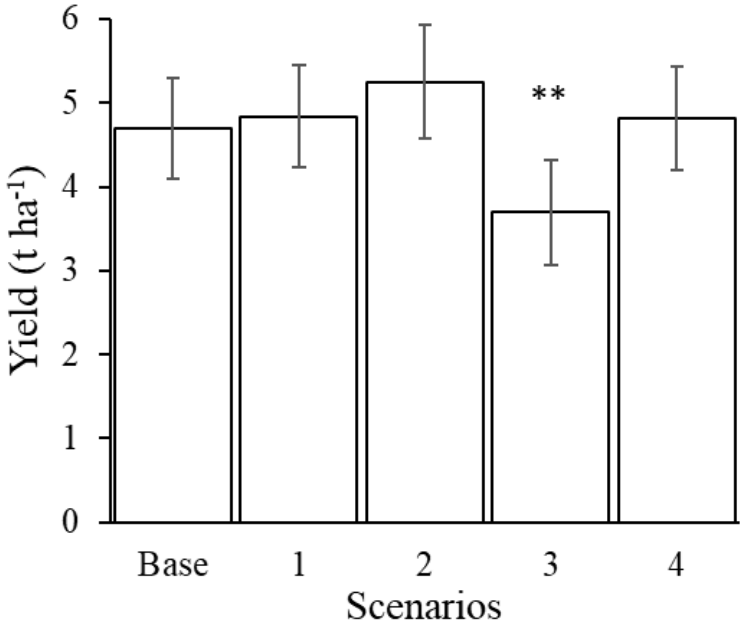

Figure 4: *Grain rice yield (mean of 20 annual simulations) achieved for the base scenarios compared to the rice yield obtained by triggering the second herbicide treatment when weed relative abundance exceeded 6.5% (scenario 1), by increasing floodwater level from 5 cm to 10 cm (scenario 2), by simulating a rice cultivar with higher thermal requirements for emergence (scenario 3) and with a higher value for maximum height (scenario 4).*

2.5. Discussion

2.5.1. Novelty of the proposed approach

WeedyCoSMo is a new model for the simulation of crop-weed interaction, based on hierarchically-arranged factors daily accounting for the suitability of the different species to environmental and management drivers. The model – derived from the CoSMo approach for the simulation of phytocoenosis dynamics – can be coupled with any generic crop model, allowing users to work with the crop model they are more familiar with, or for which parameter sets for local cultivars are already available. This allows upscaling from

single-species canopies to multi-species ones with a reduced effort compared to other approaches.

The model is characterized by a good compromise between applicability (parsimony in terms of information needed for calibration and application) and biophysical adherence to the underlying system. Indeed, despite the algorithms used for crop-weed interaction are decidedly simpler than in other approaches, good performances were achieved for the simulation of time-dynamics of key state variables and for the estimation of yield losses caused by weeds when the model was evaluated using datasets collected under different environmental and management conditions. This translates into a high usability while successfully capturing key dynamics of crop-weed interaction.

2.5.2. Reliability, domain of validity and limits

Despite the potential risks due to the calibration method and to the relationship between the number of parameters and the number of observations available for model parameterization, the absence of worsening in model performance during the evaluation against independent datasets revealed an overall good robustness of the modelling approach and of the defined parameter sets.

The simulation of rice aboveground biomass (AGB) and leaf area index (LAI) in monoculture (Fig. 2a; Table 2) revealed a degree of accuracy consistent with previous studies where rice growth was estimated using different models (Bouman and van Laar, 2006; Belder et al., 2007) or the same crop simulator (e.g., Confalonieri et al., 2009; Pagani et al., 2014). The higher uncertainty in LAI simulation (compared to other variables) was already observed by different authors (Yu et al., 2006; Confalonieri et al., 2009; Tartarini et al., 2019), and it can be partly due to the larger uncertainty in the methods used for estimating this variable.

Despite early stages are crucial for crop-weed interaction (Martin et al., 2001), Deen et al. (2003) observed during this phase a larger uncertainty in crop and weed (grown in mixture) LAI estimates in a comparative study where four crop-weed models were evaluated for wheat and Lolium rigidum. In this study, the authors underlined a general tendency of the models to decrease their accuracy while moving from species in monoculture to crop-weed mixtures. This phenomenon was not observed during the evaluation of

WeedyCoSMo, which correctly reproduced observed time dynamics of LAI in the post emergence phase and throughout the season for rice and the two weed species, whereas it underestimated observations for this variable for red rice in monoculture only for values larger than 6 m^2 m^{-2}. In general, the overall good model performance while estimating LAI should be considered of primary importance, given the role of this variable in quantifying the response of rice and weeds to radiation. This is indeed crucial for correctly reproducing changes in the relative abundance of the different species throughout the season.

WeedyCoSMo performances in estimating rice yield losses due to weeds were better than those obtained using empirical approaches based on relative leaf area (Kropff and Spitters, 1991), and similar to what achieved for the same crop and weed by Bastiaans et al. (1997) and Kropff et al. (1993) using the INTERCOM model. In particular, Kropff et al. (1993) reported that INTERCOM allowed explaining 93% of the variance in observations, whereas WeedyCoSMo – in spite of lower requirements in terms of inputs needed to run the simulation – explained only 10% variance less.

However, the model evaluation for barnyardgrass should be considered as decidedly preliminary, given the few data available. Indeed, despite the good performances achieved for rice in mixture with this weed species could be considered an indirect guarantee of the functioning of the whole system (and, thus, of the reliability of barnyardgrass parameterization), related parameter values need to be further evaluated.

One of the main limits of the current version of WeedyCoSMo is the absence of algorithms for simulating phenotypic plasticity driven by inter- and intra-specific competition (Colbach et al., 2019). This choice was due to the need of limiting model complexity to increase the potential of the model for being adopted in operational farming contexts. The quest for limiting the complexity of the model also led to design WeedyCoSMo in such a way to reproduce crop-weed interaction at canopy level, without downscaling to individual-based architectures. The good performances obtained during model evaluation further demonstrate that the model design could strictly depend on the specific objective and conditions of application (Colbach, 2010), and that increasing model complexity – when not strictly needed – could prevent models from being used for decision making under operational conditions (Park et al., 2003).

Another limit of the approach we propose deals with the absence of algorithms for simulating weed seed survival and, thus, multi-annual weed dynamics. This requires initializing the model at the beginning of each seasons. However, modelling approaches for the simulation of weed seedbank processes are available (e.g., Otto et al., 2007; Bohan et al., 2011) and will be integrated in the next version of WeedyCoSMo.

2.5.3. Application and implications for weed management support

Despite some simplifications suggest to further investigate the model behavior in response to treatments (e.g., the effect of canopy density on herbicide efficiency is not considered), the scenario analysis demonstrated the suitability of the model as a tool to support strategic decisions regarding when and how often to apply herbicides. Indeed, its capability of optimizing the timing of treatments led to an overall increase in the treatment efficiency and in avoiding the second treatment in 45% of the simulated seasons. Moreover, the model capability of reproducing the lower tolerance of weeds to the partial submersion of tissues (Hattori et al., 2009) makes the model suitable to support weed control strategies based also on the modulation of water management.

Moreover, the model sensitivity to changes in the traits of the simulated rice cultivar opens to the possibility to perform ideotyping studies for supporting breeding programs targeting an increase of rice competitiveness against weeds. This would be important especially for production contexts moving towards the reduction of the use of chemicals or their abandonment (e.g., organic farming). Indeed, despite the increasing demand for breeding programs targeting a higher competitiveness against weeds (Fontaine et al., 2009), very few studies are available where crop-weed interaction models were used to identify in a quantitative way plant traits able to maximize potential crop productivity while minimizing yield losses due to weeds (e.g., Colbach et al., 2019).

However, the model potential for being used to support decision making is limited – in its current configuration – by the absence of algorithms for the estimation of seed production and survival. This limits the types of analysis the model can be used for, although the capability to reproduce seasonal dynamics of crop-weed interaction with a low number of inputs opens to further extensions of the model that will broaden its usefulness for management support under operational farming conditions.

2.5.4. Perspectives

Thanks to the good balance between usability and capability of capturing key processes involved with crop-weed interaction, WeedyCoSMo opens up new opportunities for extending existing DSS towards the possibility to support weed management under operational farming conditions.

Further activities will refer to tests on other crops and weeds and to the model linkage to modelling approaches for the simulation of weed seedbank processes like seed mortality and dormancy (e.g., Otto et al., 2007; Bohan et al., 2011) and weed germination/emergence (e.g., Masin et al., 2010; Gardarin et al., 2012; Borgy et al., 2015), and the evaluation of the model for designing rice ideotypes more competitive against weeds (Bastiaans et al., 1997). Moreover, approaches for the simulation of the effect of mechanical weed control will also be implemented.

2.6. Conclusions

We proposed a new approach, namely WeedyCoSMo, to simulate the time dynamics involved with crop-weed interaction, based on the quantification of the suitability of the different species to the environmental and management conditions explored each day. The model was developed by targeting operational contexts, thus we paid particular attention to limit its requirements in terms of data needed for calibration and application. WeedyCoSMo can be coupled with any generic crop model, thus allowing to extend existing modelling approaches – e.g., those already implemented in operational simulation platforms – for being used to support strategic decisions on weed management.

WeedyCoSMo demonstrated its suitability in simulating the interactions between different rice cultivars and two major rice weeds, i.e., red rice and barnyardgrass, whose time trends of aboveground biomass and leaf area index were accurately reproduced, as well as rice yield losses due to weed presence. The model demonstrated its suitability also for scenario analysis, showing a good potential for being used to identify context-specific management strategies.

As demonstrated by the results achieved during model evaluation, the novel approach to upscale from single-species to multi-species canopies allows simulating crop-weed interaction without the need to implement individual-

based architectures. This makes the model easy to use because of the limited number of parameters, most of which are shared with many crop models widely used worldwide. However, despite its low complexity, the good performances achieved seem to further demonstrate what observed by Deen et al. (2003), who concluded a comparative study suggesting the absence of clear relationships between model complexity and the capability to capture most of the dynamics involved with crops response to weed competition.

The capability of WeedyCoSMo to simulate changes in the relative abundance of crops and weeds on a daily basis encourages its evaluation as a tool to support the optimization of weed management practices.

Credit Authorship Contribution Statement

Ermes Movedi: Conceptualisation, Methodology, Software, Writing – original draft, Formal analysis. Daniele Valiante: Data curation, Investigation. Alessandro Colosio: Investigation. Luca Corengia: Investigation. Stefano Cossa: Software, Validation. Roberto Confalonieri: Conceptualization, Supervision, Writing – review & editing.

Declaration of Competing Interests

The authors declare that they have no known competing financial interests or personal relationships that could have appeared to influence the work reported in this paper.

Appendix A: *WeedyCoSMo parameters for red rice (R), Barnyardgrass (E), and for the rice varieties Japonica 9,915 (J), Liangy-oupeijiu (Lo), Nanjing 9108 (N), Lebonnet (L), and Mars (M).*

Parameter name	Units	Weeds		Rice varieties				
		R	E	J	Lo	N	L	M
Parameters of the WARM model (simulation engine used within WeedyCoSMo)								
Extinction coefficient of solar radiation	-	0.5	0.55	0.5	0.45	0.45	0.45	0.45
Full canopy coefficient	-	1.05	1.05	1.05	1.05	1.05	1.05	1.05
Full canopy maximum water uptake	mm	10	10	10	10	10	10	10
Growing degree days to reach mid emergence	°C-d	80	50	150	150	150	70	70
Growing degree days to reach mid flowering	°C-d	1000	1250	1200	1300	1300	1150	1150
Growing degree days to reach harvest	°C-d	50	50	50	50	50	80	80
Growing degree days to reach mid maturity	°C-d	450	350	650	550	550	450	450
Leaf life	°C-d	800	800	950	900	900	550	600
Maximum radiation use efficiency	g MJ^{-1}	2.5	3	3.2	3	2.9	2.6	2.7
Fraction of photosynthates partitioned to leaves at emergence (0-1)	-	0.55	0.8	0.75	0.6	0.6	0.65	0.65
Specific leaf area (leaf area to leaf dry mass ratio) at emergence	$m^2 kg^{-1}$	23	30	18	25	25	29	29
Specific leaf area (leaf area to leaf dry mass ratio) at mid tillering	$m^2 kg^{-1}$	22	20	13	18	18	14	14
Threshold radiation for saturation (above which radiation use efficiency decreases)	MJ d^{-1} m^{-2}	32	30	30	30	30	32	32
Parameters used by WARM and by the crop-weed interaction component								
Base temperature for photosynthesis and development	°C	11	11	11	11	11	11	11
Cutoff temperature for photosynthesis and development	°C	42	43	43	43	43	40	40
Maximum leaf area index	m^2 m^{-2}	11	10	10	10	8	6	8
Maximum height	m	1.8	1.5	1.25	1.25	1	1	1.1
Optimal temperature for photosynthesis and development	°C	28	27	28.5	28.5	28.5	27	28
Parameters used by the crop-weed interaction component								
Percentage of maximum plant height corresponding to the floodwater level at which gas exchanges are arrested	-	0.33	0.27	0.6	0.72	0.7	0.5	0.55

3. Adaptation strategies to alleviate climate change impacts on grasslands productivity and forage quality. A case study in northern Apennines.

Ermes Movedi, Livia Paleari, Giovanni Argenti, Fosco Vesely, Nicolina Staglianò, Silvia Parrini, Roberto Confalonieri

To be submitted to:

Agricultural Systems

3.1. Abstract

Grasslands are environments characterized by an elevated biodiversity in plant species, which dynamically evolves over time as response to management practices, soil proprieties, and climate conditions. Climate change can locally affect grassland growth and floristic composition and, in turn, the quality and quantity of provided ecosystem services. We focused on mountain areas in the northern Apennines where temporary alfalfa (*Medicago sativa* L.)-dominated grasslands are sown for the production of Parmesan cheese, to evaluate climate change impacts on grassland growth and composition as well as alternative management scenarios to improve adaptation in the mid-term. The plant community CoSMo model as coupled with the crop model CropSyst was used, to explicitly account for dynamics of floristic composition. Five sites and four alternative climate scenarios (RCP4.5 and RCP8.5 projections as provided by the HadGEM2 and GISS general circulation models) were considered, to explore a wide range of agro-environmental conditions. Results showed that the observed dynamics of

floristic composition and biomass accumulation were successfully simulated, with a mean absolute error lower than 10% for floristic composition and less than 1 t ha^{-1} for total biomass. Climate change impacts were globally negative, with a clear decrease of forage production as compared to the baseline (from -3.6 % to -14.3% according to the climate scenario). The biodiversity of the phytocenosis also declined (inverse of Simpson index decreased of -12.5% on average), due to the increase in alfalfa dominance. The latter, however, led to preserve the forage crude protein content (+0.9% on average). Guidelines for optimizing grassland productivity and forage protein under future climates were defined, mainly focused on reducing the alfalfa field duration, sowing grass-legume mixtures, and delaying the last cut. These practices can be easily adopted in real farm contexts, to support the adaptation of temporary grassland systems to a changing climate.

Keywords:

Ecosystem services; CoSMo; Relative abundance; Alfalfa; CropSyst; Adaptation.

3.2. Introduction

Grasslands play a key role in the context of ecosystem services, by providing material and not material products and services that affect human activities, including economy, health, and quality of life (Tribot et al., 2018).

Grasslands are crucial for biodiversity protection, carbon and nitrogen sequestration, pollination, improvement of landscape value for tourism activities, and protection of soil from erosion (Marriott et al., 2004; Giustini et al., 2007; Schulze et al., 2009; Argenti et al., 2011; Cong et al., 2014; Hao et al., 2017; Pulina et al., 2017; van Oijen et al., 2018; Bengtsson et al., 2019; van Oijen et al., 2020; Viira et al., 2020). One of the most important ecosystem service that grasslands provide is forage production (Suttie et al., 2005), which is often linked to the production of local and traditional

delicacies. For example, temporary grasslands dominated by alfalfa (*Medicago sativa L.*) are the main forage source for more than 100 dairy farms that produce local Parmesan cheese in the mountain areas of northern Apennine (Mancini et al., 2019). Alfalfa is one the most adapted species to the local environmental conditions and, by providing forage with high nutritional value (high crude protein content) and stable yields even in low-input contexts, it plays a key role to improve the economic and environmental sustainability of dairy farms in the area (Tabacco et al., 2018; Kic, 2019).

Grasslands are environments characterized by the coexistence of a large number of herbaceous species and, therefore, by a high biodiversity (Habel at al., 2013). This richness of species has a large influence on the type and quality of ecosystem services that grasslands provide (Oliver et al., 2015), to the point that grassland floristic composition can be used as a proxy of codominance and resilience of grassland ecosystems (Simpson, 1949, Mackie et al., 2018) and, when evaluated in terms of percentage of legumes species, as a reliable indicator of quality of forage (Argenti et al., 2021).

Grassland floristic composition is highly variable as function of multiple environmental factors, such as climate conditions, soil proprieties, and management regimes (Jeangros et al., 1999; Ziliotto et al., 2004; Buxton and Fales, 1994). Agronomic practices play a relevant role especially in case of temporary grasslands, where different species are sown for hay production. These grassland evolves over time due to the settlement of wild species and are thus periodically renewed to ensure satisfactory production and quality of forage. Crop management markedly affect the dynamics of these plant communities, through the increase of water and nutrients availability (irrigation and fertilization), the frequency of mowing, the composition of the sown mixture, and the field duration before renewal (Matches, 1992; Ren et al., 2012, Argenti et al., 2021).

Variation in climate also deeply affects grassland floristic composition and growth (Mooney and Hobbs, 2010), although the impacts can largely vary as a result of heterogeneity in plant communities and local climates. By conducting an extensive meta-analysis, Dellar et al. (2018) estimated an increase of grassland productivity as response to climate change in northern Europe and, on the contrary, a decrease in central and southern areas.

Despite crop models are widely used for estimating the effects of climate change on multiple crops (Tubiello et al., 2007), only few of them can

explicitly reproduce the floristic composition of plant communities and its dynamics over time (Confalonieri, 2014). Modelling approaches accounting for inter-species competition and plant community evolution as response to environmental drivers would allow to analyse climate change impacts on grasslands floristic composition and related ecosystem services. By explicitly considering management factors, they would also allow to identify strategies to improve the adaptation of agro-ecosystems to future climate projections (Franke et al., 2022).

The focus of this study was to evaluate the impact of climate change on temporary alfalfa-dominated grasslands by explicitly considering their floristic composition. To this end, the CoSMo plant community model (Confalonieri et al., 2014) was used, focusing on the mountain northern Apennine as study area. Adaptation strategies to optimize forage production and quality under future conditions were also evaluated and discussed, to provide farmers with guidelines preserving grasslands productivity in the mid-term.

3.3. Materials and methods

3.3.1. The modelling approach

The community model CoSMo (Community Simulation Model; Confalonieri, 2014) was used to dynamically simulate the floristic composition of the plant community as response to environmental and management factors and – coupled with the generic crop model CropSyst (Stöckle et al., 2003) – the grassland productivity (Movedi et al., 2019). CoSMo daily estimates the variation in the relative abundance of the different species in the community (floristic composition) according to their suitability to environmental (E) and management (M) drivers, which account for both continuous variables (e.g., global solar radiation, soil water content) and events (e.g., cut, grazing). Drivers are used to estimate species-specific suitability factors to the conditions (E, M) explored at each time step. The overall suitability of each species is then calculated by aggregating the suitability factors estimated for each driver through a hierarchical weighting procedure, which allows to differentiate the drivers according their actual impact on the overall species suitability. Drivers representing grazing or cutting are top-ranked given the marked effect of these events on grassland composition due to the heterogeneity in species capability to restart growth after these disruptive events. Phenological development is the second high-

impact driver because after maturity annual self-seeding species do not compete anymore until the germination and emergence of the next generation of individuals. The remaining drivers are ranked in decreasing order (as air temperature, global solar radiation, soil water and nitrogen availability) in line with other modelling approaches dealing with inter-specific competition (Confalonieri et al., 2014). The overall species-specific suitability value is then used to estimate the relative abundance of the different species at the following time step. The relative abundance allows to weight the crop model parameters that describe the growth of each species in monoculture, in order to derive the crop model parameters representing the plant community as a whole. Community parameters are thus dynamic, evolving alongside phytocenosis composition. The crop model uses these parameters to simulate biophysical processes at the level of plant community at each time step, providing key variables for grassland productivity (e.g., aboveground biomass, leaf area index).

In this study the crop model CropSyst (Stöckle et al., 2003) was used as simulation engine to daily estimate the plant community growth and development as a function of weather variables, chemical and physical soil properties, and crop management. It was chosen because of its proven effectiveness for alfa-alfa (*Medicago sativa* L.) simulation in the study area (Confalonieri e Bechini, 2004) and its reliability in reproducing growth and development of plant communities when coupled with CoSMo (Movedi et al., 2019). CropSyst estimates the daily accumulation of aboveground biomass (AGB, t ha^{-1}) with a net photosynthesis approach, based on the minimum value between that derived as a function of radiation use efficiency as limited by temperature, and that estimated according to the transpiration use efficiency as corrected by vapour pressure deficit. Green leaf area expansion is simulated according to the daily aboveground biomass accumulation, the early-stages specific leaf area, and an empiric stem/leaf partition coefficient. The Beer's law approach is used to estimate the radiation intercepted daily as a function of the green LAI and of the light extinction coefficient for solar radiation. Phenological development is simulated according to the mean air daily temperature and parameters defining minimum and optimum thermal requirements, with an option to account for photoperiod. For the simulation of soil water dynamics, a cascading model with travel time (Neitsch et al.. 2002) was used together with pedotransfer functions (van Genuchten et al., 1985) to estimate hydrological soil proprieties. More details on CropSyst can be found in the reference literature

(Stöckle et al., 2003). Concerning the simulation of forage quality in terms of crude protein content on dry matter basis (CP, %), the empiric model developed by Argenti et al. (2021) for the same study area was used, which derives forage crude protein as a function of the relative abundance of legumes in the grassland. In this study, the simulated relative abundance of wild or sown legumes (alfalfa and *Trifolium* spp.) as provided by CoSMo was used.

3.3.2. Model parameterization

Field data for model parameterization were collected at five sites (Table 1) in the northern Apennine (Emilia-Romagna region) with temporary alfalfa-dominated grasslands as described by Argenti et al. (2021). In this mountain and unfavourable area, temporary grasslands and meadows represent a key support for the production of local Parmesan cheese by the about 100 farms of the consortium "Terre di Montagna" (Mancini et al., 2019). Alfalfa is one the most adapted species to local environmental conditions and, given its good productivity and high nutritional value of the forage (high protein content). The five sites were chosen as representative of the heterogeneity characterizing the area in terms of environmental conditions, presence of species, and age of the meadows. Three samplings were conducted at each site during 2019, before mowing (Appendix A). Variables measured referred to the floristic composition (visual method; Boob et al., 2019), the aboveground biomass dry matter (AGB, t ha^{-1}; oven-dried until constant weight), the leaf area index (LAI, unitless; ceptometer estimation), and the crude protein on dry matter basis (CP, %; Kjeldhal method) as a key component of forage quality. More details on the field experiments can be found in Argenti et al. (2021).

Table 1: *Description of the experimental fields (from Argenti et al., 2021).*

Site	Altitude (m a.s.l.)	Latitude (°)	Longitude (°)	Sown crop	Years since sowing
A	740	44.313808	11.031986	Alfa-Alfa	2
B	870	44.331032	10.987424	Alfa-Alfa	4
C	750	44.285525	10.946268	Alfa-Alfa	8
D	780	44.234906	10.922269	Mixture[a]	2
E	740	44.218132	10.909049	Mixture[a]	4

[a]: grasses-legumes mixture

For each site, daily minimum and maximum temperature, net solar radiation, and rainfall were retrieved from the weather service of the University of Milan Cassandra Lab, which provides historical daily weather data for the whole Europe with a spatial resolution of 0.016° × 0.016°. This weather service is based on the spatial downscaling of data from international networks (NOAA-GSOD, METAR, and SYNOP) conducted by integrating data from regional networks of agrometeorological stations and by using dedicated geo-statistical and modelling techniques also accounting for the effect of elevation (USGS Gtopo30). Reference evapotranspiration was estimated at runtime based on the Penman-Monteith method (Allen et al. 1998).

Simulations were conducted by considering crop growth and development only limited by water availability (rainfed grasslands), whereas non-limiting nitrogen supply was assumed because the experimental sites were fertilized and the presence of legumes ensures benefits from symbiotic N fixation.

Data from the first day of sampling were used for initializing the community LAI, AGB and floristic composition. For the latter, only species with a mean relative abundance higher than 2% over the three sampling events were considered (Piseddu et al., 2019). Concerning soil moisture, volumetric field capacity was assumed because of snow melting and abundant rainfall events during the early spring. Root depth were initialized to 150 cm. Concerning simulation of management, the observed mowing schedule was used.

Model evaluation was conducted by using different indices of agreement: coefficient of determination (R^2, from 0 to 1 [optimum]; Addiscott and Whitmore, 1987), slope of the regression line, relative root mean square error

(RRMSE, from 0 [optimum] to +∞; Jørgensen et al., 1986), mean absolute error (MAE, from 0 [optimum] to +∞; Jørgensen et al., 1986), and modelling efficiency (EF, from -∞ to 1 [optimum]; Nash and Sutcliffe, 1970).

3.3.3. Evaluation of climate change impacts on grasslands productivity

Future climate projections for two representative concentration pathways (RCPs, RCP4.5 and RCP8.5; IPCC 2013) as provided by two general circulation models (GCMs), HadGEM2 (Collins et al., 2011) and GISS-ES (Schmidt et al., 2006), were used to assess the impact of global warming on grasslands productivity. The use of multiple RCPs×GCMs combinations allow to handle the uncertainty in future climate projections, by considering alternative pathways of CO_2 emission in the mid-term – RCP4.5 assumes the implementation of policies for curbing GHGs emission while RCP8.5 envisages business as usual storylines – as well as GCMs with a different equilibrium climate sensitivity that can lead to alternative climate projections for the same RCP. The uncertainty in the downscaling process was accounted for by using two stochastic weather generators (WGs), LARS-WG (Semenov and Barrow, 1997) and CLIMAK (Danuso, 2002). Historical weather series for the baseline (1986 – 2005, IPCC 2013) were retrieved from the ECMWF database (Hennessy, 1986). For each of the eight climate scenarios (2 RCPs × 2 GCMs × 2 WGs), twenty-year series centred on 2040 were generated at each site. For each site and weather file, 16 independent simulations were executed simulating a sowing each 1st of October and a 5 year of field duration.

Regarding management, three main mowing events were considered (1st of June, 20th of July and 1st of October), as representative of early, medium, and late mowing periods.

The impact of climate variations on grassland productivity was evaluated by comparing the model outputs (20-year mean) obtained for the baseline and the future climate projections. Seven synthetic output variables describing the length of the growing season, the forage production, its composition and quality were analysed: the total aboveground biomass harvested yearly (AGB_{year}, t ha^{-1}) and its distributions on different mowing events (AGB_j, t ha^{-1}, aboveground biomass harvested on the j-th mowing event), the vegetative restart day and the dormancy day (day of the year in which the plant community begins and stops, respectively, to accumulate AGB), the relative abundance of plant species (p_i, from 0 to 1, i representing the ith species in

the community), the Simpson-based diversity index ($D = 1/\lambda$, the larger the value of *D*, the highest the diversity, with λ calculated according to Eq. 1; Simpson, 1949; Jost, 2006), and the forage crude protein (CP, %, estimated according to Eq. 2; Argenti et al., 2021).

$$\lambda = \sum_{i=1}^{n}(p_i)^2 \quad (1)$$

where λ is the Simpson concentration index; n is the number of herbaceous species coexisting in the grassland; i is the *i*th herbaceous species. As in the parameterization, only species with a relative abundance higher than 2% were considered.

$$CP = 4.9085 \cdot \ln(x) + 0.8017 \quad (2)$$

where CP is the crude protein content (%) in the aboveground biomass estimated as a function of the relative abundance of legumes in the grassland (x, %). To account for the dynamics of legume presence during the season affecting forage CP on different mowing events, x was derived according to Eq. 3:

$$x = \frac{\sum_{j=1}^{m} p_{lj} \cdot AGB_j}{AGB_{year}} \quad (3)$$

where m is the number of mowing events (in this study three); j is the *j*-th mowing event; p_{lj} is the relative abundance of legumes (*Medicago sativa L.* and *Trifolium* spp.), and AGB_j is the aboveground biomass harvested at each cut.

Since the analysis concerned temporary alfalfa-dominated grasslands (in most case sown in purity and then allowed to evolve with the settlement of wild grass species), the starting value of the relative abundance of *Medicago sativa L.* was set to 100% on 1st of October and that of the other relevant species initialized to 0. The simulated field duration was equal to 5 years, which is the observed optimal duration of temporary alfalfa meadows in the study area (Argenti at al., 2021). Soil moisture was initialized to field capacity.

Plant dormancy was simulated according to the approach proposed by Confalonieri and Bechini (2004). The entire plant community is considered dormant after seven consecutive days with mean air temperature below a given threshold (8°C, calibrated by Movedi et al, 2019, in a similar context)

and night length longer than 13h. In spring, plant community restarts growing when night lasts less the 13h and mean air temperature is higher than the dormancy threshold for more than seven consecutive days. In case other factors interfere with plant growth (e.g., water stress), the vegetative restart day is postponed until conditions become favourable again.

3.3.4. Definition of adaptation strategies based on management practices

Four possible adaptation strategies were tested, by considering only those highly feasible under operational farm contexts: i) modifying the mowing schedule, by testing all the possible combinations of 5, 10, and 15 days variation (bring the date forward or delay it) for each of the three mowing events and by adding a fourth cut, ii) change the initial mixture of sown species (60% *Medicago sativa L.*, 20% *Dactylis glomerata L.* and 20% *Lolium multiflorum L.*; 100% alfalfa; 70% *Medicago sativa L.*, 15% *Dactylis glomerata L.* and 15% *Lolium multiflorum L.,* named Mix1, Mix2, and Mix3 hereafter), iii) testing different alfalfa field durations among those currently in use in many farms (4 years and 5 years) and iv) all the possible combinations of the aforementioned strategies.

Since the objective of the study was to support forage production in milk dairy farms in the long term, the alternative adaptation strategies were evaluated in terms of forage quality (crude protein) and biomass production under future climate scenarios and in each of the five sites considered.

3.4. Results

3.4.1. Model evaluation

Results highlighted a good agreement between observed and simulated values for all the variables analysed (Table 2). Concerning the dynamics at the level of plant community, the model correctly reproduced the grassland floristic composition, with a MAE lower than 10% and both EF and R^2 equal to 0.87. Although the RRMSE was slightly higher than 50%, the very good performance obtained for the Simpson index underlines how the error mainly affects non-dominant species with a very low presence in the phytocenosis. This is clear in Figure 1, where the model capability of reproducing the floristic composition is evaluated by comparing observed and simulated relative abundance of single species. Values of relative abundance higher than

20% are indeed well simulated, being most of them close to the 1:1 line that indicates perfect agreement.

Table 2: *Model performance. Error metrics forvariables describing grasslands floristic composition and growth.*

Variable	Units	MAE[a]	RRMSE (%)	EF	R^2	Slope	*p*-value
Floristic composition	(%)	6.04	55.84	0.87	0.87	0.99	<0.001
Simpson Index	(-)	0.38	22.03	0.78	0.79	1.03	<0.001
AGB_{cut}[b]	(t ha^{-1})	0.83	41.39	0.00	0.57	0.53	0.01
AGB_{year}[c]	(t ha^{-1})	0.96	23.09	0.57	0.76	1.23	0.05
LAI	(m^2 m^{-2})	0.94	34.84	-0.70	0.61	0.46	0.01

[a] Mean absolute error: same units of the variable.

[b] Aboveground biomass harvested at each cut.

[c] Total aboveground biomass harvested during the year.

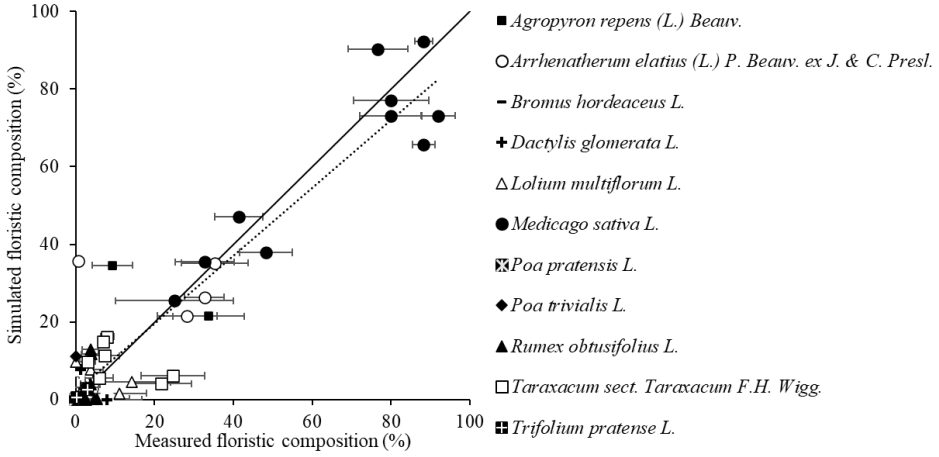

Figure 1: *Comparison between observed and simulated relative abundance (%) for the species detected in the five sites. Only species with a relative abundance higher than 2% were considered.*

The simulation of grassland growth was successfully captured, both in terms of AGB accumulation during the year and of AGB harvested at each cut.

MAE was less than one t ha^{-1} in both cases, EF was always positive and the average R^2 was equal to 0.67 (Table 2). Similar considerations apply to the model performance for leaf area index, although in this case the modelling efficiency was negative. However, this is due to the fact that the variability in observations was very low (standard deviation was equal to 0.95), which makes the mean of observations a very good estimator of single values. This, in turn, led to negative EF values even for small error in the simulations (e.g., MAE lower than 1 m^2 m^{-2}).

Parameterizations obtained for both CropSyst and CoSMo are available in appendix B and appendix C, respectively.

3.4.2. Climate change impact on forage production and quality

A clear increase in mean temperature was projected under all GCMs × RCPs combinations, regardless of the weather generator used (Fig. 2). The HadGEM2 projection showed the highest temperature increase, close to +2.1 °C for RCP 4.5 and to +2.4 °C for RCP8.5. The GISS realizations were milder for both RCPs, with values ranging from 1.0 °C to 1.2 °C. The variability due to the weather generator was clear in terms of rainfall patterns, with more evenly distributed precipitation in case of CLIMAK (Fig. 2c) and larger heterogeneity between months in case of LARS-WG (Fig. 2d).

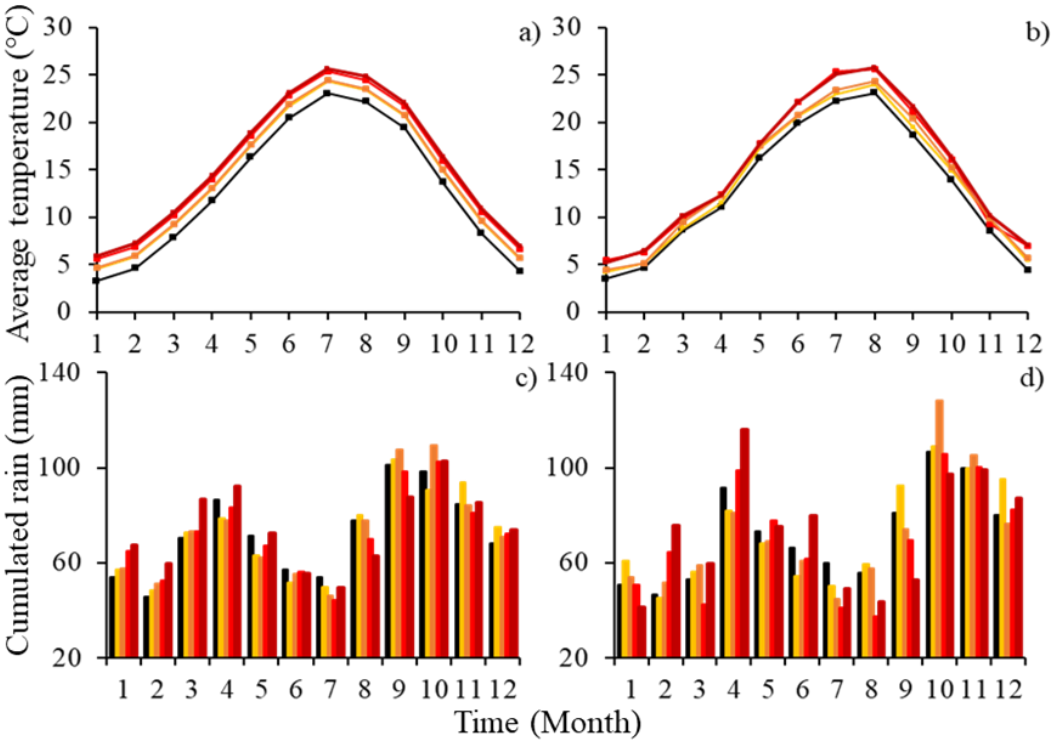

Figure 2: *Monthly average air temperature and cumulated rainfall for the baseline (black) and each GCMs × RCPs combinations (yellow: RCP4.5-GISS, orange RCP8.5-GISS, red: RCP4.5-HadGEM2, dark red: RCP8.5-HadGEM2) as downscaled with the stochastic weather generator CLMAK (a, c) and LARS-WG (b, d).*

The increase in mean temperature reflected on grassland dormancy patterns (Figure 3), with an extension of the period of active growth (+22 days on average) due to both an earlier vegetative restart day (Fig. 3, left panels) and a delay in the beginning of dormancy in winter (Fig 3, right panels). A clear variability was found among climate scenarios, with the highest impact observed for the HadGEM2 projections and the high-emissions storyline described by the RCP 8.5. On average, the vegetative restart day occurred 10 days earlier than the baseline (Fig. 3a), with values ranging from 4 days to 13 days for, respectively, the mildest (RCP4.5-GISS) and the warmest scenario (RCP8.5-HadGEM2). A similar pattern was found for the dormancy day, with an average delay equal to 12 days and values ranging between those observed for the RCP4.5-GISS scenario (9 days) and the RCP8.5-HadGEM2 (16 days). Results highlighted a marked inter-season variability (size of the boxplots in Fig. 3), whereas no clear differences among sites were observed (mean variability due to the site was less than 2%). These patterns were not affected by the weather generator used (variability in mean values due to this factor were less than 5%), which instead mainly affected the inter-season heterogeneity but without a clear pattern (Fig. 3).

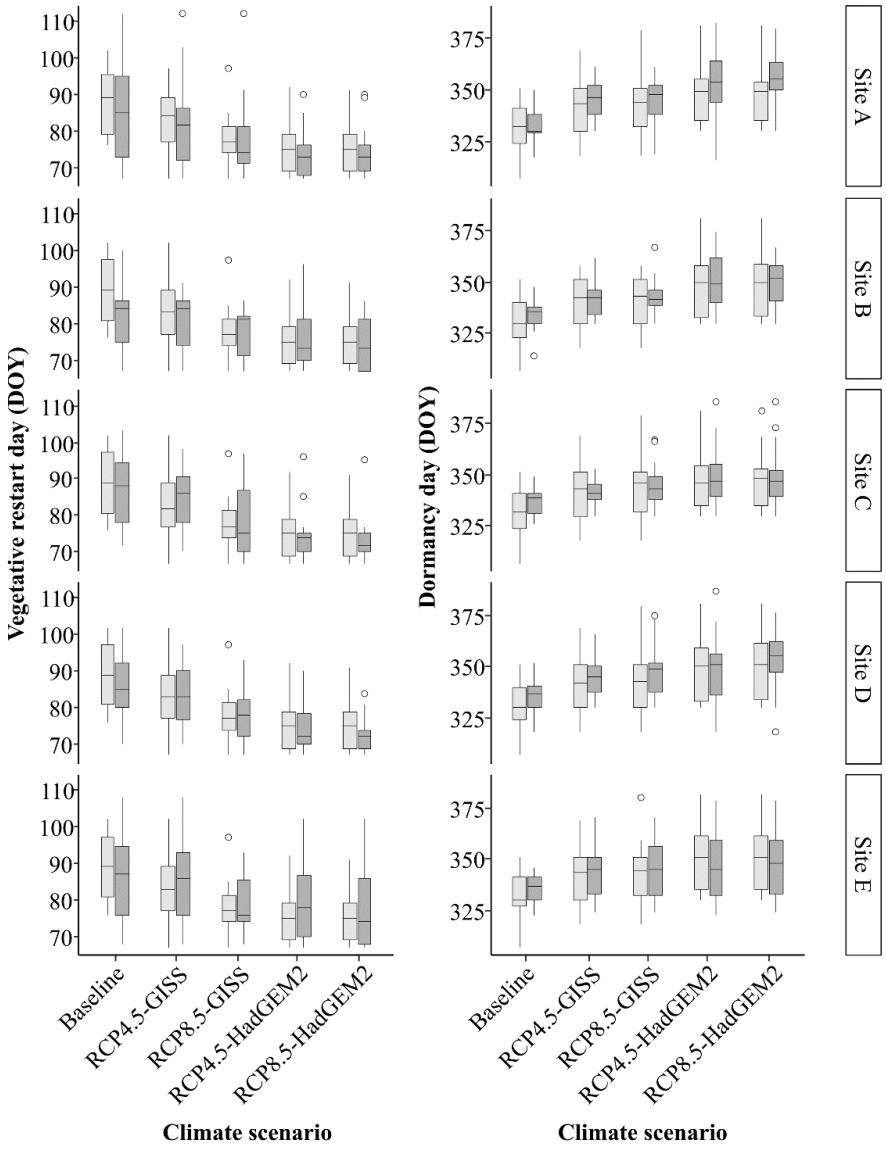

Figure 3: *Effect of climate change on the vegetative restart day (left panels) and the dormancy day (right panels) for each site and climate scenario (RCP × GCM combination) as downscaled by the two weather generators, CLIMAK (light grey) and LARS-WG (dark grey). The baseline is reported for sake of comparison. Results are shown on yearly basis as day of the year (DOY), calculated on a two-year period for dormancy day.*

Concerning the impact of climate change on grassland growth, the increase in mean temperatures was not beneficial for total biomass accumulation (Fig. 4a), which showed an average reduction of 5.7% under future scenarios as compared to the baseline. The extent of the negative impact markedly varied across climate scenarios, ranging from -3.6% (RCP4.5-GISS) to -7.4 % (RCP4.5-HadGEM). However, the decrease in biomass accumulation was not evenly distributed over mowing events. The earlier vegetative restart day (Fig.3) turned indeed into more biomass harvested at the first cut (Fig. 4b) with an average increase of +17.7% (mean of all the climate scenarios). On the contrary, biomass available at the second and third cut (Fig. 4c and Fig. 4d, respectively) under future climate projections was markedly lower than the baseline, likely due to higher temperatures and less precipitations during the summer months projected for 2040 (Fig.1). The average reduction for all the climate scenarios was equal to -29.4% and to – -31% for, respectively, the second and the third cut. Small variability related with the site was found, whereas differences due to the weather generator clearly affected grassland growth, although to a limited extent as compared to the climate scenario.

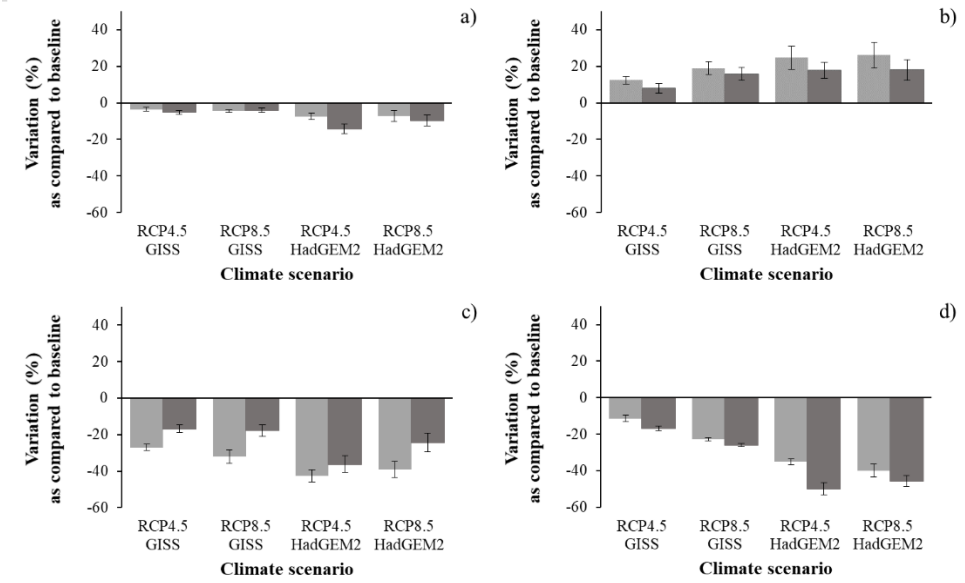

Figure 4: *Effect of climate change on grasslands growth. Percentage variation as compared to the baseline of the aboveground biomass accumulated during the entire season (a) and that harvested during the first (b), second (c), and third (d) cut. Results are reported for each climate scenario (RCP × GCM combination) as downscaled by the two weather generator, CLIMAK (light bars) and LARS-WG (dark bars). Error bars represent the variability (standard deviation) among sites.*

The analysis of plant community dynamics as response to the climate conditions highlighted a clear reduction of the grassland biodiversity, with a general decrease in Simpson index (-11.7%; Fig. 5a). As expected, alfalfa increased its relative presence (+6.8% as average of all scenarios; Fig. 5b), thanks to its macro-thermal features and its deep root system that prevented drought stress during summer months. Microthermal species (mainly grasses as *Dactylis glomerata* L.; *Poa pratensis* L. and *Lolium multiflorum* Lam.) were instead negatively affected (-8.2% on average, Fig. 5c), although a marked variability induced by the weather generator was found (average of all climate scenario equal to -12% for CLIMAK, and –4.4% for LARS-WG). Despite the increase in the relative presence of alfalfa, the overall forage protein content only slightly improved (+ 1.5% on average across scenarios, Fig. 5d). This is due to the combined effect of (i) the concentration of alfalfa growth in summer because of thermal reasons and (ii) the general reduction

of biomass harvested at the second and third cuts. This turned into less alfalfa biomass harvested yearly that counterbalanced the increase in alfalfa relative abundance in terms of overall forage quality. This highlights the relevance of dynamically simulating the plant community composition and growth to properly evaluate the effect of changing climates on forage quality.

The heterogeneity among sites in terms of floristic composition was higher than observed for other variables (e.g., biomass accumulation, Fig. 4). This is in line with the variability in plant communities characterizing the five sites, which turns into different dynamics of relative abundance according to the species-specific response to temperatures and water availability.

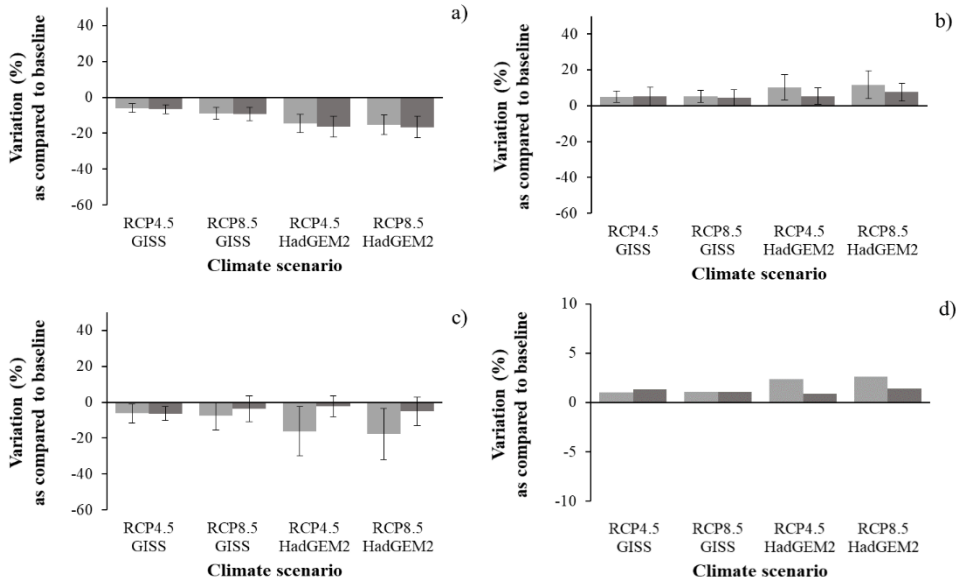

Figure 5: *Effect of climate change on grassland floristic composition and forage quality for each RCP × GCM combination as downscaled by two weather generators, CLIMAK (light grey) and LARS-WG (dark grey). Results are reported as percentage variation as compared to the baseline of the Simpson index (a), the relative abundance of alfalfa (b), the relative abundance of microthermal species (c), and the forage crude protein (d). Error bars represent the variability (standard deviation) among sites.*

3.4.3. Testing of management adaptation strategy

Of all the adaptation strategies tested (35 combinations of mowing schedule × initial mixture of sown species × and field duration), only those providing the best results in terms of total aboveground biomass accumulation (AGB, t ha^{-1}) and forage quality (crude protein concentration, CP, %) are here reported and discussed (Table 3).

Given the negative correlation between biomass accumulation and forage protein content, in general it was not possible to define a unique strategy able to optimize both factors simultaneously. Nevertheless, results were always better than those achievable with a standard management (also reported in Table 3 for sake of comparison), thus supporting the adoption of the strategies defined.

In all the climate conditions analysed, sowing pure alfalfa at the beginning of the temporary grasslands and varying the mowing schedule (moving the first cut earlier, and delaying the second and third cuts) allowed to increase the forage crude protein under future climates to an extent more than double that achievable with standard management (average for all scenarios equal to +2% CP as compared to baseline with adaptation, +0.9% with standard practices). Moreover, optimizing CP did not negatively affect the other variables, with a stable reduction of both AGB and Simpson index (average of all scenarios equal to, respectively, -6.3% and -12.1% with CP adaptation, -7% and -12.5% with standard management). As expected, a clear correlation between forage CP and relative abundance of alfa-alfa was found (Pearson's r of 0.99), given the primary role of *Medicago sativa* L. among the legume species detected in the five sites. For the same reason, the CP was negatively correlated with the Simpson index (Pearson's r of -0.91), since the increase in alfalfa presence turns into a reduction of species biodiversity.

Adaptation strategies aiming at minimizing the negative effects of climate change on forage production (total biomass) were mainly based on sowing a mixture that includes grass species (*Dactylis glomerata* L. and *Lolium multiflorum* L.) and delaying the last cut (Table 3).

Table 3: *Adaptation strategies to preserve forage production and quality under future climate projections. Percentage variation as compared to the baseline for total aboveground biomass (AGB_{year}, t ha^{-1}), crude protein (CP, %), Simpson index (-), and relative abundance of alfalfa (%) is reported for both the standard management and the best adaptation strategies identified for each climate scenario (RCP × GCM combination) and weather generator (WG) used. Values are averaged over the five sites.*

			Adaptation strategy			Variation (%) as compared to baseline			
WG	**Climate scenario**	**Target**	**Crop duration (years)**	**Change in mowing schedule (days)[b]**	**Sown species[a]**	**CP**	**AGB_{year}**	**Simpson index**	**Alfalfa relative abundance**
CLIMAK	RCP4.5 GISS	-[c]	-	-	-	0.71	-3.55	-5.83	4.76
		AGB	4	0/0/+10	Mix1	-9.04	1.41	18.46	-27.70
		CP	4	-5/+5/+10	Mix2	1.97	-3.13	-5.86	11.08
	RCP8.5 GISS	-	-	-	-	0.71	-4.54	-9.02	5.05
		AGB	4	0/0/+10	Mix1	-8.09	-0.08	14.76	-24.72
		CP	4	-5/+5/+10	Mix2	1.89	-3.75	-8.78	10.99
	RCP4.5 HadGEM2	-	-	-	-	1.72	-7.44	-15.52	9.98
		AGB	4	0/0/+10	Mix1	-5.65	-4.40	7.14	-16.46
		CP	4	-5/+5/+10	Mix2	2.48	-6.87	-14.95	14.10
	RCP8.5 HadGEM2	-	-	-	-	2.00	-7.16	-16.72	11.30
		AGB	4	0/0/+10	Mix1	-5.73	-4.97	6.03	-16.71
		CP	4	-5/+5/+10	Mix2	2.65	-6.92	-15.92	14.91
LARS-WG	RCP4.5 GISS	-	-	-	-	0.63	-5.18	-6.70	5.29
		AGB	4	-5/+5/+10	Mix1	-9.81	-0.11	15.28	-28.01
		CP	4	-5/+5/+10	Mix2	1.87	-3.90	-6.28	11.55
	RCP8.5 GISS	-	-	-	-	0.26	-4.04	-9.03	4.31
		AGB	4	-5/+5/+10	Mix3	-9.71	0.61	11.77	-27.43
		CP	4	-5/+5/+10	Mix2	1.42	-3.00	-8.44	10.06
	RCP4.5 HadGEM2	-	-	-	-	0.24	-14.23	-18.78	5.36
		AGB	4	0/0/+10	Mix1	-9.02	-11.37	4.76	-25.28
		CP	4	-5/+5/+10	Mix2	1.58	-13.85	-18.18	12.10
	RCP8.5 HadGEM2	-	-	-	-	0.70	-9.70	-18.74	7.47
		AGB	4	-5/+5/+10	Mix1	-6.78	-7.03	1.63	-17.54
		CP	4	-5/+5/+10	Mix2	2.02	-8.71	-18.51	14.22

[a]: Mix1: 60% *Medicago sativa* L., 20% *Dactylis glomerata* L. and 20% *Lolium multiflorum* L.; Mix2: 100% alfalfa; Mix3: 70% *Medicago sativa* L., 15% *Dactylis glomerata* L., and 15% *Lolium multiflorum* L.

[b]: slash-separated values refer to variation in the day of first, second and third cut, respectively, as compared to the current schedule.

[c]: standard management practices (no adaptation), see materials and methods for details.

This allowed to reduce the AGB decline under future climates of more than a half (-3.2% with adaptation and -7% without adaptation, on average for all scenarios), while even reversing the decline of Simpson index thanks to the introduction of multi-species sowing mixture. The average variation of Simpson index was indeed equal to -12.5% without adaptation, and to +10% with the adaptation strategies defined.

For both CP and AGB optimization, the best crop duration was slightly lower than the current one (4 years instead of 5), although the general effect of this management practice was limited as compared to a change on mowing schedule and in sowing mixture.

3.5. Discussion

3.5.1. Model performance

The model error in estimating floristic composition and AGB was similar to that observed in other studies, both those where the same model was used (Movedi et al., 2019) and studies based on different modelling approaches (Soussana et al., 2012). Also, the model error for the relative abundance of species (MAE < 10%) was comparable with the error found in the observations themselves (average standard deviation of observation: was equal to 5.2%, with maximum value of 27.8%), due to the high uncertainty in eye estimation of percentage presence of the two species and their relative biomass in the field. The poor agreement between simulated and observed values for the dynamics of *Agropyron repens (L.) Beauv.* and *Arrhenatherum elatius (L.) P. Beauv. ex J. & C. Presl.* were explained by the large similarity in the two species, in particular during the vegetative phase (when reproductive organs are not present), which turned into the highest standard deviation of eye-detected relative abundance (27.8%).

Concerning leaf area index, the negative modelling efficiency can be due to both the elevated uncertainty in the observations and in the simulation process, as observed by other authors (e.g., Yu et al., 2006; Tartarini et al., 2019), although the other metrics were satisfactory (MAE<1).

3.5.2. Climate change impacts and adaptation strategies

The negative impact of climate change on grassland forage production found in this study is in agreement with the meta-analysis conducted by Dellar et al.

(2018), who found a general reduction of pasture yield in terms of aboveground dry biomass as results of reduced rainfall amounts and increased temperatures. In this study the largest reduction in biomass production was observed in the summer cuts (the second and the third mowing events). This reduction was due to the increase in temperatures and the limited water availability that characterized the summer months, in particular July (when the second and the third mown are growing) which led to a clear reduction in photosynthetic efficiency. This turns into an increase of alfalfa relative abundance under future climates because this species is more resistant to high temperature and water stress as compared to the other species (Huang et al., 2018; Tang et al., 2014). The increase in the relative abundance of alfalfa had positive effects on the quality of forage (higher crude protein content; Argenti et al., 2021) but also a negative trade-off on the Simpson index, due to less diversified plant communities, and on the potential soil capability to withstand erosion, because species with tap roots are less effective in reducing the soil detachment as compared to fibrous roots (Wang and Zhang, 2017; Mackie et al., 2018).

The adaptation strategies tested in this study were defined by considering (i) the dynamics of grassland growth projected in the study area (e.g., the decline in AGB production during summer led to bringing the first cut forward and delaying the second and third cut), and (ii) the practices currently adopted by the farmers in the area, to ensure the suitability of the strategies to operational contexts. Despite the large availability of modelling studies aiming at alleviate the negative effects of climate change through crop management – e.g., by optimizing the cultivar (Zabel et al., 2021) or the crop choice (Cappelli et al., 2015), the sowing window (Zhang et al., 2012) or the irrigation techniques used (Wang et al., 2021) – studies targeting the optimization of grassland management are still scarce. The potential of crop management to counterbalance the negative impacts of climate variation on yield and food security at global scale is huge (Franke et al., 2022). Extending this approach to managed grasslands can be crucial to support their role as providers of key ecosystem services, especially in marginal areas.

3.6. Conclusions

The community model CoSMo allowed to evaluate the dynamics of growth and floristic composition of temporary alfalfa-dominated grassland as response to changes in climate projected in the northern Apennine in the mid-term. This allowed to estimate grassland-related ecosystem services (forage

production and quality, preserving biodiversity) and to suggest adaptation strategies to preserve them in the mid-term. Results highlighted a clear decline in forage production and an increase in alfalfa dominancy, due to the higher suitability of this species to warm and dry conditions. Given the key role of grasslands for forage production in the local dairy farms, adaptation strategies were evaluated by prioritizing the suitability of the proposed solutions in real farm contexts. Guidelines for optimizing grassland productivity and forage quality under future climates can be summarised in three key points: reduce the alfalfa field duration, sown mixtures including microthermal grass species and delay the third cut. These are practices that can be easily adopted and tested by farmers, to support the adaptation of agricultural systems to a changing climate.

Acknowledgements

This work was carried out thanks to the support of the project MODIPRAS (Modelling relationships between species diversity, the functioning of grassland systems and their ability to deliver ecosystem services) of the INRA metaprogramme ECOSERV (Ecosystem services). It received financial support from Emilia-Romagna Region (FEASR PSR, FOCUS AREA 3A, Operazione 16.2.01) and AGER Agroalimentare e Ricerca (IPCC MOUPA).

Appendix A. Mowing and sampling events.

Site	A	B	C	D	E
Sampling 1	5/30/2019	5/30/2019	5/30/2019	5/31/2019	5/31/2019
Mowing 1	6/15/2019	6/15/2019	6/4/2019	6/6/2019	6/15/2019
Sampling 2	7/16/2019	7/16/2019	7/15/2019	7/15/2019	7/15/2019
Mowing 2	8/1/2019	7/20/2019	7/20/2019	7/20/2019	8/1/2019
Sampling 3	8/29/2019	8/28/2019	8/28/2019	8/28/2019	8/28/2019
Mowing 3*	-	9/14/2019	-	9/2/2019	9/2/2019

* not available for site A and site C.

Appendix B. CropSyst parameters for different species (A: Agropyron repens (L.) Beauv., A1; Arrhenatherum elatius (L.), P. Beauv. ex J. & C. Presl., B: Bromus hordeaceus L., D: Dactylis glomerata L., L: Lolium multiflorum L., M: Medicago sativa L., P: Poa pratensis L., P1: Poa trivialis L., R: Rumex obtusifolius L., T: Taraxacum sect. Taraxacum F.H. Wigg., T1: Trifolium pratense L.)

Parameters	Species											Units	Description
	A	A1	B	D	L	M	P	P1	R	T	T1		
BT	4	2	2	3	2	5	2	5	6	5	5	°C	Minimum temperature to development
OT	38	33	25	28	34	38	27	25	30	33	29	°C	Optimal temperture to development
k	0.35	0.35	0.4	0.45	0.4	0.5	0.5	0.45	0.5	0.9	0.5	-	Ligth extintion coefficint
CF	0.95	0.95	0.95	0.95	0.8	1	0.95	0.9	1	0.9	0.95	-	Full canopy coefficient
MWU	8	8	8	8	8	7	8	8	8	9	8	$mm\ d^{-1}$	Maximum water uptake
LAIini	0.09	0.09	0.09	0.09	0.09	0.09	0.09	0.09	0.09	0.09	0.09	$m^2\ m^{-2}$	Initial LAI
Leaflive	600	550	500	500	1500	400	1000	400	900	800	500	°C-d	Gdd to end single leaf
NTC	18	15	18	18	18	18	18	15	25	18	18	°C	Minimum nigth temperature to translocation
NTM	24	24	24	24	24	25	24	24	30	24	24	°C	Maximum nigth temperature to translocation
RUE	2.5	2.5	2.7	2.7	3	3.3	2.7	2.2	3	2.9	4	$g\ MJ^{-1}$	Rariation use efficiency
SLA	20	20	27	23	26	28	20	26	30	30	30	$m^2\ kg^{-1}$	Specific leaf area
STP	4.5	2.5	3	4.5	1.2	3.5	1.5	3	2	0.2	1.5	-	Steam/leaf coefficient
GDDf	1000	1400	650	650	600	800	1200	1200	900	1200	800	°C-d	Gdd to flowering
TBC	4	4.5	4	4	4	4	4	5	4	4	4	$kg\ m^{-2}\ kPa\ m^{-1}$	Traspiration coefficent to biomass

Appendix C. CoSMo parameters for different species (A: Agropyron repens (L.) Beauv., A1; Arrhenatherum elatius (L.) P. Beauv. ex J. & C. Presl., B: Bromus hordeaceus L., D: Dactylis glomerata L., L: Lolium multiflorum L., M: Medicago sativa L., P: Poa pratensis L., P1: Poa trivialis L., R: Rumex obtusifolius L., T: Taraxacum sect. Taraxacum F.H. Wigg., T1: Trifolium pratense L.)

Parameters	Species											Units	Description
	A	A1	B	D	L	M	P	P1	R	T	T1		
WCC	1	0.2	0.4	0.7	0.4	0.88	0.8	0.4	0.8	0.75	0.65	-	Drought tolerance: 1 tollerant, 0 sensible
RT	0	0	0	0	0	1	0	0	1	1	1	-	Root type 1 tap root; 0 fibrous root
MinT	4	2	2	3	6	5	2	5	6	5	5	°C	Minim temperature to competition
MaxT	38	33	25	28	30	38	27	24	30	33	29	°C	Maximum temperature to competion
GDDres	0	0	100	0	0	0	0	0	0	0	0	°C-d	Growing degree days to emergence after resowing
GDDdie	-	-	2000	-	-	-	-	-	-	-	-	°C-d	Growing degree day to die
LAImax	5	4	4	7.5	6.5	5	5	4	3.5	5	4	m^2 m^{-2}	Maximum LAI
MaxH	1.2	1.6	1.3	1.5	1	1	0.8	0.9	0.7	0.35	0.8	m	Maximum plant height
OptT	22	16	13	14	15	25	15	11	16	19	16	°C	Optimal temperature
MaxRD	160	140	120	140	100	180	80	40	140	100	160	cm	Maximum rooting dept
Common													
I	80											-	Inertia coefficient of species replacement
WFMin	0.15											m^3 m^{-3}	Minimum water available for fibrous roots growth
WFMax	0.5											m^3 m^{-3}	Maximum water available for fibrous roots growth
WTMin	0.1											m^3 m^{-3}	Minimum water available for

				tap roots growth
WTMax	0.4		$m^3 m^{-3}$	Maximum water available for tap roots growth
DWT	8		°C	Average air temperature to reach after winter to restart to growth

4. Assessment of climate change impacts on alpine pastures productivity and floristic composition

Ermes Movedi, Stefano Bocchi, Livia Paleari, Fosco M. Vesely, Ilda Vagge, Roberto Confalonieri

Submitted: 1 March 2022; Actual state: under reviewing

Journal: Climate Change

4.1 Abstract

Climate change impact on pasture floristic composition needs to be carefully assessed, given its key role for the resilience of pastoral systems and related ecosystem services. Nevertheless, variations in floristic composition are rarely taken into account in climate change impact studies. Here, we used the plant community model CoSMo to simulate future dynamics of biomass accumulation and floristic composition for high-altitude alpine pastures. Dedicated multi-site field activities were conducted to collect data for model calibration. Simulations were run for four 20-year climate scenarios centred on 2040, resulting from the combination of two general circulation models (GISS-ES and HadGEM2) and two representative concentration pathways (RCP4.5 and RCP8.5). Results highlighted the capability of CoSMo to successfully reproduce the productivity and floristic composition of grazed pastures, modeling efficiency and R2 being higher than 0.90 for aboveground biomass accumulation and relative abundance of species. CoSMo simulated an overall positive effect of increasing temperatures on pasture productivity (+10.7% on average), due to higher biomass accumulation rates and longer growing seasons. However, these benefits were highly heterogeneous among the monitored pastures (ranging from -2.5% to +16.2%), because of differences in floristic composition and in species-specific thermal response that led to complex, non-linear reactions to climate variations. A negative impact of climate change was simulated for grazing value (-11.1% on average), due to the higher suitability to future conditions of species with low

palatability. Our results highlight that floristic composition must be explicitly considered while assessing climate change impacts on pasture productivity and connected ecosystem services.

Keywords:

Biodiversity; CoSMo; ecosystem services; grassland; grazing value; plant community.

4.2. Introduction

Grasslands are among the major ecosystems worldwide, covering more than 40% of the terrestrial area (Suttie et al. 2005). Along with their relevance for wildlife habitat and biodiversity reservoir (Marriott et al. 2004), one of the primary role played by grasslands is forage production for livestock feeding (Suttie et al. 2005). Given that pastures often cover areas unsuitable for conventional agriculture, the resulting livestock grazing system represents a key source of income in many areas worldwide (Godfray et al. 2010). Other benefits that grasslands provide deal with their role for carbon sequestration (Schulze et al. 2009, Cong et al. 2014), reduction of pollution and soil erosion, increase of pollination, and improvement of landscape value for tourism activities (Bellocchi et al. 2018). Grasslands thus play a pivotal role in the context of ecosystem services, which can be defined as all the material and not material benefits provided by an ecosystem that affect human activities in terms of economy, health, and quality of life (Tribot et al. 2018).

Grasslands are environments characterized by the coexistence of many different herbaceous plant species and, as such, by an elevated biodiversity (Habel at al. 2013). The floristic composition of grasslands is a key factor for the quality of the ecosystem services they provide (Oliver et al. 2015), because it can markedly affect forage quality (Daget and Poissonet 1971), as well as the resilience of the plant community to environmental constraints (Simpson 1949; Mackie et al. 2018). However, pasture floristic composition is highly variable in relation to multiple environmental factors like latitude, elevation, light intensity and quality, soil proprieties, availability of nutrients and water, and climate conditions (Buxton and Fales 1994; Jeangros et al. 1999). In the case of pasture, management also plays a key role, by defining water and nutrient availability (through irrigation and/or fertilization), the kind of grazing livestock, and the grazing intensity (Matches 1992; Ren et al. 2012). The different species of grazing animals are indeed known to have

clear preferences for some plant species, thus affecting pasture floristic composition through selective grazing (Daget and Poissonet 1971).

Ongoing and forecasted changes in climate are expected to influence the productivity and floristic composition of grasslands (Mooney and Hobbs 2010) and, in turn, the related ecosystem services (Oliver et al. 2015). However, whether this influence will be positive or negative is something still debated and likely heterogeneous across different contexts. Dellar et al. (2018) indicated a reduction of grasslands productivity as response to climate change in center and southern Europe and an opposite trend for the North of Europe. Dibari et al. (2020) estimated a general reduction of grassland suitability and a loss of biodiversity in the Alps in the coming decades, whereas Riedo et al. (2000) highlighted a positive trend in net biomass accumulation of managed grasslands at different altitudes in response to climate change. Nevertheless, most of these studies did not explicitly reproduce the climate-induced variations in grassland floristic composition, thus overlooking the effect of species-specific adaptation to climate change on the dynamics of plant competition and related pasture productivity and quality. A seminal work in this sense was conducted by Liu et al. (2018) who analyzed variations in plant community composition of alpine grasslands as response to climate variability, although the analysis was limited at the level of plant functional groups (grasses, forbs, and sedges).

Eco-physiological models are powerful tools for estimating climate change impact on cropping systems (Tubiello et al. 2007; Soussana et al. 2010) and for investigating the complex dynamics characterizing multi-species plant communities (e.g., Soussana et al. 2012; Sàndor et al. 2018). Among the models suitable for large-area applications, the CoSMo plant community model (Confalonieri, 2014) is one of the few approaches able to explicitly and dynamically simulate changes in the floristic composition of grasslands as a function of environmental and management drivers, thus allowing a comprehensive quantification of climate change impacts on pasture productivity and related ecosystem services.

The objective of this study was to assess climate change impacts on high-altitude alpine pastures productivity and floristic composition. This will allow to extend the analysis of climate change effects on pasture by accounting for aspects dealing with pasture quality and biodiversity.

4.3. Materials and methods

4.3.1. Experimental data

Field observations were carried out in 2019 at three pastures (site 1, 2, and 3, hereafter) at 2200 m above sea level on the Rhaetian Alps in the Sondrio province (site 1: 46.419° N, 10.200° E; site 2: 46.421° N, 10.198° E; site 3: 46.422° N, 10.198° E). The area is a wide moraine hollow of Val Dosdè characterised by important and typical forms left by morphogenetic agents of glacial, periglacial, fluvial and fluvioglacial origin. From a vegetational point of view, there are: acidophilous *Nardus stricta*-dominated grasslands (*Nardion strictae* Br.-Bl. in Br.-Bl. & Jenny 1926), which are being studied, silicicolous, alpine heaths dominated by nano-phanerophytes and lichens (*Loiseleurio procumbentis-Vaccinion microphylli* Br.-Bl. in Br.-Bl. & Jenny 1926), communities composed of oligotrophic to mesotrophic small sedges and bryophytes that grow in acid fens (*Caricion nigrae* Koch 1926 em. Klika 1934) and acidophilous, mesophilous and xerophilous shrub communities dominated by *Rhododendron ferrugineum* L. (*Rhododendro ferruginei-vaccinion myrtilli* A. Schnyd. 1930). These phytocoenoses form a complex mosaic reflecting the morphological and pedological micro-variations of the hollow. The phytosociological nomenclature follows the rules of the International Code of Phytosociological Nomenclature (Weber et al. 2000). For the definition of the syntaxa, the Prodrome of Italian Vegetation was followed (Biondi et al. 2014; see the specific interactive site of the Italian Botanical Society: http://www. prodromo-vegetazione-italia.org/), with reference to the Prodrome of European Vegetation (Mucina et al. 2016).

The nomenclature of the species follows Bartolucci et al. (2018).

For each site, aboveground biomass (AGB, t ha^{-1}) for the different species, canopy leaf area index (LAI, -) and height (H, cm), and floristic composition were estimated twice during the season (July 25th and August 29th). The sample size for AGB and floristic composition was 0.5 m^2, whereas LAI and canopy height were determined by using the AccuPAR ceptometer (Decagon, Pullman, WA, USA) and a ruler, respectively. All the measurements were replicated at three points randomly identified at the beginning of the season in each site. Information concerning the management of the pastures in terms of grazing period (from end of June to mid-September) and grazing pressure (around 1.4, 0.8, and 2.8 adult cattle ha^{-1} in site 1, 2, and 3, respectively) were also collected. For each site, soil texture was derived from the WISE database

(Batjes, 2016). Daily minimum and maximum temperature, net solar radiation and rainfall were retrieved from the weather service of the University of Milan Cassandra Lab, which provides historical, near real-time and forecasted daily weather data at 0.016° × 0.016° spatial resolution for the whole Europe. The service is based on the integration of data from regional networks of agrometeorological stations and dedicated geo-statistical and modelling techniques (accounting for the effect of elevation; USGS Gtopo30) to spatially downscale data from international networks (NOAA-GSOD, METAR, and SYNOP) (Mariani et al. 2012, 2016; Cola et al. 2020). Reference evapotranspiration was estimated at runtime based on the Penman-Monteith method (Allen et al. 1998).

4.3.2 The modelling approach

The grassland model CoSMo (Community Simulation Model; Confalonieri, 2014) was used to simulate the dynamics of the different species in the phytocoenosis, and it was coupled with the generic crop model CropSyst (Stöckle et al. 2003) for the simulation of the physiological processes involved with plant growth and development (Movedi et al. 2019).

CoSMo is a daily time step model that dynamically simulates changes in the composition of a phytocoenosis and – coupled with a generic crop model – its productivity. While CoSMo estimates the variations in the relative abundance of different species as a function of the species suitability to environmental and management drivers, the crop model daily reproduces soil and plant biophysical processes as a function of weather and soil properties and of the phytocoenosis composition. CoSMo represents an intermediate solution between complex individual-based models and simplified approaches relying on the calibration of a single set of parameters of a crop model to mimic the behaviour of a plant community, and it has proved to successfully reproduce the dynamics of grasslands composition and productivity (Movedi et al. 2019) and of crop-weed interaction (Movedi et al. 2022).

Basically, at each time step CoSMo estimates the suitability of each species in the community to the explored environmental and management conditions, and the overall suitability of each species is used to dynamically reproduce the changes in their relative abundance. The overall suitability is derived from factors defining the response of each species to drivers (Table 1) that may affect inter-specific competition. Drivers account for both continuous

variables (e.g., global solar radiation, soil water content) and events (e.g., cut, grazing). The overall suitability of each species is then calculated by aggregating the suitability factors – estimated for each driver – while accounting for a hierarchical weighting procedure, which allows to reduce the impact of drivers at the bottom of the hierarchy (Table 1).

The effect of grazing or cut events is top-ranked because their impact on the overall species suitability is so marked that the role of other drivers becomes negligible. Phenology is ranked second given that, for annual self-seeding species, once maturity is reached the species is considered not competing anymore until germination and emergence of the next generation of individuals. The hierarchy of the remaining drivers is consistent with other modelling approaches dealing with inter-specific competition (e.g., Kropff and van Laar, 1993). The overall suitability value for the different species is then used to derive the relative abundance of the different species at the following time step, which is in turn used to weight the species-specific parameter values of the crop model (derived for the species in monoculture) while deriving the parameter values of the crop model for the community as a whole. The resulting community parameter values – which dynamically change at each time step as the phytocoenosis evolves – allow the crop model to simulate key biophysical processes of the community at each time step. As a result, rate and state variables from the crop model (e.g., AGB, LAI) are available at the level of whole plant community, whereas the relative abundance of species – needed to update the crop model parameter values for the phytocoenosis at each time step – is provided by CoSMo.

The effect of grazing livestock is accounted for by CoSMo both directly – by estimating the amount of AGB daily grazed (Eq. 1) (Minson and McDonald, 1987) – and indirectly, because grazing affects the community LAI and thus light interception and photosynthesis. Grazing, also, affects the relative abundance of the different species, thanks to functions representing (i) the degree of the liking of different categories of animals for the different species ($f_{[liking]}$; Table 1), (ii) the species-specific capability to restart after a grazing event (SL; Table 1), and (iii) the effect of LAI and height on the species competitiveness for light ($f_{[rad]}$; Table 1).

(1)

$$AGB_g = \begin{cases} 0.108 \cdot AW^{0.719} & AGB \geq 0.108 \cdot AW^{0.719} + AGB_{min} \\ AGB - AGB_{min} & AGB_{min} < AGB < 0.108 \cdot AW^{0.719} + AGB_{min} \\ 0 & AGB \leq AGB_{min} \end{cases}$$

where AGB_g (kg ha^{-1} day^{-1}) is the daily grazed AGB, AW is the livestock live weight per unit surface (kg ha^{-1}), and AGB_{min} is the minimum AGB to allow grazing (set to 50 kg ha^{-1}). In this study, the value of AW was derived by assuming an average weight of an adult cattle of 800 kg and the site-specific animal pressure (adult cattle ha^{-1}) collected during the field activities. The same percentage reduction of community AGB due to grazing is applied to the community LAI and height.

For the description of the remaining CoSMo equations, readers may refer to Confalonieri (2014) and Movedi et al. (2019).

Concerning the crop model to be coupled with CoSMo, CropSyst (e.g., Stockle et al. 2003) was chosen because of its favorable relationship between parsimony (in terms of number of parameters) and reliability, as shown in previous studies dealing with mown grasslands (Movedi et al. 2019). CropSyst is a generic, daily time-step model that reproduces crop growth and development as a function of weather variables, physical and chemical soil properties, and crop management practices. Phenological development is simulated as a function of mean air daily temperature and of parameters defining minimum and optimum thermal requirements, with an option to account for photoperiod. Light interception is estimated from LAI and extinction coefficient for solar radiation according to the Beer's law analogy, and daily biomass accumulation (net photosynthesis) is derived as the minimum between the two values estimated using a temperature-limited radiation use efficiency approach and a vapor pressure deficit-corrected transpiration use efficiency one. Green leaf area expansion is calculated from AGB daily rate and state, the early stages specific leaf area and the empiric stem/leaf partition coefficient. Leaf senescence is simulated when daily-emitted LAI units reach a specific thermal time threshold. Concerning the simulation of soil water dynamics, a cascading model with travel time (Neitsch et al. 2002) was used, whereas hydrological soil proprieties were estimated by using the van Genuchten et al. (1985) pedotransfer functions.

Table 1: *Drivers affecting the competition capability of different species in the CoSMo model, with their category, hierarchical position, and associated suitability factor (from Confalonieri, 2014; Movedi et al. 2019).*

Driver	Category	Hierarchical position	Suitability factors
Grazing/cut	Event	1	$f_{[liking]}$ (liking of the grazing animals), SL (length of the shock period after the event)
Phenology (maturity reached)		2	M (is maturity reached?)
Air temperature	Continuous	3	$f_{[temp]}$
Global solar radiation		4	$f_{[rad]}$ (competition for light)
Soil water availability/excess		5	$f_{[water]}$ (competition in case of insufficient water availability or in case of water excess)
Nitrogen availability		6	$f_{[N]}$ (competition for soil N)

4.3.2.1. Model initialization and parameterization

Simulations were carried out by considering plant growth as limited by water – given the experimental sites were not irrigated – but not by nitrogen availability because of the continuous livestock presence. Concerning model initialization, the first observed values of floristic composition, AGB, LAI and plant height were used. The initial soil moisture was assumed to be at

field capacity, considering the autumn and spring rainfalls characterizing the area and the contribution of melting snow to soil moisture.

Model parameters (Table S1, Online Resource 1) were set to values from the literature for the same species, to values determined on the species in monoculture in experimental plots or – in case of unavailability of observations – to values from similar species or to values defined by calibration within the parameters biophysical range. The parametrization was carried out independently for the two models (Tables S2 and S3, Online Resource 1) and, for the calibrated parameters, the trial-and-error approach was used, by targeting the highest agreement between observed and simulated state variables. The parameterization was performed only for the species representing more than 0.75% of the sampled AGB (average of the two sampling events).

The agreement between observed and simulated floristic composition, AGB, LAI and plant height was quantified by using the relative root mean square error (RRMSE, from 0 to $+\infty$, optimum: 0; Jørgensen et al. 1986), the mean absolute error (MAE, from 0 to $+\infty$, optimum: 0), the modelling efficiency (EF, from $-\infty$ to 1, optimum: 1; Nash and Sutcliffe, 1970), the R^2 and the slope of the linear regression equation between observed and simulated values.

4.3.2.2. Evaluation of climate change impacts

The impact of projected changes in climate on each of the three sites was evaluated by running the model for two 20-year time frames, representing the baseline (1986-2005) and near future (centred on 2040) climate conditions. This allowed considering the effect of seasonality on yearly trends of weather variables. For each weather series, five additional years were considered to initialize the model (spin-up period) (Movedi et al. 2019). The uncertainty in future climate projections was handled by using the realizations of two representative concentration pathways (RCPs) – RCP 4.5 and RCP 8.5 (IPCC, 2013) – as provided by two general circulation models (GCMs) – HadGEM2 (Collins et al. 2011) and GISS-ES (Schmidt et al. 2006). The two RCPs were selected to explicitly consider a wide range of potential future climate evolution, given they represent an optimistic (RCP 4.5; moderate increase in CO_2 emissions in response to the adoption of mitigation strategies) and a pessimistic (RCP 8.5; no reduction in CO_2 emissions) scenarios. Spatial and temporal downscaling of GCM outputs was carried out using the stochastic weather generator LARS WG (Semenov and Barrow, 1997) and the historical

weather series (1986-2005) retrieved from the European Center for Medium Range Weather Forecasts database (ECMWF). LARS-WG was used given its proved reliability for climate change studies (e.g., Höglind et al. 2013; Vesely et al. 2019). Beside variations in temperature and rainfall, the projected increase in atmospheric CO_2 concentration for each climate scenario was provided to the model to account for the CO_2-fertilization effect on AGB accumulation.

The model outputs obtained for the four climate change scenarios (RCP4.5-HadGEM2, RCP4.5-GISS-ES, RCP8.5-HadGEM2, and RCP8.5-GISS-ES) were compared with those simulated for the baseline using the following synthetic variables: the 20-year mean cumulated AGB, including grazed AGB (AGB_{avg}, t ha^{-1}), the 20-year mean daily rate of AGB during the period of active growth (AGB_r, t ha^{-1} day^{-1}), the 20-year mean relative active growth duration (TAG, from 0 to 1; fraction of days in a year when the community AGB rate is not null), the 20-year mean relative abundance of plant species (p_i, from 0 to 1, i representing the ith species in the community), the Simpson-based diversity index ($D = 1/\lambda$, the larger the value of D, the highest the diversity, with λ calculated according to Eq. 2; Simpson, 1949; Jost, 2006), and the grazing value (GV, the larger, the better, indicating forage value and palatability; Eq. 3; Daget and Poissonet, 1971):

$$\lambda = \sum_{i=1}^{n}(p_i)^2 \quad (2)$$

$$GV = \sum_{i=0}^{n}(p_i \cdot GV_i) \quad (3)$$

where λ is the Simpson concentration index; n is the total number of herbaceous species that coexist in the pasture; i is the ith herbaceous species; GV_i is an empiric parameter to evaluate the single herbaceous species. In this study, the relative abundance daily estimated by CoSMo was used for each time frame (average of the 20-year simulation), and the values of GV_i reported by Daget and Poissonet (1971) were used (Tables S4, Online Resource 1).

4.4. Results

4.4.1. Floristic composition, growth dynamics and grazing value

The floristic composition and the relative abundance of species detected during the two sampling events are reported in Table 2, whereas Table 3 shows pasture productivity and quality by reporting AGB, LAI, plant height,

grazing value and Simpson diversity index. Overall, 88 herbaceous species were detected in the three sites, but only ten of them presented a relative abundance higher than 0.75% in at least one of the two sampling events (Table 2). Field observations highlighted a marked variability among the three monitored sites in terms of relative abundance of species (Table 2). The pasture in site 2 was a peat bog with prevalence of *Trichophorum cespitosum* (first part of the season) and *Eriophorum* sp.pl., whereas sites 1 and 3 were largely characterized by *Deschampsia cespitosa* and *Nardus stricta*, respectively. In site 3, the prevalence of *N. stricta* is explained by its low palatability and by the high grazing pressure that characterized the site. In site 1, the presence of *N. stricta* was relevant but the dominant species was *D. cespitosa* likely because the lower grazing pressure generated conditions less penalizing for this species as compared to site 3.

The relative abundance of the species changed to large extent over time, with an increased diversity in the second sampling event (Table 2) because of the presence of species not previously detected or whose relative abundance was negligible (e.g., *Carex nigra* and *Poa alpina* in site 3, *Eriophorum angustifolium* in site 2). These temporal dynamics in the community composition reflected in the Simpson diversity index, which increased from 1.33 to 2.03 (average of the three sites) while moving from the first to the second sampling event (Table 3).

The mean AGB observed in the three sites ranged from 1.07 t ha^{-1} in site 2 to 6.84 t ha^{-1} in site 1, with small variability between the two sampling events. The lower grazing pressure in site 1 as compared to site 3 clearly reflected in the sampled AGB, which was 83% higher in the first site (mean of the two sampling events). The difference between AGB values in these two sites increased over time, with the largest difference observed during the second event (114% higher in site 1). This is likely due to the continuous presence of the grazing livestock in site 3 starting from the end of June. The pasture in site 2 showed instead an overall low productivity, due to the peculiar edaphic conditions (peat bog soil) that favored the presence of species with a low potential in terms of AGB accumulation (*T. cespitosum* and *Eriophorum* sp.pl.).

To a certain extent, a similar pattern was found for LAI and height, with the largest and lowest values observed in site 1 and 2, respectively, although AGB was poorly correlated with both LAI ($R^2 = 0.51$; $p = 0.11$) and height ($R^2 = 0.57$; $p = 0.08$). The differences in the species relative abundance observed in

the two sampling events explain the different temporal dynamics observed for AGB and LAI. Indeed, despite LAI was always decidedly lower in the second sampling event, AGB was more stable in sites 2 and 3 and increased in site 1, likely because of a lower LAI to AGB ratio in *N. stricta* compared to *D. cespitosa* (Table 2).

The highest diversity was observed in site 2 at the second sampling event, because of the largest homogeneity in the relative presence of *T. cespitosum*, *E. angustifolium* and *E. vaginatum*, whereas the pasture in site 1 had the highest grazing value, regardless of the sampling time (Table 3).

Table 2: *Floristic composition and relative abundance (%) of the species detected in the three sites during the two sampling events. Only the species with more than 0.75% of the sampled AGB are reported and were used to calculate the relative abundance.*

Site	Species	25 July 2019	8 August 2019
1	*Deschampsia cespitosa* (L.) P. Beauv.	85.96	64.64
	Nardus stricta L.	10.25	34.47
	Anthoxanthum nipponicum Honda	3.06	0.00
	Mutellina adonidifolia (J. Gay) Gutermann	0.73	0.89
2	*Trichophorum cespitosum* (L.) Hartm.	87.30	26.24
	Eriophorum angustifolium Honck.	0.00	50.89
	Eriophorum vaginatum L.	12.70	22.87
3	*Nardus stricta* L.	84.45	77.44
	Anthoxanthum nipponicum Honda	8.35	11.47
	Mutellina adonidifolia (J. Gay) Gutermann	4.59	3.40
	Scorzoneroides helvetica (Mérat) Holub	2.61	2.23
	Poa alpina L.	0.00	3.30
	Carex nigra (L.) Reichard	0.00	2.16

Table 3: *Observed dry aboveground biomass (AGB), leaf area index (LAI), height (H), grazing value, and Simpson diversity index of the pastures in the three sites at each sampling event. The grazing value and the Simpson diversity index were calculated considering only the species listed in Table 2.*

Sampling event	Site	AGB (t ha^{-1})	LAI (m^2 m^{-2})	H (m)	Simpson diversity index	Grazing value
25 July 2019	1	5.99	2.17	0.46	1.33	2.23
	2	1.17	0.80	0.30	1.28	1.00
	3	4.03	1.23	0.32	1.39	0.51
29 August 2019	1	7.68	1.37	0.37	1.85	1.68
	2	0.96	0.22	0.24	2.63	1.00
	3	3.44	1.20	0.26	1.61	0.69

4.4.2. Model evaluation

The agreement between observed and simulated variables describing pasture growth, composition and grazing value was overall satisfactory (Table 4), with the values of all metrics achieving values close to their optima for all the variables and sites. The only exception was the relative abundance in site 2, for which the values of the agreement metrics were less satisfactory. CoSMo successfully reproduced pasture productivity: the values of MAE and RRMSE for AGB were 0.42 t ha^{-1} and 15.55%, EF and R^2 were higher than 0.95, and systematic under- or over-estimations were not observed. Despite the capability of CoSMo to reproduce community LAI and height was never evaluated before against observations, the results obtained are promising, especially for canopy height (MAE equal to 0.03 m and EF higher than 0.5). The simulation of community LAI was instead affected by higher uncertainty and – despite the overall trend in LAI values was successfully captured (positive EF, R^2 and MAE equal to 0.73 and 0.4 m^2m^{-2}, respectively), the model presented a certain tendency to overestimate observations.

The model accurately reproduced the relative abundance of species in site 1 and site 3 (Table 4): MAE was lower than 3%, EF and R^2 were equal to 0.99 and RRMSE was always lower than 17%. The peculiarities of site 2 (peat bog and periods with few cm standing water) that clearly defined its floristic composition (prevalence of species not detected in the other sites) were instead not properly interpreted by the model, this leading to poorer results with respect to the other two sites.

The comparison between observed and simulated relative abundance for all the single species is reported in Fig. 1. Most of the points are close to the 1:1 line, emphasizing the capability of CoSMo to successfully reproduce the time dynamics of floristic composition in the three pastures. The model reliability while simulating the relative abundance of the single species in the phytocoenosis clearly reflected on the agreement obtained for the grazing value and the Simpson diversity index, which were both successfully simulated, with all the metrics close to their optima (Table 4).

Parameter values are presented in Tables S2 and S3, Online Resource 1.

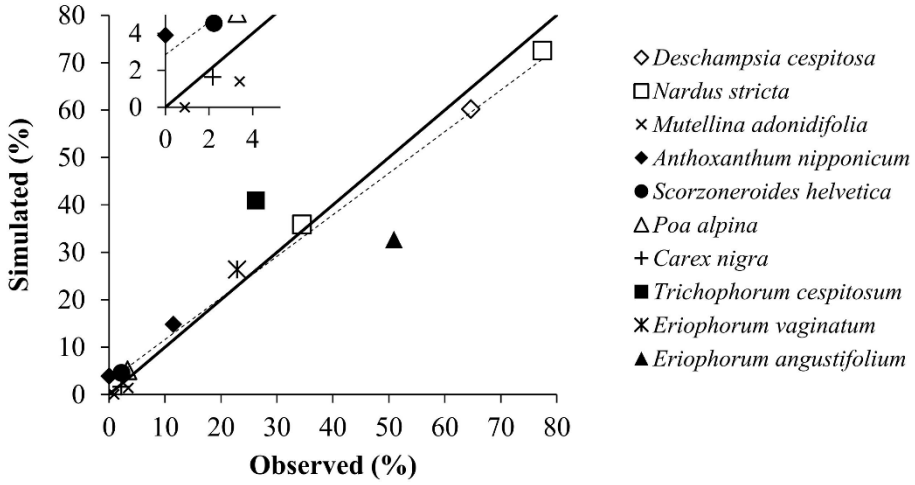

Figure 1: *Observed and simulated relative abundance of single species (percentage contribution of each species to the community AGB). The small chart zooms in the range 0 to 5% to increase readability for values close to zero. Solid line: 1:1 line, representing the perfect agreement between observed and simulated values. Dotted line: linear regression equation between simulated and observed data.*

Table 4. *Agreement between observed and simulated variables describing pasture growth, floristic composition and grazing values in the three sites. AGB, LAI and H are the community aboveground biomass, leaf area index and height, respectively. The relative abundance represents the percentage contribution of each species to the community AGB.*

Variable	MAE [a]	RRMSE (%)	EF	R^2	Slope
AGB (t ha^{-1})	0.42	15.55	0.95	0.97	1.02
LAI (m^2 m^{-2})	0.40	53.80	0.03	0.73	0.71
H (m)	0.03	13.91	0.53	1.00	0.61
Grazing value (-)	0.08	8.73	0.94	1.00	1.30
Simpson diversity index (-)	0.21	10.52	0.75	1.00	0.90
Relative abundance (%), Site 1	2.65	12.23	0.99	0.99	1.08
Relative abundance (%), Site 2	12.11	40.89	-0.19	0.00	0.08
Relative abundance (%), Site 3	2.48	16.97	0.99	0.99	1.08
Relative abundance (%), All sites	4.76	30.47	0.92	0.93	1.06

[a] units for MAE are the same as reported in the first column.

4.4.3. Climate change impacts

According to the climate change scenarios considered, the mean annual temperature in the study area is expected to increase from the 3.99 °C of the baseline to 4.76, 5.18, 5.76 and 5.93 °C, respectively, for the scenarios RCP4.5-GISS-ES, RCP8.5-GISS-ES, RCP4.5-HadGEM2, and RCP8.5-HadGEM2. In general, the increase in temperature was more marked during the summer months, with the maximum monthly increase in temperature (+3.09 °C) achieved in September for the scenario RCP8.5-HadGEM2. Concerning precipitations, the total annual rainfall was equal to 1270 mm in

the baseline and to 1304 mm, 1300 mm, 1155 mm and 1217 mm for, respectively, the scenarios RCP4.5-GISS-ES, RCP8.5-GISS-ES, RCP4.5-HadGEM2, and RCP8.5-HadGEM2. A small increase in annual rainfall was thus projected by the GCM GISS-ES, whereas HadGEM2 indicated a decrease – especially for RCP 4.5 – with the largest reduction during summer months.

Simulations highlighted how these climate variations will have an overall positive impact on pasture productivity (Fig. 2a), with an expected increase in cumulated AGB regardless of the climate scenario considered (+10.7% on average). This positive effect on biomass accumulation is explained by the average increase in the number of days in which pastures are actively growing (+6.7% on average, Fig. 2a) and by the higher daily rate of AGB accumulation during the growing season (+4.1% on average, Fig. 3) as compared to current climate conditions. The differences in the temperature increase projected by the four climate scenarios reflected in the extent of the changes simulated for both biomass accumulation and duration of the active growth period, with warmest scenarios (RCP4.5-HadGEM and RCP8.5-HadGEM) achieving the higher daily rate of AGB accumulation (Fig. 3) and the lowest extension of active growth period (Fig. 2a), the latter being explained by the faster accumulation of thermal time as compared to the scenarios characterized by milder temperature increase (GISS-ES realizations of RCP4.5 and RCP8.5).

The heterogeneity in the results obtained for the different sites (Figs. from 2b to 2d) highlighted how changes in climate will not affect the different pastures in the same way, since their different floristic composition (Table 2) and the heterogeneity in the response to temperature of the species in the communities (Tables S2 and S3, Online Resource 1) will turn into complex, non-linear responses to changes in climate. The geographical position of the three pastures excludes indeed that the variability between sites is due to differences in future climate projections. Site 3 (Fig. 2d) showed the most positive variation of pasture productivity under climate change scenarios, with an average increase in biomass accumulation and length of active growth period equal to 16.2% and 7.2%, respectively (mean of the four climate scenarios). On average, no benefits due to climate change were instead simulated for Site 1 in the mid-term, with daily rate of AGB accumulation ranging from -11.1% to +4.6% as compared to the baseline (-2.5% was the mean for the four climate scenarios). In this site, the climate scenario with the largest reduction of daily AGB accumulation (RCP4.5-HadGEM2) was also the only one for which a shortening – although negligible – in the active

growth period was simulated (-1.5%). For all the other combinations site × climate scenario, in fact, the active growth duration is expected to increase, to an extent that ranges from 1.8% (site 1, RCP8.5-HadGEM2) to 15.8% (site 2, RCP8.5-GISS-ES).

Considering climate change impact on floristic composition, no marked variations were simulated, with an average (all site × climate scenario combinations) variation of the Simpson diversity index equal to -1.0%, with values ranging between -4.1% (Fig. 2d) and +3.4% (Fig. 2b). This indicates a similar level of codominance between the different species under future climate projections. On the contrary, the grazing value showed a clear decrease under climate change scenarios (-11.1% on average; Fig. 2a), with values ranging from -5.5% to -15.7% (average of all sites). This negative trend was especially marked in site 1 (-22.9%; Fig. 2b), and this can be explained by the fact that *N. stricta* – which has a poor value for livestock feeding (Table S4, Online Resource 1) – is expected to increase its relative abundance under future climate conditions (Fig. 4), thus leading to a worsening of the overall pasture grazing value. A similar trend was observed for site 3 (Fig. 2d), although to a lesser extent (-6.5% on average), given *N. stricta* is already dominant in this site under baseline conditions (Table 2), thus leading to lower relative worsening under future climate projections. Concerning site 2 (Fig. 2c), no changes in the grazing values under future climate conditions were simulated, given the three species that coexist in this site have the same specific grazing value (Table S4, Online Resource 1). This means that any changes in the floristic composition will not affect the grazing value of the pasture in site 2.

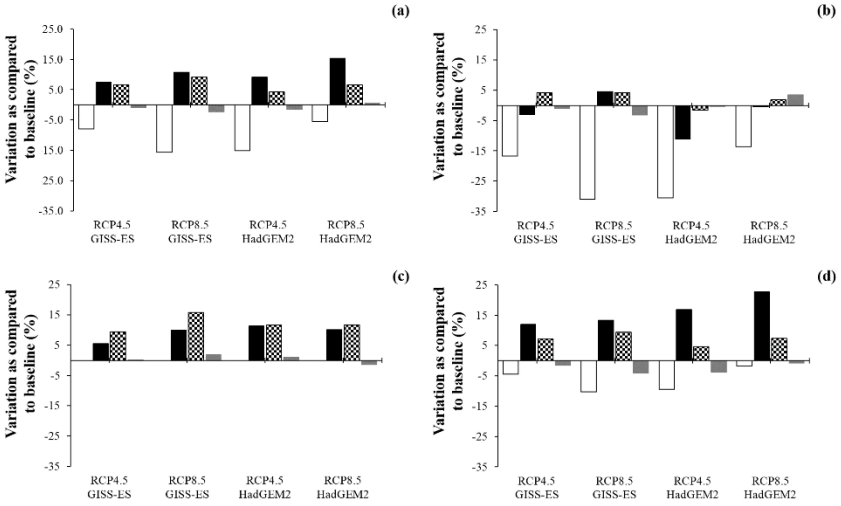

Figure 2: *Climate change impacts quantified in terms of percentage variation of aboveground biomass accumulation (black bars), length of the active growth period (checkered bars), grazing value (white bars), and Simpson diversity index (grey bars) with respect to the baseline. Panel a, b, c, and d, refer to the results obtained for, respectively, the three sites (averaged together), site 1, site 2, and site 3.*

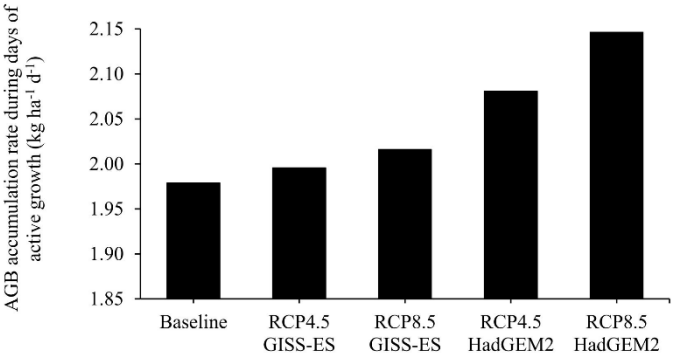

Figure 3: *Daily rate of aboveground biomass accumulation during the active growth period simulated for the current conditions (baseline) and the four climate scenarios.*

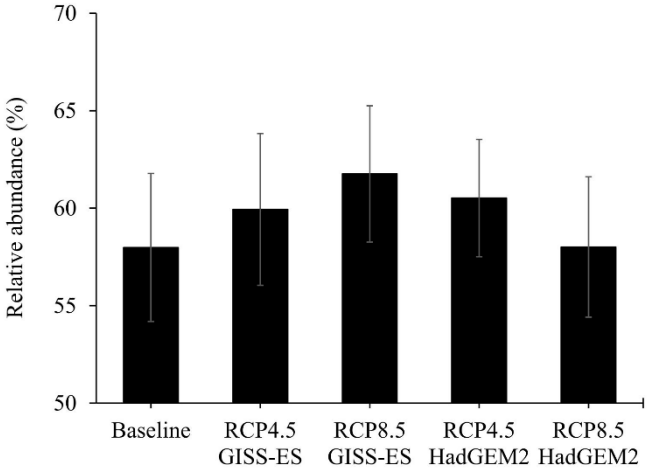

Figure 4: *Relative abundance (%) of Nardus stricta simulated for current conditions (baseline) and for future climate scenarios in the two sites where this species is currently present (sites 1 and 3). For each climate scenario, the mean (error bars indicate the standard deviation) of the values from the two sites is reported.*

4.5 Discussion

The modelling solution developed by coupling the CoSMo plant community model and the crop model CropSyst demonstrated its suitability for reproducing key dynamics involved with biomass accumulation and floristic composition in alpine pastures. Concerning the simulation of pasture productivity, the model performance can be regarded as satisfactory, especially if compared to results from other grassland models (e.g., Soussana et al. 2012) and from previous works where the CoSMo model was used (Movedi et al. 2019). Despite the higher complexity compared to single-species system, the degree of accuracy in the simulation of pasture AGB was consistent with most studies where single crops were simulated (e.g., Belder et al. 2007, Coucheney et al. 2015). The only variable involved with pasture growth for which the agreement with observations was – to a certain extent – less satisfying was LAI. Besides the uncertainty intrinsic in whatever modelling approach, the lower accuracy in LAI simulation is often underlined in modelling studies (e.g., Yu et al. 2006; Tartarini et al. 2019) and it is partly due to the larger uncertainty in the methods for estimating this variable as

compared to methods for estimating, e.g., AGB or plant height (e.g., Confalonieri et al. 2009).

The changes in the relative abundance of the different species were successfully captured, thus allowing to extend the evaluation of climate change impacts at the level of changes in floristic composition and related ecosystem services provided by pastures (e.g., feeding grazing livestock). The results obtained in this study highlighted how this is a key point for a comprehensive evaluation of climate change effects, given the complex interactions between the current floristic composition, the heterogeneity in the response to environmental drivers of the different species in the community, and the variability in pasture management. All these factors can lead to divergent dynamics in the mid-term for pasture biomass accumulation and grazing value. A better understanding of the drivers at the basis of climate change impacts on pasture productivity is indeed a crucial prerequisite for developing effective adaptation strategies (Soussana et al. 2010).

Our estimates of a general increase in pasture biomass accumulation as response to expected climate variation are in partial agreement with other studies. They are in line with results reported by Riedo et al. (2000), who outlined a positive trend in net biomass accumulation for managed grasslands, but differ from other authors who highlighted a reduction in pasture productivity in the mid-term (Dellar et al. 2018; Dibari et al. 2020). However, the heterogeneity in the results we obtained for the different sites suggests that the variability in floristic composition can markedly affect the dynamics of pasture growth under future climate projections, thus partly explaining the variability in results from different studies. The increase in the length of the active growth period also varied across the different sites, in line with the expected variability in the occurrence of vegetative restart in spring and the end of the growing season in autumn outlined by different authors (e.g., Schwartz et al. 2006; Ren et al. 2018). Concerning the floristic composition, the projected reduction of forage quality under future climate conditions due to the increase in the relative presence of *N. stricta* is in agreement with the findings from Dibari et al. (2020), who underlined how pastures macro-types dominated by this species will expand in the Alps in the coming decades.

4.6. Conclusions

We showed how the plant community model CoSMo can successfully reproduce the dynamics of grazed pastures in terms of biomass accumulation, growing season duration, floristic composition, biodiversity and, in turn, forage quality. This – together with the low requirements in terms of data needed to parameterize the model and running simulations – makes CoSMo a valuable tool to support the estimate of forage production in pastures, which is one of the most important ecosystem service provided by grasslands.

Our results highlighted that the projected mid-term increase in temperatures will favor high-altitude pastures in two ways: by increasing the daily biomass accumulation rate and by extending the length of the active growth period. However, despite the biodiversity is expected to increase, the quality of the forage could be negatively affected because of the positive response to future climate conditions of species with a low grazing value. This underlines once more how the evaluation of climate change impacts on pastures cannot overlook the effects on the floristic composition of the community, this being a crucial issue to obtain a comprehensive evaluation of pasture responses to climate change and to target the definition of effective adaptation strategies.

Moreover, this study opens to new opportunities in the analysis of ecological scenarios involved with the mid-term assessment of the capability of plant species to persist in a given site or to successfully invade new areas.

Ethical approval

The authors have no relevant financial or non-financial interests to disclose.

No human participants and/or animals were involved in the research.

Consent to Participate

Not applicable (no human participants were involved in the research).

Consent to Publish

The authors declare they all agreed with the content of the manuscript and that all gave explicit consent to submit and to publish.

Author Contributions

R. C. and S. B. provided study conception and funding acquisition. Material preparation, data collection and analysis were performed by E. M., I. V., L. P., and F.M. V. The first draft of the manuscript was written by E. M., L. P. and R. C. All authors read and approved the final manuscript.

Funding

This research has been founded by the AGER Interdisciplinary Project for assessing current and expected Climate Change Impact on MOUntain PAsture (IPCC MOUPA), Grant number 2017-1176.

Competing interest

The authors have no relevant financial or non-financial interests to disclose.

Data Availability

The datasets generated and analysed during the current study are available from the corresponding author on reasonable request.

4.7. Electronic Supplementary Material

ESM 1 - Supplementary Tables

Table S1. Description of parameter acronyms.

Acronym	Description	Unit
k	Radiation extinction coefficient	-
LeafLife	single leaf life duration	°C-d
RUE	Maximum radiation use efficiency	g MJ^{-1}
SLA	Specific leaf area	m^2 kg^{-1}
SLP	Stem leaf partitioning	-
GDDFl	Growing degree day to flowering	°C-d
TUE	Maximum water transpiration use efficiency	(kg m^{-2})kPa m^{-1}
WST	Water stress tolerance	-
WCF	Water competition factor	-
R	Root type (0 fibrous, 1 tap)	-
BT	Base Temperature	°C
CoffT	Cut-off temperature	°C
AL	Animal liking	-
LAImax	Maximum leaf area index	m^2 m^{-2}
Hmax	Maximum plant height	m
OptT	Optimal temperature	°C
RD	Maximum rooting depth	cm

Table S2. Calibrated CropSyst parameters (see Table S1 for parameter acronyms).

	k	Leaf Life	RUE	SLA[a]	SLP	GDDFl[b]	TUE	WST[b]
Anthoxanthum nipponicum	0.35	450	1.5	13.0	4.00	650	3.0	0.50
Carex nigra	0.35	400	1.6	9.0	3.00	550	3.0	0.00
Descampsia cespitosa	0.35	600	1.8	11.0	5.00	650	3.5	0.50
Eriophorum angustifolium	0.35	500	1.0	8.0	5.50	400	2.0	0.00
Eriophorum vaginatum	0.35	500	0.9	8.0	5.00	400	3.0	0.00
Mutellina adonidifolia	0.80	500	1.2	12.0	2.00	650	3.0	0.50
Nardus stricta	0.30	500	1.7	8.0	3.50	650	3.0	0.50
Poa alpina	0.35	400	1.8	12.0	3.00	400	3.0	0.20
Scorzoneroides helvetica	0.80	450	1.7	14.0	2.00	650	3.0	0.50
Trichophorum cespitosum	0.35	500	0.7	8.0	5.00	400	2.0	0.00

[a]: from Turtureanu et al. (2020) for *Nardus stricta*.

[b]: from Longo et al. (2021) for all the species.

Table S3: Calibrated CoSMo parameters (see Appendix A for parameter acronyms).

	WCF[a]	R	BT[a]	OptT[a]	CoffT[a]	AL[b]	LAI max	H max[c]	RD
Anthoxanthum nipponicum	0.50	0	2	11	20	0.70	2.0	0.25	150
Carex nigra	0.00	1	2	12	25	0.70	2.0	0.25	100
Descampsia cespitosa	0.72	0	3	12	25	0.70	4.0	0.70	150
Eriophorum angustifolium	0.00	0	-1	10	25	0.10	3.0	0.30	100
Eriophorum vaginatum	0.00	0	2	13	25	0.20	3.0	0.30	100
Mutellina adonidifolia	0.50	1	0	10	21	0.82	2.0	0.25	150
Nardus stricta	0.70	0	1	11	24	0.30	4.0	0.30	150
Poa alpina	0.50	0	1	11	21	0.75	2.5	0.30	150
Scorzoneroides helvetica	0.50	0	1	11	18	0.77	3.5	0.20	150
Trichophorum cespitosum	0.00	0	3	18	25	0.80	3.0	0.25	100

[a]: from Longo et al. (2021) for all the species.

[b]: estimated from the grazing value reported by Daget and Poissonet (1971) for all the species but *Eriophorum angustifolium, Eriophorum vaginatum,* and *Trichophorum cespitosum* (calibrated value in that case).

[c]: from Longo et al. (2021) for all the species but *Nardus stricta*, which is from Turtureanu et al. (2020).

Table S4: Grazing value for each of the species considered as reported by Daget and Poissonet (1971).

Species	Grazing value (from 0 to 7)
Anthoxanthum nipponicum	1.0
Carex nigra	1.0
Descampsia cespitosa	2.5
Eriophorum angustifolium	1.0
Eriophorum vaginatum	1.0
Mutellina adonidifolia	7.0
Nardus stricta	0.0
Poa alpina	7.0
Scorzoneroides helvetica	4.0
Trichophorum cespitosum	1.0

5. Development of a new model for simulating the interaction between olive trees, olive fly and fly predators

Ermes Movedi, Sofia Tartarini, Fosco Vesely, Livia Paleari, Luca Radegonda, Andrea Pietrasanta, Raffaele Grasso, Giacomo Facelli, Roberto Confalonieri

To be submitted to:

Agriculture, Ecosystems & Environment

5.1. Abstract

Olive groves (*Olea europea L.*) play a significant role in Mediterranean agriculture, where the olive fruit fly (*Bactrocera oleae (Rossi, 1790)*) is the major pest. Plant–pest interaction models do exist in this context but are poorly documented or oversimplified. In this study, starting from the literature, we have developed, documented and evaluated a new, biologically interpretable and operationally usable model. Field-scale canopy layers (not individual olive trees) are dynamically simulated on a daily time step. The behaviour of the model was assessed by sensitivity analysis and its performance was tested on measured data from the scientific literature and alert bulletins. The optimum temperature for olive-tree growth and development and the maximum pupae death temperature for olive fly population and infection are the most relevant parameters. The model error was low (MAE <1 t in the simulation of fruit dry biomass and ~ 5% in the percentage of olive fruits infected by olive fruit fly). The new model is usable in operational context.

Keywords:

Olive trees, olive fruit flies, crop model, plant-pest interactions, process based, plant organs, fly population

5.2. Introduction

The olive tree (*Olea europea L.*) is a long-lived and water-stress tolerant species, endemic to the Mediterranean basin, where olive groves are widely distributed and play an important economic role (Vossen, 2007; Iraldo et al., 2013; Palese et al., 2013). In fact, 95% of the 20.7 million tonnes of worldwide olive production and 97% of the 10.7 million hectares of worldwide olive groves (on average between 2010 and 2020) are concentrated in Mediterranean countries (FAOSTAT database; Kasnakoglu, 2006). In this region, the olive fruit fly (*Bactrocera oleae (Rossi, 1790)*) is the major pest of olive trees (Manousis and Moore, 1987; Tzanakakis, 2003; Tzanakakis, 2006).

The host plant and the pest coexist in the same environment and both interact with each other and other species (Gutierrez et al., 2009). For example, (*Lasioptera berlesiana (Paoli, 1907)*) is a predator of olive fruit fly larvae and eggs, but it affects olive fruits with a fungus, *Sphaeropsis dalmatica* (Thüm.) Zachos & Tzav.-Klon., the agent of olive drop and rot.

Olive fruit fly damage is a lesion on the fruit mainly due to the holes dug by the larvae's bites and also the lesion of the female ovipositor. Subsequently, the lesions of the olive fruit fly are used as access to the olive fruits by various microorganisms. The damage to harvested olives is twofold, both in terms of quantity (Rojnić et al., 2015) due to the fall of some infected fruits and the portion of fruit eaten (reduction of olive fruit weight), and in terms of quality (Kyriakidis and Dourou, 2002) of the harvested fruits (fly-infected), which are often rotten and acidic due to the microorganisms.

Climate change could influence species interactions (e.g. Saier, 2007) and modify the olive fruit fly range (Gutierrez et al., 2009). In this changing context, crop simulation models are powerful tools to estimate biotic dynamics, interactions and crop damage (Tubiello et al., 2006). However, available olive crop models may not be suitable for accurate simulations and operational use. According to Moriondo et al. (2019), the model of López-Bernal et al. (2018) is too complex and needs a lot of specific inputs, which make it difficult to use in large-scale applications. At the same time, models by Moriondo et al. (2019), Morales et al. (2016), Villalobos et al. (2006) and Abdel-Razik (1989) are available, but these are simplistic representations of olive-tree physiology and often lack explicit host-plant interaction. For example, tree reserves are not considered in Moriondo et al. (2019), whose

model does not take into account the damaging effect of olive fruit fly. The latter is considered in the model of Gutierrez et al. (2009), which, however, does not consider water stress in olive trees and is not well documented.

Our aim was to develop a new process-based crop model estimating the interaction between olive trees and olive fruit fly population dynamics (also considering the predator population), able to consider water and other abiotic stresses and the dynamic partitioning of reserves during olive tree growth. The new model had to be well documented and easy to understand, in order to consider using it in an operational context: as a decision support system or in a parametric insurance.

5.3. Materials and methods

5.3.1. Model description

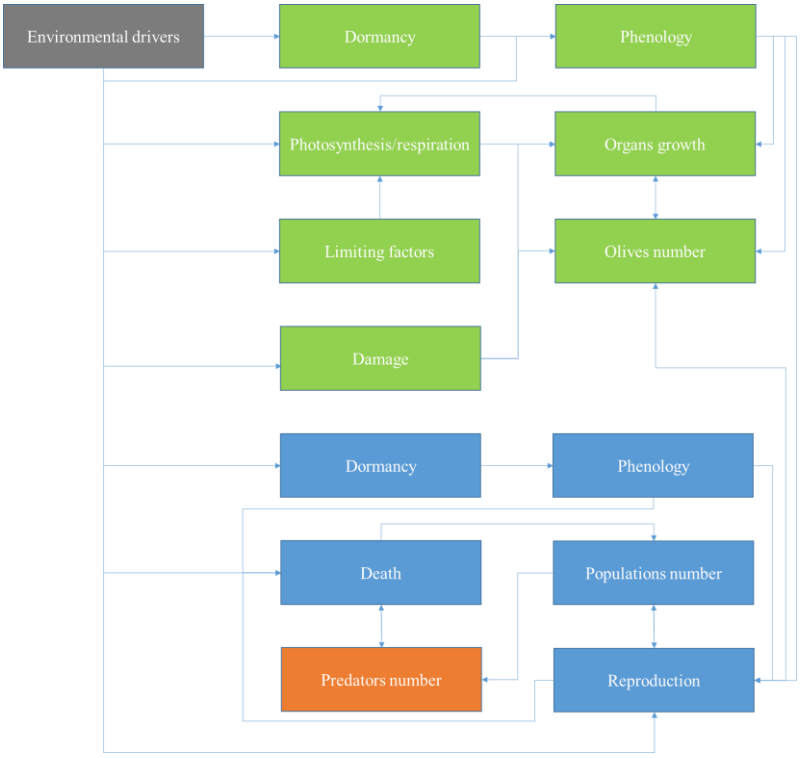

Figure 1: *Model diagram: olive tree model (green boxes), olive fruit fly model (blue boxes) and fly predators (orange box). Environmental drivers summarise management, weather and soil factors.*

The new model, “Olive trees olive fruit flies and predators - interactions process-based, dynamic model” (OOPS), summarises the current knowledge by implementing and summarising equations from Moriondo et al. (2019), López-Bernal et al. (2018) and Gutierrez et al. (2009). It works on a daily time step and field level. Model inputs (environmental drivers) are (Figure 1): soil properties (organic carbon, depth and texture); weather variables (minimum and maximum air temperature, cumulated rain, average wind, evapotranspiration and solar radiation); latitude and day of the year. Other inputs are the management events: harvesting, pruning, irrigation and chemical treatment on the olive fruit fly and the initialisation values (e.g. leaf area index, plant biomass, number of flies). The main outputs of the model are woody, green and fruit biomass, number of olive fruit flies and their predators, infected fruits, fallen fruits, leaf area index (LAI) and phenological state of olive trees and flies. Output variables refer to one hectare.

The model is divided into three independent sub-models (Figure 1): a biophysical model for olive tree growth and development, and two population models for estimating the dynamics of the olive fruit fly and its natural predators.

All equations are available in the supplementary material.

5.3.1.1. Olive plant sub-model (biophysical model)

This sub-model works at the field level; at the individual plant level, it only estimates the canopy radius and the number of dead plants (in the case of severe damage), in order to estimate the canopy gap and overlap to correct for daily photosynthesis.

Only the aboveground part of the plant is considered. For roots, a parameter is considered that manages the maximum rooting depth, which is constant for all simulations and consists of the maximum depth at which soil water is available to the plant.

The main biophysical processes simulated are: plant phenology; photosynthesis; partitioning; organs, canopy, diameter and height growth; senescence; fruit drop; evapotranspiration; respiration (only in specific cases); lignification; winter hardening; yield alternation; shading; and abiotic damage (Sanzani et al., 2012). The abiotic damage simulated are: thermal shock (heat or cold), excess rainfall, water stress, wind limitation during

flowering and excess light (photosynthetic reduction). Thermal shock causes: flower sterility or death of the organs or the plant, depending on the severity; excess rainfall causes flower sterility; water stress causes: photosynthetic reduction, flower sterility, death of the organs or the plant depending on the severity (Sanzani *et al*., 2012). Abiotic damage could be turned off by users. If the wind limitation is off, wind speed is not required by the sub-model; the same for rainfall if both the excess rainfall and water constraint are turned off.

Figure 1 reports only a simplification of the process estimated by sub-model to better show the interaction with the olive fruit fly.

In detail, plant phenology encompasses various sub-processes, including: winter dormancy, chilling unit accumulation, bud differentiation, regrowth, thermal time accumulation, gradual flowering, seed harness, fruit demand and maturity, and twig lignification. Plant phenology is primarily driven by temperature, day length and water deficit; for bud differentiation, the plant reserves play a crucial role. Vice versa, twig lignification is only driven by the age in term of number of spring regrowths: at the beginning of the second regrowth, the twig is considered lignified and this mass is considered in the woody mass (Gutierrez et al., 2009).

Photosynthesis is based on the interception of light from all photosynthetic surfaces and we adopted the Lambert-Beer law (Swinehart, 1962) and the net radiation use efficiency as in Moriondo et al. (2019). Photosynthesis production is limited by temperature (via a beta function - not switchable off, always on) and water (switchable off). In case of exceptional heat events, photosynthesis is automatically turned off and respiration is simulated with a general loss of biomass, limited by temperature (using a beta function - not switchable off, always on).

Partitioning, remobilisation and fruit accumulation are mainly driven by phenology, photosynthesised mass and the availability of reserves. The sub-model considers five organs plus constant roots: leaves, woody organs, twigs, reserve organs and reproductive organs (the olive fruit).

In detail, a mobilisation of reserves is estimated after regrowth, and the reserves and the new photosynthesised mass are partitioned between vegetative (leaves and twig) and woody organs. After mobilisation of the reserves and before flowering, partitioning occurs between leaves, twigs, woody organs and reserves. Starting from flowering until the harvest or

physiological maturity of fruits, the olive trees sub-model tries to satisfy the mass demand of the fruits. If the photosynthesised mass is enough, it also breaks down into reserves and, if the plant is not in winter dormancy, also into woody and vegetative organs, otherwise the reserves are mobilised until the fruit demand is satisfied or the reserves are ended. If the photosynthesised mass and reserves do not satisfy at least a certain quote of fruit demand, an olive fruit drop is estimated. After harvesting or full maturation, if the plant is actively growing, the photosynthesised mass is partitioned into reserve, woody and vegetative organs, else only in reserves.

The partitioning, utilisation of reserves and the role of reserves in the diversification of buds is crucial in the sub-model for the indirect estimation of alternation in production and have an effect on the memory of previous damage.

The leaves are organised into coeval daily cohorts, characterised by a number, a leaf area index (LAI), a thermal age, and for each leaf there is a bud, and for each leaf pair an internode is estimated with an increase in height and length.

Flowering is estimated in a scalar way: there is a thermal time period in which a quota of flower bods bloom, which depends on the thermal time accumulation relative to the total thermal time length in this period. The flowers of the quota of the bloomed flower bods last only one day and the sub-model estimates a fruit set that depends on wind speed, rain, water stress and temperature limitations (cold or/and hot).

The effects of pruning consist mainly of a reduction in the biomass of all organs (AGB), LAI, height and canopy diameter, and a variation in the ration of flower buds to vegetative buds through a reduction in the total number of buds.

5.3.1.2. Olive fruit fly sub-model (population model)

The olive fruit fly population is organised in coeval cohorts, and cohort phenology is estimated. The phenology is driven by two process: dormancy and thermal time accumulation (Figure 1). Seven phenological phases are considered: egg, larva I, larva II, larva III, pupae, non-reproductive adult and reproductive adult.

The insect population is driven daily by deaths and emigrations that reduce the number of flies, and by ovipositions and immigrations that increase the number of flies.

Death can occur due to exceeding a threshold of thermal time accumulation or due to various external factors: temperature (too cold or too hot), predators, olive fruit drops, dry condition at the time o to ecdysis and unknown causes (Giglioli and Pasquali 2007; Genc and Nation, 2008). The effects of management on fly mortality in terms of fruit harvesting and chemical treatments are also simulated (by applying a chemical abatement efficiency to the fly population, varying by phenological phase).

Oviposition is limited by temperature, wind speed, day length, fly phenology and population, and interactions between olive trees and fruits.

There are five estimated interactions between olive trees and olive fruit fly (Figure 1) by: i) the oviposition of the olive fruit fly and thus the olive infection; ii) a limit on oviposition related to the number of olive fruits and the level of infection (if there was or is an egg in an olive, this olive is considered infected); iii) a limit of oviposition related to the hardness of olive seeds; iv) a limit on the fly population during olive drop and harvest; and v) the dropping of an infected portion of the olives.

The immigration or emigration approach only acts on adult flies and starts below or above a threshold value of the fly population: if the number of flies is too high, migration is estimated, if it is too low, immigration.

The effects of rain on disrupting the flight of adults and thus oviposition were not taken into account because in the Mediterranean environment summer most rain events are short-lived (e.g. Saaroni and Ziv, 2000).

The olive tree sub-model requires initialisation, while for the olive fruit fly sub–model, initialisation is optional.

5.3.1.3. Olive fruit fly predator sub-model (population model)

The predator sub-model estimates at the daily time step the number of flies eaten (for each phenological phases as a function of different liking function) in a delay function of the fly population (Gutierrez et al., 2009). This sub-model does not require initialisation.

5.3.2. Reference data

The reference data have a double bibliographic source: for the olive sub-model states: aboveground biomass (AGB), LAI, total fruit weight (yield), plant height (H) and canopy radius (R) the source is scientific journals (Hernandez-Santana et al., 2017; Fernández et al., 2013; Villalobos et al., 2006; Di Vaio et al., 2012; Mariscal et al., 2000; Table 1); for olive plant phenology and infected olive fruits (by flies), the health service of the Apulia region of Italy (Assopropoli Bari).

A complete dataset in which olive trees and olive fruit fly states were measured together was not find.

Table 1: *Number of available observations in olive groves by variable and their sources.*

Source	LAI	Yield	AGB	Plant height (H)	Canopy radius (R)
Hernandez-Santana et al. (2017); Fernández et al. (2013)	31	5	-	-	-
Villalobos et al. (2006)	23	4	4	25	25
Di Vaio et al. (2012)	5	-	-	-	-
Mariscal et al. (2000)	-	-	12	48	48

5.3.2.1. Olive tree data

For the olive tree conditions, we focused on data from orchards without growth limitation, in order to avoid confusion in the evaluation of the parameters involved in the simulation of stress intensity and plant productivity.

The works of Hernandez-Santana et al. (2017) and Fernández et al. (2013) (years 2010–2012 and 2014–2015; 37° 15’ N, 5° 48’ W; Seville, Spain) concerned the same olive grove composed by young but adult trees. The works of Villalobos et al. (2006) (years 1998–2002; 37° 52’ N, 4° 49’ W;

Cordoba, Spain), Di Vaio et al. (2012) (year 2004; 40° 49' N, 14° 20' E; Naples, Italy) and Mariscal et al. (2000) (years 1995-1997; 37° 52' N, 4° 49' W; Cordoba, Spain),were about young trees.

Daily weather data were derived from the European Centre for Medium-Range Weather Forecasts (ECMWF) Era-Interim database (Hennessy, 1986; Dee et al., 2011). They spanned the entire data collection period plus five years before, with a spatial resolution cell of 0.25° including the study sites plus one site in the Apulia region (years 2011-2020; 40° 38' N, 17° 38' E).

The parameter ranges used in the sensitivity analysis (SA) and calibration were derived from the literature (Villalobos et al., 2006; Connor et al., 2012, Mohammed and Noori 2008; López-Bernal et al., 2018; Gutierrez et al., 2009; Moriondo et al., 2019). For the new parameters, the adopted ranges were set based on the coherence of the output provided by the equation in question.

5.3.2.2. Olive phenology and fly data

The dataset counted 141 data on olive fruit infected by the fly in the seasonal peak and 292 data on plant phenology. The monitoring service started in 2015 and ended in 2020, in 31 experimental farms (the time series in not continuous in all farms and the monitored field might change from year to year).

For these farms, daily weather data were derived from the Cassandra Lab weather service at the University of Milan (Italy), which provides historical, near real-time and forecast daily weather data with a resolution of 0.016° × 0.016° for the whole Europe. This system (Mariani et al., 2012, 2016; Cola et al., 2020) uses geo-statistics and modelling to spatially downscale rough data retrieved from international networks (NOAA-GSOD, METAR and SYNOP).

Finer weather data were adopted because of often more than one fields, were physically located in a 0.25° × 0.25° cell so with the same model input but with different state of fly infection; the reason probably is the complex orography of the zone (47% are hills and mountains) and thus the weather micro-variability derived.

Finer data were not available for olive states and rates because the finer weather system is temporally lacking.

5.3.3. Sub-models sensitivity analysis and calibration

Sensitivity analyses (SA) were carried out separately for the model and a three-step calibration was carried out, two automatic and one manual.

E-Fast (Saltelli et al., 1999) total order index (Homma and Saltelli, 1996) was adopted as the SA method to detect the most influential parameters to support the calibration and to understand the model behaviour. This method relies on the variance ratio to quantify the relevance of the parameters and provides a measure of the overall effect on the selected output of one parameter at a time, considering interactions with all others. We used 450 iterations for each parameter tested (the list of model parameters, the description of the distribution used in SA and the values used in the parametrisation phase can be found in Appendix A).

The automatic calibration method used is a bounded version (for parameter ranges) of the downhill simplex (Nelder and Mead, 1965). The simplex has N+1 vertices interconnected by line segments and polygon faces in an N-dimensional parameter hyperspace and moves in this space according to three basic rules: reflection, contraction and expansion. Although other optimisation methods are available (e.g., Kirkpatrick et al., 1983; Glover, 1986), simplex guarantees a balance of performance and complexity (Matsumoto et al., 2002; Press et al., 2007). Relative root mean square error (RRMSE, from 0 to +∞, optimum: 0; Jørgensen et al., 1986) was optimised (minimised).

5.3.3.1. Olive trees sub-model SA and calibration

The SA was performed on 36 parameters (16200 iterations). All five available daily weather series were used in the SA. The five additional weather data before the start of data collection were used to initialise the sub-model (Movedi et al., 2019). To avoid the overlapping of the effect of a single weather year and total fruit weight alternation, three simulation runs a weather series was carried out, recombining the weather series. Each series consisted of the first five years of the weather series and three additional years (6th, 7th and 8th / 7th, 8th and 9th /8th, 9th and 10th).. The SA was carried out averaging a set of nine simulated years: the last three years of the three simulation runs. The variables tested was leaf area index (m^2 m^{-2}), olive number (#), olive dry weight (kg ha^{-1}) and olive dry weight standard deviation (kg ha^{-1}). The initial values used were to simulate young but productive trees:

canopy radius: 1.5 m; plant height: 3.5 m; dry mass of twigs: 2000 kg ha^{-1}; dry mass of woody organs: 15000 kg ha^{-1}; reserve woody organ ratio: 0.15; percentage of flowering buds: 50%; leaf area index: 2.5 m^2 m^{-2} (split into 400 leaf cohorts of different ages on regular scale). Considering the features of the dataset, in the sub-model, plant growth limitations were turned off, with the exception of rain and wind speed in flowering, self-shading and excess light. Management included automatic pruning (at spring regrowth) and harvesting at the day of year (DOY) 300.

The calibration of the sub-model was carried out only on the parameters that had more than 0.05 in the SA index for at least one variable and one site. The average RRMSE of LAI, AGB, olive fruit weight and canopy height and radius was optimised.

All simulations lasted from the planting of the olive trees to the end of data collection, with no re-initialisation in between. Initialisation and management were set based on field data or estimated if measured data were not available.

5.3.3.2. Olive fruit fly and their predator sub-models SA and calibration

The parametrised version of the olive tree sub-model was adopted. In order to correct for seed hardening and thus the appearance of the first fly infections, a manual adjustment of the plant phenology was performed using phenological data from Assopropoli Bari.

The SA was carried out on 23 parameters (10350 iterations). The same (weather) procedure of the olive tree sub-model was used, but only on a point in Apulia; management included automatic pruning (at spring regrowth) and harvesting at the day of the year (DOY) 300. The olive fruit fly population was initialised at 900 pupae and 10% of olive fruit remained in the field after harvest. The variables tested through SA were: total numbers of flies (#), olives dropped due to the fly (%) and infected olives (%).

The calibration of the sub - model was only carried out on the parameters that had more than 0.05 in the SA index for at least one variable. The RRMSE of infected olive fruits was optimised.

The sub-model, in the calibration phase, started on the 1st of January and ended on the yearly end date of data collection. The simulation was re-initialized every year because between the end of data collection and the

restart we do not know whether the monitored field was the same, and even if it was, whether the farmers carried out some chemical treatments. To avoid this uncertainty, we considered each simulation (location x year) as totally independent and initialised with a unique calibrated value of the fly population at the pupae stage.

5.3.4. Model evaluation

The agreement between the observed and simulated variables was quantified using: i) mean absolute error (MAE, from 0 to +∞, optimum: 0; Jørgensen et al., 1986), ii) coefficient of determination (R^2; from 0 to 1, optimum: 1; Addiscott and Whitmore, 1987) – considering slope, intercept and significance of regression –, iii) relative root mean squared error (RRMSE, from 0 to +∞, optimum: 0; Jørgensen et al., 1986), iv) modelling efficiency (EF, from -∞ to 1, optimum: 1; Nash and Sutcliffe, 1970), and v) coefficient of residual mass (CRM, from -∞ to + ∞, optimum: 0; negative values indicate model overestimation, positive values underestimation; Loague and Green, 1991). A graphical comparison was also carried out.

5.3.5. Model test

To test the behaviour of the three sub-models and their interactions, the OOPS model was tested on the same cell in the Apulia region where the SA was carried out. No modifications were made to the model set and parameterisation. The daily outputs were analysed graphically and compared with the output of an unpruned model run for the olive tree sub–model for eight years, and only the last year of the pruned version for the olive fruit fly sub-model.

5.4. Results

5.4.1. Sensitivity analysis

The most influential parameters of the olive sub-model is, in the majority of the tested sites and variables, the optimal temperature for growth and development.

For the single year variables (Figure 2 a, d), the olive sub-model is mainly sensitive to a few parameters, especially the optimum temperature (2) and the maximum radiation use efficiency (17), and the order of the parameters that

have an SA >0.05 is similar among sites. For the variables that are highly correlated for the previous year (number of olives; Figure 2 c) and years (yield variation; Figure 2 b), on the other hand the sub-model is sensitive to various parameters and the parameters involved to reserve use and translocation (from 10 to 15 included) have become relevant. For the yield variation, the behaviour is different among sites in terms of the order of the most sensitive parameters (Figure 2b).

The cut-off temperature of respiration, all parameters involved in vernalisation and the leaf area index for maximum self-shading were never relevant (SA index > 0.05). The latter probably for the estimation of pruning, and the former two for the climate in which the model was tested: warm but not too hot to influence respiration and vernalisation.

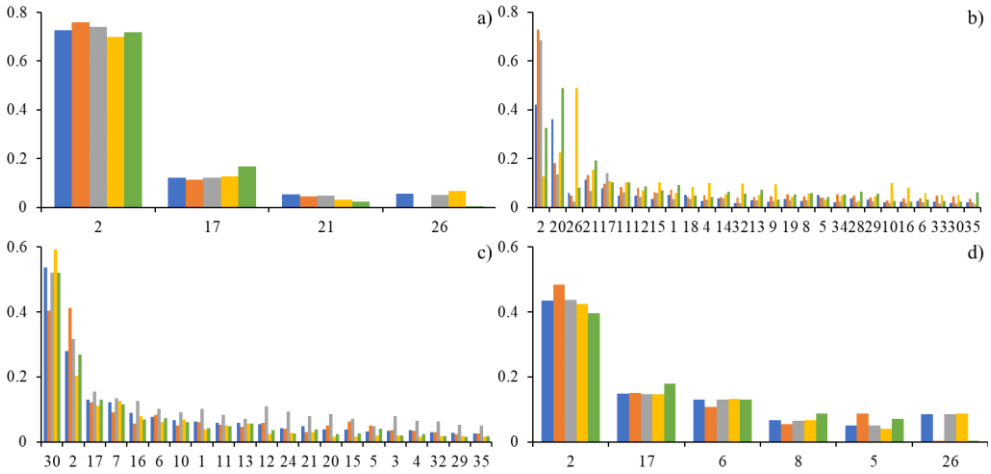

Figure 2: *Sensitivity analysis total order results for olive sub-model: the results are ordered by the mean SA index in all sites and the parameters are drown until at least one site has a value is greater than 0.05 (5%). The number of parameters is reversible in parameter name according to the ID in Appendix A. Blue bars for the site of Mariscal et al. (2000); orange bars for the site of Di Vaio et al. (2012); grey bars for Villalobos et al. (2006); yellow bars for Hernandez-Santana et al. (2017) and Fernández et al. (2013); green bars for a site in Apulia region. a) annual olive fruit yield, b) interannual variation of olive fruit yield; c) number of olive fruits; d) leaf area index.*

For the olive fruit fly model, the total order was above 0.05 for all the parameters in all variables excluding for the higher optimum number of adults

for oviposition in the infected olive percentage estimation (Appendix B). The most sensitive parameter for the first order in all variables is the maximum temperature threshold for pupae death (Appendix C).

5.4.1. Model calibration

The results of the olive-tree sub-model were overall satisfactory with EF>0.45, R^2>0.7, a significant regression of the estimates versus observations ($p<0.01$) with intercept and slope close to 0 and 1, respectively, for each variable (Table 2).

Following the results of the new model on the data found in literature are commented in detail.

The sub-model is able to estimate fruit production in young olive trees (dataset of Villalobos et al., 2006) and the interannual trend of production in adult olive trees (dataset of Hernandez-Santana et al., 2017 and Fernández et al., 2013 - Figure 3a, Table 2). For LAI (Figure 3c and Table 2), the sub-model estimated well the growth of young plants (dataset of Villalobos et al., 2006 and Di Vaio et al., 2012) but underestimated the value in the adult plants and not follow the LAI growth trend for this plant (low R^2 and negative EF), but the absolute and relative error was low (MAE = 0.4; RRMSE = 32.4% in Hernandez-Santana et al., 2017 and Fernández et al., 2013). The overall AGB was well simulated (Figure 3b and Table 2; EF and R^2=0.85), but in both datasets of Mariscal et al. (2000), the sub-model overestimated the observed values of biomass, while in contrast sub-model performed satisfactorily in Villalobos et al. (2006). For plant height (Table 2, Figure 3e), the sub-model performed well in all datasets used. There was only one underestimation of dataset of Mariscal et al. (2000) (low density; CRM=0.28). For canopy radius (Figure 3d and Table 2), there was an overall underestimation of the observed values (CRM=0.26), higher in Mariscal et al. (2000) low density (CRM=0.46).

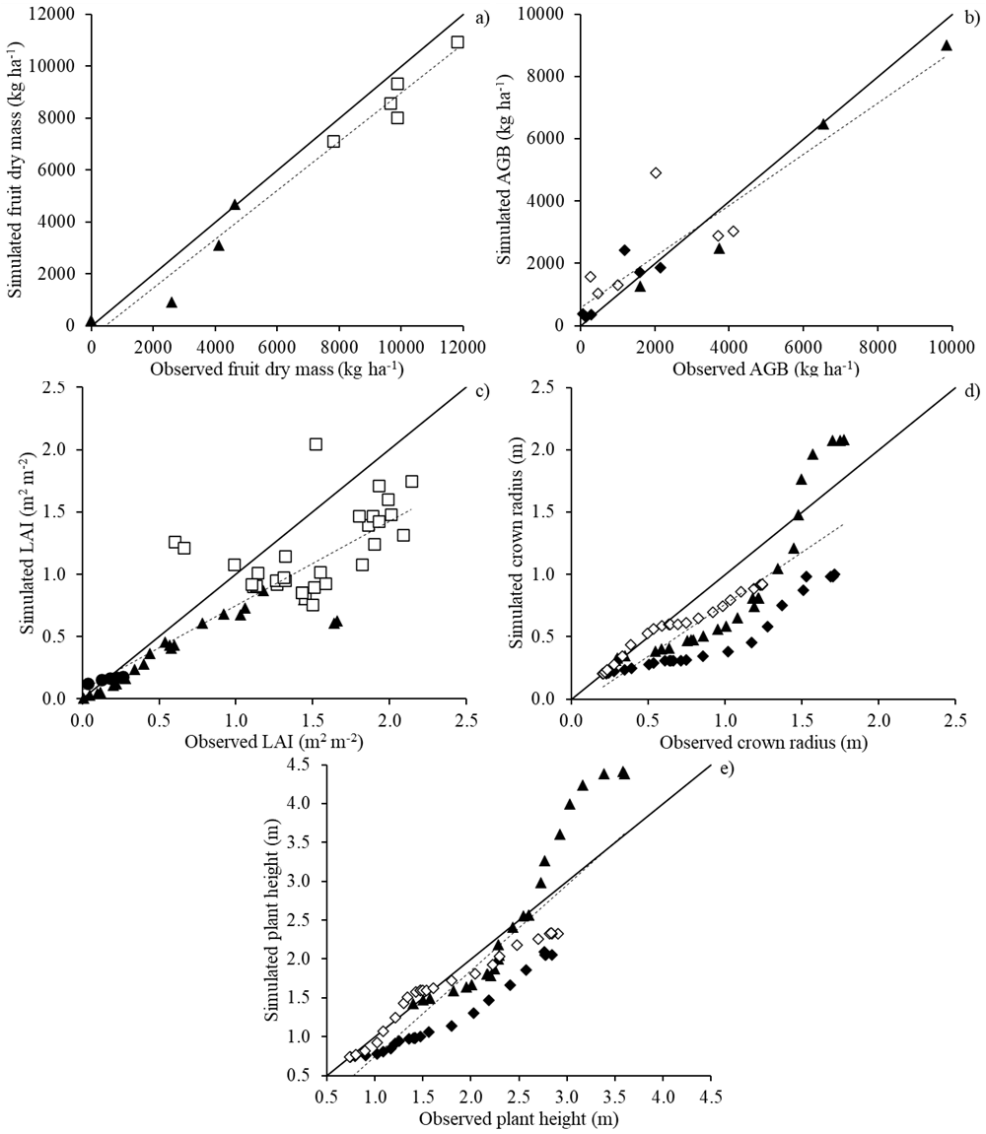

Figure 3: *Model parameterisation results for the olive sub-model: black line: 1:1 line; dotted line: overall trend line; filled triangles: Villalobos et al. (2006); empty squares: Hernandez-Santana et al. (2017) and Fernández et al. (2013); empty diamonds: Mariscal et al. (2000) high density; filled diamonds: Mariscal et al. (2000) low density; filled circles: Di Vaio et al. (2012).*

Table 2: *Model performance*

Variable / dataset	MAE	RRMSE (%)	EF	CRM	R^2	Slope	Intercept	Signif.
LAI / Villalobos et al. (2006)	0.24 $m^2 m^{-2}$	59.05	0.44	0.38	0.80	1.64	-0.01	0.00
LAI / Hernandez-Santana et al. (2017) and Fernández et al. (2013)	0.45 $m^2 m^{-2}$	32.41	-0.51	0.22	0.26	0.64	0.75	0.00
LAI / Di Vaio et al. (2012)	0.05 $m^2 m^{-2}$	35.61	0.44	0.04	0.97	3.74	-0.43	0.00
LAI / overall	0.33 $m^2 m^{-2}$	40.29	0.58	0.25	0.76	1.12	0.18	0.00
R / Villalobos et al., (2006)	0.28 m	29.55	0.52	0.13	0.82	0.67	0.45	0.00
R / Mariscal et al. (2000) high density	0.13 m	24.65	0.74	0.17	0.97	1.51	-0.19	0.00
R / Mariscal et al., (2000) low density	0.40 m	54.42	0.13	0.46	0.91	1.68	0.08	0.00
R / overall	0.27 m	38.46	0.45	0.25	0.70	0.84	0.32	0.00
H / Villalobos et al. (2006)	0.37 m	20.23	0.30	-0.05	0.92	0.56	1.02	0.00
H / Mariscal et al. (2000) high density	0.20 m	15.24	0.85	0.07	0.94	1.33	-0.41	0.00
H / Mariscal et al. (2000) low density	0.47 m	30.83	0.40	0.28	0.97	1.42	-0.04	0.00
H / overall	0.35 m	22.47	0.64	0.08	0.80	0.73	0.65	0.00
AGB / Villalobos et al. (2006)	0.63 t ha^{-1}	14.38	0.94	0.12	0.98	0.99	0.68	0.01
AGB / Mariscal et al. (2000) high density	1.16 t ha^{-1}	74.06	0.10	-0.27	0.32	0.64	0.36	0.24
AGB / Mariscal et al. (2000) low density	0.36 t ha^{-1}	59.94	0.53	-0.29	0.71	0.77	0.00	0.04
AGB / overall	0.73 t ha^{-1}	41.93	0.85	-0.06	0.85	1.04	-0.23	0.00
Fruit dry mass / Villalobos et al. (2006)	0.74 t ha^{-1}	35.11	0.69	0.22	0.82	0.92	0.80	0.09
Fruit dry mass / Hernandez-Santana et al. (2017) and Fernández et al. (2013)	1.00 t ha^{-1}	11.27	0.24	0.10	0.87	0.92	1.73	0.02
Fruit dry mass / overall	0.88 t ha^{-1}	15.77	0.92	0.12	0.97	1.03	0.64	0.00
Percentage of olive infected by olive fruit fly / Apulia region	5.50 %	90.11	-0.03	0.53	0.52	0.62	5.70	0.00

After a recalibration of the phenology on the available data of Apulia region (overall MAE=8.57 d and CRM=0.00), the sub-model of the olive fruit fly population was tested on the percentage of infected olives. The result was satisfactory, with MAE =5.5% and R^2>0.5. The sensitivity of the sub-model is low for low values of infection (Figure 4).

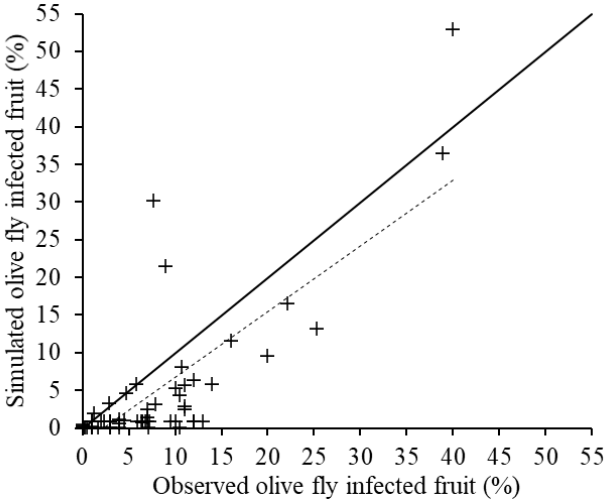

Figure 4: *Parameterisation results for the olive fruit fly sub-model: black line: 1:1 line; dotted line: trend line.*

5.4.3. Model test

The main differences between the management (pruning - Figure 5a - or not - Figure 5b) are the higher non-wooded mass and the presence of an alternating production of olive fruit mass in the unpruned olive groves. For both types of management, the plasticity of the mass production of olive fruits is visible: in years of low production, the mean weight of an olive is higher than in years of high production. It is also apparent that reserves are estimated to be replenished in low production years and depleted in high production years. This behaviour is followed by the non-wooded mass (more accentuated in unpruned management).

The non-wooded mass in the pruning simulation example shows a decrease in tree steps at the end of the year or the beginning of the new one: olive harvesting, twig lignification and removal of pruning (Figure 5a); and only two steps without pruning (Figure 5b).

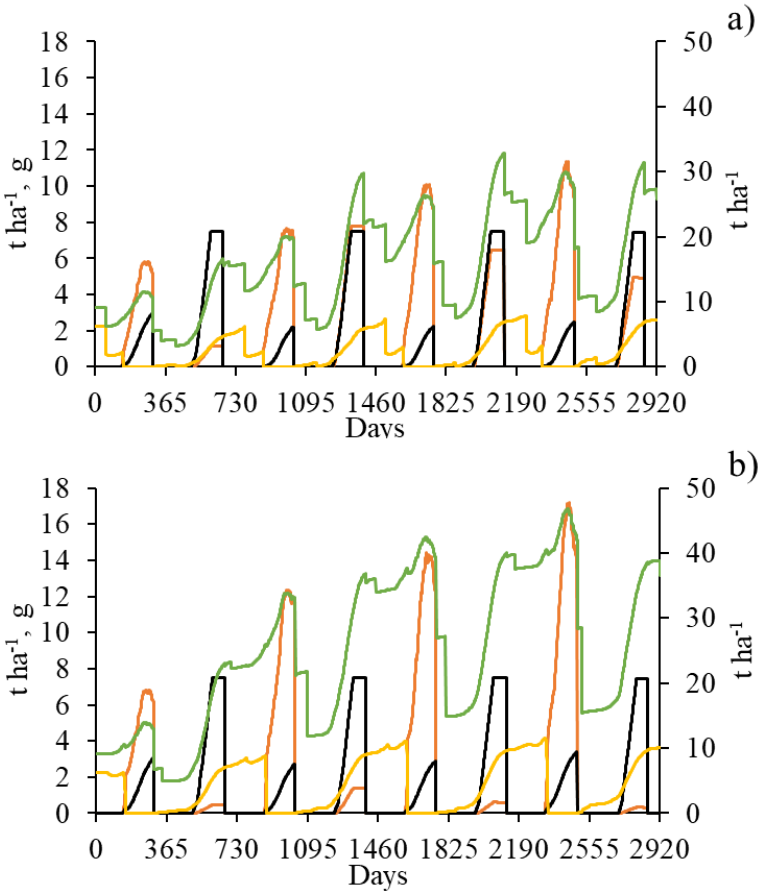

Figure 5: *Olive tree sub-model test: a) pruned conditions, b) unpruned conditions. Green line: non-woody mass (leaves, fruits, reserves and non-woody twigs; right axis; t ha^{-1}); orange line: olive fruit mass (left axis; t ha^{-1}); yellow line: reserve mass (left axis; t ha^{-1}); black line: single mean olive fruit mass (left axis; g).*

After seven years of initialisation, the olive fly population starts with adults, pupae and larvae III (Figure 6).

A first generation, DOY 100-200, borne by olive fruit residual and three other generations (DOY: 200-250; 250-300; 300-350) are responsible of the infection of more than 30% of seasonally produced olive fruits (Figure 6). The population is divided into consecutive phenological phases: egg, larva (from I to III), pupa and adult. Not all individuals reach the following

phenological phases, for prey simulation (Figure 6) and for other causes. For example, pupae do not become adults and the adult population is declining (Figure 6) for the absence of rain in summer (during ecdysis; data not shown).

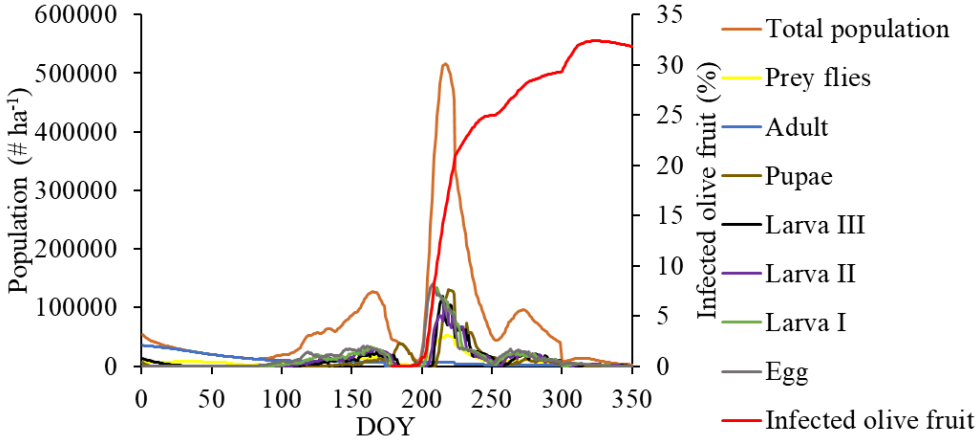

Figure 6: *Olive fruit fly sub-model test*

5.5. Discussion

The new model has fewer parameters than other models (e.g. López-Bernal et al., 2018), which facilitates meta-modelling (Colbach, 2010) and a possible future use in operative context as parametric insurance, or decision support systems (DSS) to support the manage olive fruit fly.

5.5.1. Olive trees sub-model

The model is able to simulate the interannual fluctuation of olive dry mass production (Figure 5), not simulated in López-Bernal et al. (2018), in which the outputs of a biennium were averaged, as there is an empirical but explicit approach to estimate the reserves. The relevance of this approach can also be seen through the sensitivity analysis, as variables such as the number of olives and the variation of olive mass are sensitive to the parameters of this sub-model, whereas the mean olive mass (subject to compensation over the years) is not sensitive to these parameters.

The errors in the parameterisation of AGB, canopy radius and plant height could be explained by the simulation of pruning, which in the model is performed on the day the plant grows back after winter dormancy, whereas we do not know when it was done in the observed data. Furthermore, we used the same set of parameters for all sites, but the varieties and pruning management were different. For final yield, with R^2=0.95, the model performed as well as Moriondo et al. (2019).

For LAI, plant growth was well simulated as in Moriondo at al. (2019), but at full canopy, the model was not able to follow the LAI trend. This variable is difficult to measure in tree plants (Jonckheere et al., 2004) and is variable over space. It is thus difficult to estimate with modelling approaches (Yu et al., 2006; Confalonieri et al., 2009; Tartarini et al., 2019).

5.5.2. Olive fruit fly and their predator sub-models

Considering the limitations of the model: migration/emigration is only related to the number of adult olive fruit flies in the model and not to weather, management and plant conditions, the model is point-like with no relation to nearby points, the model does not consider wild plants in which the olive fruit flies might lay eggs. Despite these limitations, the olive fruit fly model performed well and contrariously to other models (Gutierrez et al., 2009) a comparison whith observation was carried out.

The slightly negative EF (-0.03) and the relatively high RRMSE (90.1%) and CRM (0.53) values are mostly due to the limited sensitivity of the model to the low observed infection values: the majority of the observed values are below 15% but the model for this value estimated an infection near 0%. The high presence of a low measured value resulted in a very low observed mean (about 8%) and the small mean absolute error (MAE=5.5%) resulted in a negative EF (Criss and Winston, 2008) and a high RRMSE. The highest value was well simulated, but the underestimation of the low value is high, resulting in a high CRM.

5.6. Summary and concluding remarks

The model developed here includes a set of empirical equations, which make it relatively simple and usable for the estimation of several processes. The substantial agreement between the simulations and experimental data, obtained under a range of environmental and management conditions in olive

groves representative of Mediterranean areas, demonstrates that the new model is an appropriate approach for estimating the dynamic behaviour of olive trees and olive fruit fly populations.

This study is one of the few to consider explicit and dynamic modelling of olive trees and the main pest of olive groves and, although its limitations, it holds potential (with a different calibration or small modifications) for extension to the estimation of the interaction between other tree crops and insect species. However, the point-like nature of the model and the situations used for modelling raise the need for a broader assessment. First, this means that solutions based on the new model may potentially be suitable for applications at other olive grove areas if the model parameters are documented for those areas other than the ones investigated here. Then, it is desirable to better understand the evolution of olive grove functioning in the current context of global change in order to study whether the interaction between olive trees and its main pest can be modelled at the local scale, projected to the long term and extended to other regions.

In conclusion, this study confirms that the new olive tree-olive fruit fly modelling solution can be easily implemented, although some basic knowledge is needed to parametrize each individual sub-model in an olive grove. As the biophysical structure of the model reflects important determinants of the functioning of olive tree systems, we advocate its use to predict the behaviour of relevant olive grove outputs. We recommend that further tests be carried out in different areas, given the need to evaluate the modelling approach in contrasting biogeographical regions (beyond the Mediterranean region), where the olive fly is also present. Further research aimed at developing scalable and open solutions for a wide range of olive groves, while addressing issues of reuse and interconnection of model components, can be seen as the natural evolution of this study. Not negligible is the possibility use the model in operative context for the tested region to support the olive grove directly as DSS or indirectly as parametric insurance via metamodeling techniques.

Acknowledgements

The study has been funded by Generali Italia S.p.A.

5.7. Supplementary material

Appendix A., Model parameters: *Parameters: is the name used in equation; Default: the value used as default and as average of a normal distribution (with 5% -of average- as standard deviation and queue trunked to 0.1- exceptions are reported in footnotes); Value: parametrized value; ID: sensitivity analysis number: not used for fly model; if it is "-" this parameter are not used in sensitivity analysis.*

Parameters	Description	Default	Value	Units	ID
		Olive trees			
Dl_{PAo}	Threshold daylength to dormancy or regrowth	10.5[f]	10.5 [f]	Hours	20
T_{PAo}	Threshold temperature to dormancy or regrowth	9.1 [f]	9.1 [f]	°C	21
$T_{max,od}$	Cut-off temperature to development	37 [f]	39.2734	°C	1
$T_{opt,od}$	Optimal temperature to development	32 [f]	31.8521	°C	2
T_{vopt}	Optimal temperature to vernalize	7.3 [f]	7.3	°C	22
T_{vmax}	Maximum temperature to vernalize	20.7 [f]	20.7 [f]	°C	23
$deCU$	Maximum de-vernalization rate	-0.56 [f]	-0.56 [f]	°C d	24
CU_v	Chilling unit to vernalization	469 [f]	469 [f]	°C d	25
$GDD_{o,fl}$	Thermal time to flowering	400 [f]	550	°C d	3
$GDD_{o,mat}$	Thermal time to fruit maturity	3200 [f]	2600	°C d	4
k	Extinction coefficient	0.578	0.49651	(-)	5[a]
$T_{max,PhO}$	Cut-off temperature to growth	37 [f]	39.2734	°C	1
$T_{b,PhO}$	Base temperature to growth	9.1	9.1	°C	21
$T_{opt,PhO}$	Optimal temperature to growth	32 [f]	31.8521	°C	2
WS_{tol}	Water stress tolerance	3	3	(-)	-

RAD_t	Threshold of radiation to photosystems saturation	30	30	MJ m^{-2}	26
SLA	Specific leaf area	4.5 [f]	5.52717	m^2 kg^{-1}	6
LA	Average single leaf area	0.00048	0.00052	m^2	7[b]
$GDD_{s,oCLdie}$	Thermal time for leaves senescence	10000	10229.2	°C d	8
SOW	Single olive fruit dry weight	0.0005 [f]	0.00621	kg	9
$PBud$	Normal percentage of flowering buds	0.5	0.5	(-)	10
R_{gMinFl}	Minimum percentage of reserves to flowering	0.07	0.29708	(-)	11
$R_{min,m}$	Minimum percentage of reserves to allocate them	0.05	0.04968	(-)	12
R_q	Maximum reserve quote translocated in a day	0.1	0.1	(-)	13
$GDD_{o,Rend}$	Thermal time to end initial reserve remobilization	100	66.793	°C d	14
$EffR$	Reserve translocation efficiency	0.55	0.54225	(-)	15
rHr	Relation between radius and height of canopy	0.45	0.69793	(-)	18
K_c	Crop evapotranspiration coefficient	1	1	(-)	-
$T_{max,RespO}$	Cut-off temperature to respiration	40	40	°C	27
SFA	Specific fruit area	0.00001	0.00001	m^2 kg^{-1}	28
STA	Specific twig area	0.00002	0.00002	m^2 kg^{-1}	29
$GDD_{o,flini}$	Thermal time to start flowering	340	490	°C d	-
$GDD_{o,flend}$	Thermal time to end flowering	640	790	°C d	-

$AllC$	Allegation coefficient	0.07	0.14593	(-)	16
$BudNFl$	Number of flowers a bud	12	12	#	30[c]
$T_{hot,die}$	Maximum temperature for total defoliation	55	55	°C	-
$T_{Ster,hot,crit}$	Threshold maximum temperature for hot sterility	33	33	°C	-
$T_{Ster,hot,die}$	Critical maximum temperature for hot sterility	37	37	°C	-
$T_{Ster,cold,die}$	Threshold minimum temperature for cold sterility	8	8	°C	-
$T_{Ster,cold,crit}$	Critical minimum temperature for hot sterility	15	15	°C	-
$T_{hot,crit}$	Critical maximum temperature for defoliation	40	40	°C	-
$p,period,pl$	Critical consecutive days of drouth for plant die	30	30	d	-
$WS_{crit,pl}$	Water strass threshold to plant die	0.01	0.01	(-)	-
$p,period,wo$	Critical consecutive days of drouth for branch die	20	20	d	-
$WS_{crit,wo}$	Water strass threshold to branch die	0.02	0.02	(-)	-
$p,period,ts$	Critical consecutive days of drouth for twigs death	10	10	d	-
$WS_{crit,ts}$	Water strass threshold to twigs death	0.1	0.1	(-)	-
$p,period,le$	Critical consecutive days of drouth for leaves death	10	10	d	-

$WS_{crit,le}$	Water strass threshold to leaves death	0.3	0.3	(-)	-
$T_{freeze,tw,die}$	Minimum temperature for twigs death	-12	-12	°C	-
$T_{freeze,pl,crit}$	Threshold minimum temperature for plant	-10	-10	°C	-
$T_{freeze,le,crit}$	Threshold minimum temperature for leaves	-2	-2	°C	-
$T_{freeze,le,die}$	Minimum temperature for leaves death	-7	-7	°C	-
$T_{freeze,tw,crit}$	Threshold minimum temperature for twigs	-3	-3	°C	-
$T_{freeze,pl,die}$	Minimum temperature for plant death	-20	-20	°C	-
$T_{freeze,wo,crit}$	Threshold minimum temperature for branch	-8	-8	°C	-
$T_{freeze,wo,die}$	Minimum temperature for branch death	-18	-18	°C	-
$T_{freeze,of,die}$	Minimum temperature for fruit death	-4	-4	°C	-
$T_{freeze,of,crit}$	Threshold minimum temperature for olive	0	0	°C	-
LAI_{SC}	Leaf area index for maximum self-shading	8	8	$m^2\ m^{-2}$	31
LAI_{ST}	Threshold leaf area index to self-shading	3	3	$m^2\ m^{-2}$	33
RUE	Maximum radiation use efficiency	2[h]	2.22216	$g\ MJ^{-1}$	17
$GLAI_r$	Minimum leaf area index to re-growth	0.8	0.8	$m^2\ m^{-2}$	32
OD_{PTh}	Minimum rate of olive demand to olive drop	0.5	0.5	(-)	34
ODr_R	Olive drop tolerance	0.05	0.05	(-)	35
Id	Internode distance	20	11.8413	cm	19
	Olive fruit fly				
NEM	Max daily number of egg produced by a female	15[g]	15[g]	#	[d]

W_t	Threshold of wind to limit the fly	5	4.86779	m s^{-1}	
W_m	Threshold of wind to stop the fly	20	18.6187	m s^{-1}	
$T_{b,4}$	Base temperature for adult development	8 [g]	8 [g]	°C	
$T_{max,4}$	Maximum temperature for adult development	33 [g]	33 [g]	°C	
$T_{opt,4}$	Optimal temperature for adult development	29 [g]	29 [g]	°C	
$T_{b,1}$	Base temperature for egg development	6.3 [g]	6.3 [g]	°C	
$T_{max,1}$	Maximum temperature for egg development	35 [g]	35 [g]	°C	
$T_{opt,1}$	Optimal temperature for egg development	31 [g]	31 [g]	°C	
$T_{b,2}$	Base temperature for larvae development	6.3 [g]	6.3 [g]	°C	
$T_{max,2}$	Maximum temperature for larvae development	35 [g]	35 [g]	°C	
$T_{opt,2}$	Optimal temperature for larvae development	29 [g]	29 [g]	°C	
$T_{b,3}$	Base temperature for pupae development	8 [g]	8 [g]	°C	
$T_{max,3}$	Maximum temperature for pupae development	33 [g]	33 [g]	°C	
$T_{opt,3}$	Optimal temperature for pupae development	29 [g]	29 [g]	°C	
$T_{CH,4}$	Maximum temperature for adult	36 [g]	35.6729	°C	
$T_{TH,4}$	No damage maximum temperature for adult	29 [g]	29.3711	°C	
$T_{CC,4}$	Minimum temperature for adult	-9.75 [g]	-9.3849	°C	
$T_{TC,4}$	No damage minimum temperature for adult	0 [g]	0 [g]	°C	[e]
$T_{CH,2}$	Maximum temperature for larvae	40 [g]	34.6804	°C	

$T_{TH,2}$	No damage maximum temperature for larvae	29 [g]	30.4271	°C	
$T_{CC,2}$	Minimum temperature for larvae	-12 [g]	-12 [g]	°C	
$T_{TC,2}$	No damage minimum temperature for larvae	0 [g]	0 [g]	°C	e
$T_{CH,3}$	Maximum temperature for pupae	36 [g]	38.8763	°C	
$T_{TH,3}$	No damage maximum temperature for pupae	29 [g]	29.7902	°C	
$T_{CC,3}$	Minimum temperature for pupae	-12 [g]	-12 [g]	°C	
$T_{TC,3}$	No damage minimum temperature for pupae	0 [g]	0 [g]	°C	e
$T_{CH,1}$	Maximum temperature for egg	42	42	°C	
$T_{TH,1}$	No damage maximum temperature for egg	35 [g]	35 [g]	°C	
$T_{CC,1}$	Minimum temperature for egg	-1	-1	°C	
$T_{TC,1}$	No damage minimum temperature for egg	0	0	°C	e
FN_{min}	Minimum number of adult for oviposition	3	3	#	d
FN_{opt}	Optimal number of adult for oviposition	6	6	#	d
FN_{opt1}	Optimal 2 number of adult for oviposition	700	700	#	
FN_{max}	Maximum number of adult for oviposition	800000	800000	#	
$T_{max,o}$	Maximum temperature for oviposition	33	33	°C	
$T_{min,o}$	Minimum temperature for oviposition	12	12	°C	
$T_{o,o}$	Optimal temperature for oviposition	29	29	°C	
Dl_{ov}	Threshold day-length for oviposition	13.4	13.4	Hours	

cum, px	Number of day to consider the rain to pupae metamorphosis	15	15	d	[d]
R_{CM}	Critical cumulated rain to pupae metamorphosis	5	8.13541	mm	
R_{TM}	No damage cumulated rain to pupae metamorphosis	15	36.7238	mm	
$PLik_{c,ph1}$	Predation coefficient egg	0.1	0.1	(-)	
$PLik_{c,ph2}$	Predation coefficient larvae I	0.3	0.3	(-)	
$PLik_{c,ph3}$	Predation coefficient larvae II	0.3	0.3	(-)	
$PLik_{c,ph4}$	Predation coefficient larvae III	0.4	0.4	(-)	
$PLik_{c,ph5}$	Predation coefficient pupae	0.4	0.4	(-)	
$PLik_{c,ph6}$	Predation coefficient adult	0.05	0.05	(-)	
fM	Minimum death daily coefficient	0.0001	0.0001	(-)	
DM_{Ph1}	Drop death coefficient egg	0.8	0.8	(-)	
DM_{Ph2}	Drop death coefficient larvae I	0.75	0.75	(-)	
DM_{Ph3}	Drop death coefficient larvae II	0.55	0.55	(-)	
DM_{Ph4}	Drop death coefficient larvae III	0.15	0.15	(-)	
DM_{Ph5}	Drop death coefficient pupae	0.01	0.01	(-)	
$t - x$	Day of delay of predator population	5	15	d	[d]
$EFpPor$	Optimal number of fly daily eaten by a predator	0.2	1	#	

$TFPE$	Theoretical fly predator ratio at equilibrium	50	50	#
Dl_{PA}	Day-length to dormancy	11	11	hour
T_{PA}	Temperature to dormancy	7	7	°C
GDD_{hat}	Thermal time to reach larvae I	56.55 [g]	56.55 [g]	°C d
GDD_{l2}	Thermal time to reach larvae II	118.8 [g]	118.8 [g]	°C d
GDD_{l3}	Thermal time to reach larvae III	181.2 [g]	181.2 [g]	°C d
GDD_{pu}	Thermal time to reach pupae	243.55 [g]	243.6 [g]	°C d
GDD_{AD1}	Thermal time to reach adult	491.6 [g]	491.6 [g]	°C d
GDD_{die}	Thermal time to reach die	1503.8 [g]	1119.6	°C d
PO_t	Predisposition to do only a single egg to olive	0.3	0.00848	(-)
ODC_f	Coefficient of infected olive fruit drop	0.001	0.001	(-)
GDD_{AD2}	Thermal time to reach sexual maturity	573.75[g]	573.75[g]	°C d

[a]: used standard deviation of 0.089044 and average (default value) from Villalobos et al., 2006 and Connor et al., 2012.

[b]: used standard deviation of 0.000041 and average (default value) from Villalobos et al., 2006 and Mohammed and Noori 2008

[c]: uniform, only the integer included in the average ±2 range (extreme and average included).

[d]: uniform, only the three integers of average ±1.

[e]: used standard deviation of 0.05.

[f]: value from López-Bernal et al., 2018.

[g]: value from Gutierrez et al., 2009.

[h]: value from Moriondo et al., 2019.

Appendix B., First order of sensitivity analysis indices for olive fruit fly model.

Parameters	Fly population (#)	Infected olive fruit (%)	Dropped olive fruit (%)
NEM	0.01	0.01	0.01
W_t	0.00	0.00	0.00
W_m	0.00	0.00	0.00
$T_{b,4}$	0.01	0.02	0.01
$T_{max,4}$	0.01	0.02	0.01
$T_{opt,4}$	0.02	0.03	0.03
$T_{b,1}$	0.00	0.00	0.00
$T_{max,1}$	0.00	0.00	0.00
$T_{opt,1}$	0.00	0.00	0.00
$T_{b,2}$	0.00	0.00	0.00
$T_{max,2}$	0.00	0.00	0.01
$T_{opt,2}$	0.00	0.00	0.00
$T_{b,3}$	0.00	0.00	0.01
$T_{max,3}$	0.00	0.00	0.01
$T_{opt,3}$	0.00	0.00	0.01
$T_{CH,4}$	0.00	0.00	0.00
$T_{TH,4}$	0.07	0.13	0.02
$T_{CC,4}$	0.00	0.00	0.01
$T_{TC,4}$	0.00	0.00	0.01
$T_{CH,2}$	0.00	0.00	0.01
$T_{TH,2}$	0.19	0.14	0.03
$T_{CC,2}$	0.00	0.00	0.00
$T_{TC,2}$	0.00	0.00	0.00
$T_{CH,3}$	0.00	0.00	0.00
$T_{TH,3}$	0.22	0.24	0.07
$T_{CC,3}$	0.00	0.00	0.00
$T_{TC,3}$	0.00	0.00	0.00
$T_{CH,1}$	0.00	0.00	0.00

$T_{TH,1}$	0.00	0.00	0.00
$T_{CC,1}$	0.00	0.00	0.00
$T_{TC,1}$	0.00	0.00	0.00
FN_{min}	0.00	0.00	0.01
FN_{opt}	0.00	0.00	0.00
FN_{opt1}	0.00	0.00	0.00
FN_{max}	0.00	0.00	0.00
$T_{max,o}$	0.00	0.00	0.00
$T_{min,o}$	0.00	0.00	0.00
$T_{o,o}$	0.02	0.01	0.00
Dl_{ov}	0.01	0.00	0.00
cum,px	0.04	0.03	0.06
R_{CM}	0.00	0.00	0.00
R_{TM}	0.00	0.00	0.00
$PLik_{c,ph1}$	0.00	0.00	0.00
$PLik_{c,ph2}$	0.00	0.00	0.00
$PLik_{c,ph3}$	0.00	0.00	0.01
$PLik_{c,ph4}$	0.00	0.00	0.00
$PLik_{c,ph5}$	0.00	0.00	0.00
$PLik_{c,ph6}$	0.00	0.00	0.00
fM	0.00	0.00	0.00
DM_{Ph1}	0.00	0.00	0.00
DM_{Ph2}	0.00	0.00	0.00
DM_{Ph3}	0.00	0.00	0.00
DM_{Ph4}	0.00	0.00	0.00
DM_{Ph5}	0.00	0.00	0.01
$t-x$	0.00	0.00	0.00
$EFpPor$	0.00	0.00	0.01
$TFPE$	0.00	0.00	0.00
Dl_{PA}	0.02	0.04	0.01
T_{PA}	0.01	0.01	0.00
GDD_{hat}	0.00	0.00	0.00
GDD_{l2}	0.00	0.00	0.00
GDD_{l3}	0.00	0.00	0.01
GDD_{pu}	0.02	0.01	0.00

GDD_{AD1}	0.06	0.02	0.01
GDD_{die}	0.05	0.12	0.02
PO_t	0.01	0.00	0.00
ODC_f	0.00	0.00	0.00
GDD_{AD2}	0.00	0.00	0.00

Appendix C., Total order of sensitivity analysis indices for olive fruit fly model.

Parameters	Fly population (#)	Infected olive fruit (%)	Dropped olive fruit (%)
NEM	0.13	0.09	0.46
W_t	0.07	0.06	0.43
W_m	0.12	0.10	0.53
$T_{b,4}$	0.12	0.10	0.52
$T_{max,4}$	0.13	0.12	0.51
$T_{opt,4}$	0.14	0.14	0.62
$T_{b,1}$	0.11	0.07	0.47
$T_{max,1}$	0.13	0.09	0.48
$T_{opt,1}$	0.10	0.08	0.36
$T_{b,2}$	0.10	0.07	0.38
$T_{max,2}$	0.12	0.09	0.58
$T_{opt,2}$	0.13	0.09	0.56
$T_{b,3}$	0.13	0.09	0.52
$T_{max,3}$	0.12	0.09	0.43
$T_{opt,3}$	0.11	0.07	0.46
$T_{CH,4}$	0.10	0.07	0.48
$T_{TH,4}$	0.23	0.24	0.55
$T_{CC,4}$	0.10	0.08	0.47
$T_{TC,4}$	0.11	0.09	0.45
$T_{CH,2}$	0.11	0.08	0.46
$T_{TH,2}$	0.34	0.24	0.55
$T_{CC,2}$	0.12	0.08	0.49
$T_{TC,2}$	0.10	0.07	0.55
$T_{CH,3}$	0.09	0.06	0.41
$T_{TH,3}$	0.39	0.37	0.62
$T_{CC,3}$	0.13	0.08	0.54

$T_{TC,3}$	0.10	0.06	0.44
$T_{CH,1}$	0.09	0.06	0.38
$T_{TH,1}$	0.12	0.09	0.49
$T_{CC,1}$	0.10	0.07	0.45
$T_{TC,1}$	0.11	0.07	0.36
FN_{min}	0.10	0.06	0.45
FN_{opt}	0.11	0.07	0.39
FN_{opt1}	0.07	0.04	0.40
FN_{max}	0.10	0.09	0.42
$T_{max,o}$	0.13	0.09	0.46
$T_{min,o}$	0.12	0.08	0.46
$T_{o,o}$	0.16	0.08	0.45
Dl_{ov}	0.12	0.10	0.45
cum, px	0.15	0.12	0.54
R_{CM}	0.12	0.09	0.51
R_{TM}	0.12	0.09	0.48
$PLik_{c,ph1}$	0.10	0.06	0.41
$PLik_{c,ph2}$	0.10	0.07	0.39
$PLik_{c,ph3}$	0.12	0.08	0.43
$PLik_{c,ph4}$	0.11	0.08	0.36
$PLik_{c,ph5}$	0.09	0.07	0.49
$PLik_{c,ph6}$	0.10	0.07	0.43
fM	0.10	0.07	0.46
DM_{Ph1}	0.09	0.07	0.49
DM_{Ph2}	0.09	0.06	0.40
DM_{Ph3}	0.07	0.05	0.42
DM_{Ph4}	0.09	0.05	0.45
DM_{Ph5}	0.13	0.09	0.48
$t - x$	0.11	0.08	0.53
$EFpPor$	0.09	0.06	0.44
$TFPE$	0.11	0.07	0.40
Dl_{PA}	0.15	0.14	0.50
T_{PA}	0.13	0.12	0.43
GDD_{hat}	0.15	0.11	0.47
GDD_{l2}	0.08	0.06	0.43
GDD_{l3}	0.11	0.08	0.46
GDD_{pu}	0.15	0.10	0.42

GDD_{AD1}	0.17	0.10	0.46
GDD_{die}	0.24	0.28	0.74
PO_t	0.12	0.07	0.43
ODC_f	0.09	0.06	0.33
GDD_{AD2}	0.11	0.08	0.48

Olive fruit fly sub-model

The Model is a population model as in Gutierrez *et al*., 2009. It divides the population in cohorts of fly that are born contemporaneously at same time step (daily).

Thermal time

The model starts the simulation updating olive fruit fly (*Bactrocera oleae* (Gmelin)) phenology (eq. 2) basing on temperature $GDD_{r,i}$ using a no linear function (Gutierrez *et al*., 2009) the equation used was a beta function as in plant phenology of WOFOST_GT2 (Stella *et al*., 2014 - eq. 1)

Equation 1

$$\forall_{i=1}^{4} \begin{cases} Active & GDD_{r,i} = \left(\frac{T_{avg} - (T_{b,i} - 2)}{T_{opt,i} - (T_{b,i} - 2)} \cdot \left(\frac{(T_{max,i} + 2) - T_{avg}}{(T_{max,i} + 2) - T_{opt,i}}^{\frac{(T_{max,i}+2)-T_{opt,i}}{T_{opt,i}-(T_{b,i}-2)}} \right) \right)^{s} \cdot (T_{opt,i} - T_{b,i}) \\ Dormancy & GDD_{r,i} = 0 \end{cases}$$

Where i, is the considered phenological stage that have different phenology parameters (table 1), T_{avg} is the average daily air temperature is a weather variable, $T_{b,i}$ is the base temperature to develop at a specific phenological stage, $T_{opt,i}$ is the optimal temperature to develop at a specific phenological stage, $T_{max,i}$ is the maximum temperature to develop at a specific phenological stage the lasts are parameters and the value are derived from Gutierrez *et al*., 2009 and Giglioli and Pasquali 2007; s is an empiric shape coefficient and its value is set to 1.8. If T_{avg} is below $T_{b,i}$ or above $T_{max,i}$, there is not accumulation of thermal time for the selected phenological stage. The dormancy status is described tanks the equation 3.

Table 1: *Phenological stage that use different temperature for development: the whole list of phenological phasis are available in table 2 according to Gutierrez et al., 2009*

Code (i)	Phenological stage
1	Egg
2	Larva
3	Pupae
4	Image or adult

At each time step (day) the accumulation of thermal time ($GDD_{s,i,c}$) is updated according the equation 2

Equation 2

$$\forall_{i=1}^{4}[\![\forall_{c=1}^{c=n}[\![GDD_{s,i,c} = GDD_{s,i,c,t-1} + GDD_{r,i}$$

Where c, is the cohorts of the olive fruit flies that belong to the same phenological stage, n is the total number of cohorts and $GDD_{s,i,c,t-1}$ is the thermal time of the previous day

Dormancy

The effect of dormancy is a stop of phenological development and of reproductive activities. Dormancy effects and estimation are transversal to all phenological phases. It is estimated according temperature and day length (eq. 3).

Equation 3

$$\begin{cases} Active & \begin{cases} Dl < Dl_{PA} \,\&\, T_{avg7} < T_{PA} & Dormancy \\ else & Active \end{cases} \\ Dormancy & \begin{cases} Dl > Dl_{PA} \,\&\, T_{avg7} > T_{PA} & Active \\ else & Dormancy \end{cases} \end{cases}$$

In were Dl is the day length Dl_{PA} is the threshold of day length to phenological activity, T_{avg7} is the average temperature of the current day and six previous days and T_{PA} is the threshold temperature to phenological activity.

Phenological phases

For each cohort, the accumulation of thermal time is compared to a threshold parameter to estimate the phenological progress at the next phenological phase as in table 2

Table 2: *Considered phenological phases and relative parametres to reaching*

Criteria	Phenological phase (ph)
$0 \leq GDD_{s,c} < GDD_{hat}$	Egg ($ph1$)
$GDD_{hat} \leq GDD_{s,c} < GDD_{l2}$	Larva 1st stage ($ph2$)
$GDD_{l2} \leq GDD_{s,c} < GDD_{l3}$	Larva 2nd stage ($ph3$)
$GDD_{l3} \leq GDD_{s,c} < GDD_{pu}$	Larva 3rd stage ($ph4$)
$GDD_{pu} \leq GDD_{s,c} < GDD_{AD1}$	Pupae ($ph5$)
$GDD_{AD2} \leq GDD_{s,c} < GDD_{AD2}$	Not reproductive adult ($ph6$)
$GDD_{AD2} \leq GDD_{s,c} < GDD_{die}$	Reproductive adult ($ph6$)
$GDD_{s,c} \geq GDD_{die}$	Death

Where GDD_{hat} is the thermal time to egg hatching, GDD_{l2} is the minimum thermal time to have larva of 2nd stage, GDD_{l3} is the minimum thermal time to have larva of 3rd stage, GDD_{pu} is the minimum thermal time to have pupae, GDD_{AD1} is the minimum thermal time to have adult forms, GDD_{AD2} is the minimum thermal time to have reproductive adult forms and GDD_{die} is the average thermal time of flies death.

Reproduction

The daily eggs production (eq. 4, E_t) is estimated by the sum of the eggs produced by all the cohorts in reproductive adult phases. E_t value is considered the number of individuals of a new cohort (FN_a) of eggs.

Equation 4

$$E_t = \sum_{a=1}^{n} E_a$$

Where a are the cohorts that are in active reproductive phase and E_a (eq. 5) is the number of eggs produces by a specific cohort.

Equation 5

$$E_a = MET \cdot C_{m,a} \cdot C_{age,a} \cdot FN_a$$

Where MET is a variable that describe the actual eggs production per olive fruit fly at the today environmental conditions (eq. 7) $C_{m,a}$ is the coefficient of males in the cohort (it is set for each cohort to 0.5), $C_{age,a}$ is the age coefficient of the cohort (eq. 6) introduced also in Gutierrez *et al*., 2009 and FN_a is the total flies number of the cohort.

Equation 6

$$C_{age,a} \begin{cases} GDD_a < GDD_{optE} & \left(\frac{GDD_a - (GDD_{AD2} - 2)}{GDD_{o,E} - (GDD_{AD2} - 2)} \cdot \left(\frac{(GDD_{die} + 2) - GDD_a}{(GDD_{die} + 2) - GDD_{o,E}} \right)^{\frac{(GDD_{die}+2) - GDD_{o,E}}{GDD_{o,E} - (GDD_{AD2} - 2)}} \right)^{s} \\ GDD_a \geq GDD_{optE} & 1 - \frac{GDD_a - GDD_{o,E}}{GDD_{die} - GDD_{o,E}} \end{cases}$$

Where $GDD_{o,E}$ is a parameter to the optimum thermal time to eggs production and $GDD_a$is the thermal time accumulated by the specific cohort of reproductive adults.

Equation 7

$$MET = NEM \cdot (1 - fWO) \cdot (1 - fPOO) \cdot (1 - fPO) \cdot (1 - fPODO) \cdot (1 - fFPO) \cdot (1 - fTO)$$

Where NEM is a parameter that describe the pick of possible number of eggs produced by a female, fWO is the wind effect on oviposition (eq. 8), $fPOO$ is the effect of the olive phenology on oviposition (eq. 9), fPO is the effect of the photoperiod on oviposition (eq. 11), $fPODO$ is the effect of the percentage of infected olive fruits on oviposition (eq. 12), $fFPO$ is the effect of the olive fruit fly population on oviposition (eq.14) and fTO is the effect of air temperature on oviposition (eq. 15).

Equation 8

$$fWO\begin{cases} W < W_t & 0 \\ W_t \leq W \leq W_m & \dfrac{W - W_t}{W_m - W_t} \\ W > W_m & 1 \end{cases}$$

Where W is the daily average wind speed W_t is the threshold of wind speed to disturb the flight of flies and W_m is the maximum wind speed to the flight of flies. The wind effect is to intend as a redaction of flights done by female flies in case of excessive wind.

Equation 9

$$fPOO\begin{cases} GDD_{s,o} < 900 & 1 \\ 900 \leq GDD_{s,o} \leq GDD_{sen} & 1 - \dfrac{GDD_{s,o} - 900}{GDD_{sen} - 900} \\ GDD_{s,o} > GDD_{sen} & 0 \end{cases}$$

In which: $GDD_{s,o}$ is the thermal time accumulate by olive trees (eq. 34) and GDD_{sen} is the thermal time to sensible period (eq. 10; hardening of seed; Gutierrez *et al*., 2009).

Equation 10

$$GDD_{sen} = 500 + GDD_{fl}$$

In which GDD_{fl} is the thermal time to olive trees flowering

Equation 11

$$fPO\begin{cases} Dl < Dl_{PA} & 1 \\ Dl_{PA} \le Dl \le Dl_{ov} & 1 - \dfrac{Dl - Dl_{PA}}{Dl_{ov} - Dl_{PA}} \\ Dl > Dl_{ov} & 0 \end{cases}$$

Where Dl_{ov} is the optimal day length to eggs production.

Equation 12

$$fPODO\begin{cases} I_{Dolive} < PO_t & 0 \\ PO_t \le I_{Dolive} \le 600 & \left(\dfrac{I_{Dolive} - (PO_t - 2)}{600 - (PO_t - 2)} \cdot \left(\dfrac{(652) - I_{Dolive}}{52}^{\frac{52}{600-(PO_t-2)}}\right)\right)^s \\ I_{Dolive} > 600 & 1 \end{cases}$$

Where I_{Dolive} is an index of olive fruit infected by olive fruit flies (eq. 13), it range between 0 and 600 it means 0 no infection 600 each olive fruit has been hit 6 time by olive fruit fly (it is not taken into account if the insects are still in fruit or not) and PO_t is a parameter that describe the minimum percentage of infected olive to have an olive hit at least twice. The olive fruit fly has the preference to do a unique egg per olive fruit but if olive fruits are not reachable or are hit in large part the olive fruit are re-hit but in this case the oviposition activity decreases. A similar approach is used in Gutierrez at al., 2009.

Equation 13

$$I_{Dolive} = \frac{6 \cdot N_{olive,t} - E_{y,t}}{6 \cdot N_{olive,t}} \cdot 600$$

Where $N_{olive,t}$ is the olive fruit number at current time-step and $E_{y,t}$ is the total number of produced eggs in the current season updated at current time step.

Equation 14

$$fPODO\begin{cases} FN < FN_{min} & 0.5 \\ FN_{min} \le FN < FN_{opt} & 0.5 \cdot \left(1 - \dfrac{FN - FN_{min}}{FN_{opt} - FN}\right) \\ FN_{opt} \le FN \le FN_{opt1} & 0 \\ FN_{opt1} < FN \le FN_{max} & \dfrac{FN - FN_{opt2}}{FN_{opt2} - FN_{max}} \\ FN > FN_{max} & 1 \end{cases}$$

Were FN is the total number of reproductive adults, FN_{min} is the number of adult to reduce of the half the meeting probability FN_{opt} and FN_{opt1} are the population level that minimizes the disturbance effect and maximizes the probability to meet and FN_{max} is the total number of adults in which the disturbance effect inhibits the oviposition. The assumption is that a low number of olive fruit flies per hectare limit the olive fruit fly meeting and a higher number, at opposite, favours the meeting and it disturbs the female during oviposition.

Equation 15

$$fTO\begin{cases} T_{min,o} \le T_{avg} \le T_{max,o} & 1 - \left(\dfrac{T_{avg} - (T_{min,o} - 2)}{T_{o,o} - (T_{min,o} - 2)} \cdot \left(\dfrac{(T_{max,o} + 2) - T_{avg}^{\frac{(T_{max,o}+2) - T_{o,o}}{T_{o,o} - (T_{min,o} - 2)}}}{(T_{max,o} + 2) - T_{o,o}}\right)\right)^{s} \\ else & 1 \end{cases}$$

Where $T_{min,o}$ is the minimum air temperature to ovopositon, $T_{max,o}$ is the maximum air temperature for ovoposition and $T_{o,o}$ is the optimal temperature to oviposition.

Impacts on olive

The model considers both impacts: on quality of the harvested olive (infected olive; eq. 16) and on the quantity of production considering the olive fruits that drop (eq. 17).

Equation 16

$$IOP\begin{cases} I_{Dolive} < PO_t & I_{Dolive} \\ else & Max\left\{ \frac{PO_t}{100} + \left(1 - \frac{PO_t}{100}\right) \cdot \left(\frac{I_{Dolive} - (PO_t - 2)}{600 - (PO_t - 2)} \cdot \left(\frac{(652) - I_{Dolive}}{52}^{\frac{52}{600-(PO_t-2)}} \right) \right)^{s} \cdot 100 \right. \end{cases}$$

Where $IOP$is the percentage of infected olive.

Equation 17

$$N_{olive,df} = N_{olive,t} \cdot \frac{IOP}{100} \cdot ODC_f$$

Where $ODC_f$is the olive drop coefficient due to fly infections, it is a parameter, $N_{olive,d}f$ is the infected olive fruits dropped today due to olive fruit fly.

Mortality

The model estimate a mortality trigged by environmental, management, aging and unknown causes (Genc and Nation, 2008; Gutierrez *et al*., 2009).

For eggs, larvae (all three phases) and pupae we estimated the mortality ($M_{I,r}$; eq. 18) at the same way using parameters phase specific. For the adult form ($M_{A,r}$; eq. 19) a natural mortality (per aging) it is added when the GDD_{die} is reached; it is also added a mortality coefficient in transition between pupae and adult (fMM; eq. 29).The adult mortality does not consider the olive drop ($fMDO$; eq. 21).

Estimation of mortality is done at cohort level.

Equation 18

$$M_{I,r} = FN_a \cdot (1 - fMP) \cdot (1 - fM) \cdot (1 - fMDO) \cdot (1 - fMC) \cdot (1 - fMT) \cdot (1 - fMFH)$$

In which fMP is the mortality due to the presence of natural predators, fM is a parameter that describe young case of death apparently without explanation,

$fMDO$ is the death due to the drop of host olive fruit (eq. 21) , fMC is the effect of the chemical treatment: the efficiency of the treatment, fMT is the effect on death of air temperature (eq. 20), $fMFH$ is the effect of olive harvest: only a percentage of immature olive fruit fly satays in the field according to the harvest efficiency.

Equation 19

$$M_{A,r}\begin{cases} GDD_{a,t-1} < GDD_{AD1} \leq GDD_a & FN_a \cdot (1-fMP)\cdot(1-fM)\cdot(1-fMC)\cdot(1-fMT)\cdot(1-fMM) \\ GDD_a \geq GDD_{die} & FN_a \\ else & FN_a \cdot (1-fMP)\cdot(1-fM)\cdot(1-fMC)\cdot(1-fMT) \end{cases}$$

Equation 20

$$fMT = \begin{cases} T_{CC,i} < T_{avg} < T_{TC,i} & \left(\frac{T_{avg} - (T_{CC,i} - 3)}{3} \cdot \left(\frac{(T_{TC,i}+2) - T_{avg}}{(T_{TC,i}+2) - T_{CC,i}}^{\frac{(T_{TC,i}+2)-T_{CC,i}}{3}}\right)\right)^s \\ T_{TC,i} < T_{avg} < T_{TH,i} & 1 \\ T_{TH,i} < T_{avg} \leq T_{CH,i} & 1 - \left(\frac{T_{avg} - (T_{TH,i} - 3)}{3} \cdot \left(\frac{(T_{CH,i}+2) - T_{avg}}{(T_{CH,i}+2) - T_{TH,i}}^{\frac{(T_{CH,i}+2)-T_{TH,i}}{3}}\right)\right)^s \\ else & 0 \end{cases}$$

Where $T_{CC,i}$ is the critical cold temperature below witch all fly die, $T_{TC,i}$ is the threshold cold temperature below witch flies start to die, $T_{TH,i}$ is the threshold hot temperature above witch flies start to die, $T_{CH,i}$ is the critical hot temperature above witch all flies die. Those parameters are specific per the phenological phases listed following: 1) Egg, 2) Larva, 3) Pupae and 4) adults (without discrimination between mature or not); and they assume different values per phenological phase.

Equation 21

$$fMDO = \frac{IF_d}{IFN} \cdot DM_{Ph}$$

For each phenology stage· DM_{Ph} assume different values. This parameter is the mortality rate at drop eventuality, IF_d is the total amount of immature olive fruit flies that drop (eq. 22).

Equation 22

$$IF_d = N_{olive,di} \cdot IF_o$$

Where $N_{olive,di}$ is the total number of olive dropped in which there is the active infection of fly and IF_o is the number of immature forms that are in average present in an infected olive fruit (eq. 23).

Equation 23

$$N_{olive,di} = \frac{N_{olive,AI}}{N_{olive,I}} \cdot \left(N_{olive,df} + N_{olive,dnf} * IOP/100\right)$$

Where $N_{olive,AI}$ is the number of olive fruits in which there are an active infection (eq. 25), $N_{olive,I}$ is the number of olive fruit infected in total (active or not; eq. 24), $N_{olive,dnf}$ are the olive that drop for other causes.

Equation 24

$$N_{olive,I} = N_{olive} \cdot IOP/100$$

Equation 25

$$N_{olive,AI} = N_{olive} \cdot IOP_{at}/100$$

Where IOP_{at} is the active level of infections (eq. 26).

Equation 26

$$IOP_{at} \begin{cases} IOP_{at6} < PO_t & I_{Dolive} \\ else & Max \begin{cases} \frac{I_{Dolive}}{6} \\ \frac{PO_t}{100} + \left(1 - \frac{PO_t}{100}\right) \cdot \left(\frac{IOP_{at6} - (PO_t - 2)}{600 - (PO_t - 2)} \cdot \left(\frac{(652) - IOP_{at6}^{\frac{52}{600-(PO_t-2)}}}{52}\right)\right)^s \cdot 100 \end{cases} \end{cases}$$

Where IOP_{at6} is the actual percentage of olive infected without considering multiple ovoposition (eq. 27).

Equation 27

$$IOP_{at6} = \frac{IFN}{N_{olive,t}} * 100$$

Where IFN is the total number of immature flies (eq. 28).

Equation 28

$$IF_o = \frac{IFN}{N_{olive,AI}}$$

Equation 29

$$fMM \begin{cases} R_{cum,px} < R_{CM} & 1 \\ R_{CM} \leq R_{cum,px} \leq R_{TM} & 1 - \dfrac{R_{cum,px} - R_{CM}}{R_{TM} - R_{CM}} \\ R_{cum,px} > R_{TM} & 0 \end{cases}$$

Where $R_{cum,px}$ is the cumulated daily rain of a fixed number of previous day R_{CM} is the critical cumulated rain value at witch all pupae in metamorphose die and R_{TM} is the threshold cumulated ran above witch there is no fly death.

Migration / Immigration

The fly movements (in and out the simulated field) are simulated but the unique driver that is involved is the adult population number.

The emigration (C_e; eq. 30) is estimated only if adults are active (not dormant), and all the olive fruits were hit 6 time.

Equation 30

$$C_e \begin{cases} FN \geq FN_{opt} & Max\left(0.99, \dfrac{FN - FN_{opt}}{FN_{max} - FN_{opt}}\right) \\ FN < FN_{opt} & 0 \end{cases}$$

C_e is applied to the adult population to determinate the number of adults remained in the field (FN_f) according to equation 31.

Equation 31

$$FN_f = FN \cdot (1 - C_e)$$

Also immigration is estimate if population are too low (lower than 2) and if the olive has already been harvested. The approach generates a new cohort of 100 reproductive adults.

Olive sub-model

The olive trees model is a crop model able to estimate at daily time step various process of the olive trees including lignification, photosynthesis, phenological development, organ growth, respiration, lignification senescence in function to various environmental and management driver, the model is linked to the olive fruit flies model thanks the olive fruit weight and phenology.

Phenology

The phenology development is reset at plant regrowth, after the winter dormient period. The dormancy or active growth phase is estimate according the equation 32

Equation 32

$$\begin{cases} Active & \begin{cases} Dl < Dl_{PAo} \,\&\, T_{avg7} < T_{PAo} & Dormancy \\ else & Active \end{cases} \\ Dormancy & \begin{cases} Dl > Dl_{PAo} \,\&\, T_{avg7} > T_{PAo} & Active \\ else & Dormancy \end{cases} \end{cases}$$

As in olive fruit fly the dormancy per olive tree is estimated according to the threshold day length that induce dormancy or phenological activity Dl_{PAo} and a threshold temperature (T_{PAo}).

Phenology development is trigged by temperature (eq. 35, eq. 36) and water stress (eq. 91) and is summarized in a code (DVS; eq. 33).

Equation 33

$$DVS \begin{cases} GDD_{s,o} \leq GDD_{o,fl} & \dfrac{GDD_{s,o}}{GDD_{o,fl}} \\ else & 1 + \dfrac{GDD_{s,o} - GDD_{o,fl}}{GDD_{o,mat} - GDD_{o,fl}} \end{cases}$$

The Development stage code (DVS) indicate the flowering when assume value of 1 or closed and the full olive fruit maturation if it assumes value of 2. Its estimation is based on the growing degree days accumulation $GDD_{s,o}$ (eq. 34).

Equation 34

$$GDD_{s,o} = GDD_{s,o,t-1} + GDD_{r,o}$$

Where $GDD_{s,o,t-1}$ is the thermal time accumulated at previous time step and $GDD_{r,o}$ is the current thermal accumulated in current time step (eq. 35, eq. 36, eq. 91).

Equation 35

$$GDD_{r,o} = \left(\frac{T_{avg} - (T_{PAo} - 2)}{T_{opt,od} - (T_{PAo} - 2)} \cdot \left(\frac{(T_{max,od} + 2) - T_{avg}}{(T_{max,od} + 2) - T_{opt,od}}^{\frac{(T_{max,od}+2) - T_{opt,od}}{T_{opt,od} - (T_{PAo} - 2)}} \right) \right)^{s} \cdot (T_{opt,od} - T_{PAo})$$

Where $T_{opt,od}$ is the optimal temperature to olive tree development and $T_{max,od}$ is the maximum temperature for development if $T_{avg}$is higher than $T_{max,od}$ or lower than T_{PAo} no accumulation of thermal time is simulated.

Vernalization

To flower, olive trees need of cold time accumulation (Villalobos et al., 2006; Moriondo *et al*., 2019). The accumulation of cold time CU_s starts when the plant starts the dormancy period and it ends at regrowth (eq. 32). An

insufficient cold accumulation has an effect (CU_e; eq. 37) on a reduction of development rate (eq. 36) and a reduction of flowers next spring.

Equation 36

$$GDD_{r,o} = GDD_{r,o} \cdot (1 - CU_e)$$

Equation 37

$$CU_e = 1 - \frac{CU_m}{CU_v}$$

Where CU_m is the peak of cold time accumulation (CU_s; eq. 38) before the regrowth CU_v is parameter to describe the required cold time to be vernalized.

Equation 38

$$CU_s = \begin{cases} CU_{s,t-1} < CU_v & Max\left(CU_{s,t-1} + CU_r\,, CU_v\right) \\ CU_{s,t-1} \geq CU_v & CU_v \end{cases}$$

Where CU_r is the daily rate of cold time accumulation (eq. 39) and $CU_{s,t-1}$ is cold time at previous time step (daily).

Equation 39

$$CU_r = \begin{cases} T_h \geq 0 & 0 \\ 0 < T_h \leq T_{vopt} & T_h / T_{vopt} \\ T_{vopt} < T_h \leq T_{vmax} & 1 - \left(\left(T_h - T_{vopt}\right) \cdot \frac{1 - deCU}{T_{vmax} - T_{vopt}} \right) \\ T_h > T_{vmax} & deCU \end{cases}$$

Where $T_h$is the hurly air temperature T_{vopt} is the optimal temperature to vernalize T_{vmax} is the maximum temperature to vernalize and $deCU$ is the maximum devernalization rate.

Plant growth

The biomass accumulation (AGB_s; eq. 40) is estimated trough the net photosynthesis (eq. 41) as in Moriondo *et al*., 2019). The radiation interception is estimated according to the beer-lambert law (Swinehart, 1962).

Equation 40

$$AGB_s = AGB_{s,t-1} + AGB_r$$

Where AGB_r is the biomass accumulation rate (eq. 41).

Equation 41

$$AGB_r = (1 - e^{-k \cdot PAI_{s-1}}) \cdot RUE \cdot PAR \cdot 10 \cdot Min(0.95, SCOV)$$

Where k is the coefficient of extinction of solar radiation by canopy, $PAI_{s-1}$is the totality of photosynthetic areas (eq. 43), RUE is the maximum radiation use efficiency, PAR is the photosynthetic active radiation (eq. 42), $SCOV$ is the proportion of covered soil by canopy and 10 is to convert between different units a similar approach is used in Moriondo et al., 2019 (eq. 76).

Equation 42

$$PAR = 0.5 \cdot RAD$$

RAD is the solar radiation that reaches the top of the canopy.

Equation 43

$$PAI_{s-1} = GLAI_{s-1} + (OFM_{s-.1} \cdot SFA) + (TM_{s-1} \cdot STA)$$

Where $GLAI_{s-1}$is the living leaves area index state at previous time step (day), $OFM_{s-.1}$ is the olive fruit mass state at previous time step (day), SFA is the specific olive area, $TM_{s-1}$is the green twigs mass state at previous time step (day) and STA is the specific area of twig.

Limitation on photosynthesis

There is considered two environmental drivers to limit the photosynthesis a thermal limitation (eq. 44) and a self-shading limitation ($SRAD$; eq. 45).

Temperature

Cold and thot temperatures limit the photosynthesis (T_{PhLim}) as below (eq. 44).

Equation 44

$$T_{PhLim} = 1 - \left(\frac{T_{avg} - (T_{b,PhO} - 2)}{T_{opt,PhO} - (T_{b,PhO} - 2)} \cdot \left(\frac{(T_{max,PhO} + 2) - T_{avg}}{(T_{max,PhO} + 2) - T_{opt,PhO}} \right)^{\frac{(T_{max,PhO}+2)-T_{opt,PhO}}{T_{opt,PhO}-(T_{b,PhO}-2)}} \right)^{s}$$

$T_{b,PhO}$ is the base temperature to have photosynthesis, $T_{opt,PhO}$ is the optimal temperature to have photosynthesis and $T_{max,PhO}$ is the max temperature to have photosynthesis. The function is limited to 1 if temperature is above $T_{max,PhO} + 2$ or below $T_{b,PhO}$

Saturation Light

Equation 45

$$SRAD = \begin{cases} RAD \geq 25 \;\&\&\; RAD \geq RAD_t & 1 - (2 - 0.4 \cdot RAD) \\ else & 0 \end{cases}$$

Where $SRAD$ is the radiation saturation coefficient, RAD_t is the threshold above which the photosytwig are saturated.

The actual AGB_{ar} is limited by both T_{PhLim} and $SRAD$ (eq. 46).

Equation 46

$$AGB_{ar} = \begin{cases} T_{avg} \leq T_{max,PhO} & AGB_r \cdot (1 - T_{PhLim}) \cdot (1 - SRAD) \cdot (1 - W_p) \\ T_{max.PhO} < T_{avg} \leq T_{max,PhO+2} & -AGB_{s-1} \cdot (1 - T_{PhLim}) \end{cases}$$

If the temperature is elevated, it is estimated that respiration rate exceeds photosynthesis rate and the accumulation of biomass tend to be 0 or negative. if temperature is too elevated: (above $T_{max,RespO}$)also respiration is null.

Where W_p is the water stress coefficient (eq. 85)

Partitioning

If actual aboveground biomass rate is positive is partitioned in 5 organs: i) leaves, ii) twigs, iii) storage organs (fruits), iv) woody twig, branch and trunk, and v) reserves; according to the development stage code as in López-Bernal *et al.,* 2018, but in opposite our model do not neglect the growing of other organs during ripening phases.

Our model changes partitioning behaviour according to phenological phasis. Starting from regrowth, there is a first phase in which plant growth depends on reserve and the produced organs are only leaves twigs and wood. When a threshold of accumulated thermal time ($GDD_{o,Rend}$) is reached the plant is in vegetative phase and it stops to use reserves and start to accumulate them, biomass is partitioned also to leaves twig and wood. After flowering plant start to accumulate in priority way fruit organ, in this phase if biomass produced exceeds olive demand the biomass in excess is partitioned to reserve leaves, wood and twig else the reserves are used to cover the gap. After olive harvest (or drop) the plant if is in active growth there is in a condition (in terms of partitioning) equal to the vegetative phase mentioned above. If plant is dormant and olive are not ripe, the plant provide to olive demand in opposite the photosynthesized mass is partitioned in reserve.

If $GDD_{s,o} \leq GDD_{o,Rend}$ then the coefficients of partition are 0.3 for leaves, 0.3 for woody organs and 0.4 for green twigs. After this threshold of thermal time if olive fruits are not present, the partition coefficients are 0.3 for leaves, 0.2 for woody organs and 0.4 for green twigs and 0.1 for reserve.

If olive fruit is present, the priority of plant becomes satisfy the olive demand (OD; eq. 48) according equation 47.

Equation 47

$$OFM_r = \begin{cases} AGB_r \leq OD & AGB_r \\ else & \text{Max}(1.5 \cdot OD, 0.5 \cdot (OD + AGB_r)) \end{cases}$$

Where OFM_r is the increasing of olive fruit mass rate.

The remaining quote of AGB_r (if present) is partitioned to various organs basing on the coefficient written above.

Olive demand

The model estimates the daily mass that olive fruits require to growth basing on phenology.

Equation 48

$$OD = \begin{cases} GDD_{s,o} \geq GDD_{o,flini} & \begin{cases} \frac{OFM_{s-.1}}{N_{olive,t-1}} \geq 1.2 \cdot SOW & 0 \\ else & SOW \cdot N_{olive,t-1} \cdot \frac{GDD_{r,o}}{GDD_{o,mat} - GDD_{o,flini}} \end{cases} \\ else & 0 \end{cases}$$

Where $GDD_{o,flini}$ is the thermal time in which olive trees start to flower, SOW is the weight of a single olive fruit and $N_{olive,t-1}$ is the number of olive of previous time step.

Reserve remobilization

Reserves are mobilized (R_{mob}) only in special occasion for example: 1) when respiration exceed photosynthesis (eq. 49), 2) growth restarting after dormancy (López-Bernal *et al.,* 2018; eq. 50), 3) traumas (eq. 51), 4) if photosynthesis rate is lower than olive demand (López-Bernal *et al.,* 2018; eq. 52).

Case 1

Equation 49

$$R_{mob} = -\frac{AGB_r}{effR}$$

In case of respiration the reserves recover the consummated mass.

Case 2

Equation 50

$$R_{mob} = \begin{cases} GDD_{s,o} \leq GDD_{o,Rend} \ \& \ R_g < R_{min,m} & \frac{GDD_{r,o} \cdot \left(R_{s-1} - Wood_{s-1} \cdot R_{min,m}\right)}{GDD_{o,Rend}} \cdot T_{res} \\ else & 0 \end{cases}$$

Case 3

Equation 51

$$R_{mob} = \begin{cases} GLAI_{s-1} \leq GLAI_r \ \& \ active & R_q \cdot R_{s-1} \cdot T_{res} \\ else & 0 \end{cases}$$

In case of dramatic damage to canopy the plant, if it is in active growth, re-growths.

Case 4

Equation 52

$$R_{mob} = \begin{cases} R_g < R_{min,m} & \frac{OD - AGB_r}{effR} \\ else & 0 \end{cases}$$

In case of olive demand is higher than AGB_r reserve cover the olive demand.

Equation 53

$$T_{res} = \begin{cases} T_{avg} \geq T_{b,PhO} & \frac{R_q \cdot R_{s-1} \cdot \left(Min\left(T_{avg}, T_{opt,PhO}\right) - T_{b,PhO}\right)}{T_{opt,PhO} - T_{b,PhO}} \\ else & 0 \end{cases}$$

The effective amount of reserve used (R_{mobEff}, eq. 54) take in consideration of the efficiency of remobilization

Equation 54

$$R_{mobEff} = R_{mob} \cdot effR$$

Where $effR$ is the efficiency of reserve mobilization:

$R_{min,m}$ minim reserve to mobilization;

EffR is the efficiency to reserve mobilization;

R_q is the maximum reserve quote of mobilization;

R_{s-1} is the reserve state of time step before;

$GDD_{o,Rend}$ is the growing degree day at which the plant ends the reserve mobilization after regrowing;

$R_{min,m}$ is the minimum reserve relation on wood mass to have mobilization;

$Wood_{s-1}$ is the woody organs mass at pervious time step;

R_g is the relation between reserve mass and woody organs mass;

T_{res} is the effect of temperature on reserve mobilization equation 53;

The R_{mob} is added to the amount of biomass rate coming to photosynthetic activity, to have the pool of mass to be partitioned in the various organs according the thermal time accumulation.

Olive drop

The model estimates the drop of some olive fruit if the olive demand is not achieved according to equation 55.

Equation 55

$$\begin{cases} OFM_r < OD \cdot OD_{QTh} & \left(1 - \left(\frac{OFM_r}{OD \cdot OD_{QTh}}\right)\right) \cdot ODr_R \\ else & 0 \end{cases}$$

Were OD_{PTh} is a parameter that describe the threshold quote of olive demand at which olive fruits starts to drop and ODr_R is an olive drop resistance parameter

LAI accumulation and senescence

Each day the partitioned biomass to leaves is converted in cohorts of contemporary leaves (LN_c; leaves number; eq. 57) with a certain value of leaves area index ($GLAI_c$; eq. 56).

Equation 56

$$GLAI_c = \frac{SLA \cdot LM_r/10000}{Min(0.95\,, SCOV)}$$

Equation 57

$$LN_c = \frac{SLA \cdot LM_r}{LA}$$

Where SLA is the specific leaf area index LM_r is the partitioned mass to leaves and LA is the single leaf area.

Each cohort of leaves accumulates thermal time ($GDD_{s,oCL}$; eq. 58) until the reaching of the growing degree day to leaf senescence ($GDD_{s,oCLdie}$) at which the cohort of leaves dies.

The thermal time accumulated is $GDD_{r,o}$ for the youngest cohort and the next equation for the others.

Equation 58

$$GDD_{s,oCL} = GDD_{s,oCL,t-1} + GDD_{r,o} \cdot (2 - SSC)$$

Where $GDD_{s,oCL,t-1}$ is the growing degree days of a specific cohort of olive leaves at previous time step and SSC is a self-shading coefficient (eq. 59).

Equation 59

$$SSC = \begin{cases} LAI_{ST} \cdot 3 \le LAI_{SS} \le LAI_{SC} \cdot 3 & \frac{LAI_{SS} - LAI_{ST} \cdot 3}{LAI_{SC} \cdot 3 - LAI_{ST} \cdot 3} \\ LAI_{Ss} > LAI_{Sc} \cdot 3 & 1 \\ LAI_{Ss} < LAI_{St} \cdot 3 & 0 \end{cases}$$

Where LAI_{SS}(eq. 60) is the considered leaves area index to shading LAI_{SC} is the critical leaves area index above which the old leave are shaded, and LAI_{ST} is the threshold below which the leaves are not shaded.

The self-shading has an increasing response on leaves aging.

Equation 60

$$LAI_{SS} = GLAI_s \cdot k \cdot Max(1, SCOV)$$

The LAI and leaf biomass is reduced of $1 - SSC$

Twigs accumulation and buds

In similar way of leaves also the partitioned mass to twig generate at each vegetative season a cohort of twig. The last have mass and buds. The buds number (Bud) is equal to the new number of leaves (LN_c) in the $GLAI_c$ just generated.

The twig and so the buds also die if shaded applying to twig mass half of SSC.

At the end of the restart all the twig produced 2 years before became woody organs, and there is the estimation of the potential number of flowering bud is estimated according to the bud number of the previous year, the percentage of flowering bud ($RPBud$; eq. 62) and the vernalization coefficient (CU_e; eq. 37).

Equation 61

$$FlBud = CU_e \cdot Bud \cdot RPBud$$

Equation 62

$$RCBud = \frac{PBud \cdot R_g}{R_{gMinFl}}$$

Where $PBud$ is the normal ratio between flowering and vegetative buds, and R_{gMinFl} is the minimum ratio between wood and reserve mass for differentiation occurrence.

The $FlBud$ is limited between 0.8 and 0.001.

The flowers do not flower together but in a period around flowering and the allegation is limited by rain and wind.

The total number of flowers today (FF) is estimated as below (eq. 63).

Equation 63

$$FF = \frac{GDD_{r,o}}{GDD_{o,flend} - GDD_{o,flini}} \cdot FlBud \cdot BudNFl$$

Where $GDD_{o,flend}$ is the maximum thermal time to flower $FlBud$ remain constant $BudNFl$ is the number of flowers a bud

The derived number of olive fruit ($N_{olive,r}$) is estimated by equation 64

Equation 64

$$N_{olive,r} = FF \cdot AllC \cdot \left(1 - W_p\right) \cdot (1 - Win_{al}) \cdot (1 - REF_{al})$$

Where $AllC$ is the allegation coefficient Win_{al} is the effect on wind on allegation (eq. 66) and REF_{al} is the rain effect on allegation (eq. 65).

Equation 65

$$REF_{al} = \begin{cases} R_d > 2 & 1 \\ else & 0 \end{cases}$$

Where R_d is the daily rain.

Equation 66

$$Win_{al} = \begin{cases} 1 < W < 10 & 0.5 \\ else & 0 \end{cases}$$

Canopy growth

The canopy growth is in function to leaves growth: the model estimates the increasing of plant height (H_r; eq. 68) and the radius (r_r; eq. 67) of vegetal canopy

Equation 67

$$r_r = NLA \cdot (1 - rHr) \cdot Id$$

Equation 68

$$H_r = NLA \cdot rHr \cdot Id$$

Where NLA is the new area of generated leaves (eq. 69), rHr is the relation between plant height and radius of canopy and Id is a coefficient to take into account the internode length and the overlapping and thickening of leaves.

Equation 69

$$NLA = \frac{SM_r \cdot 0.75 \cdot SLA}{10000 \cdot Min(0.95\,, SCOV)}$$

Where 0.75 is a coefficient derived by the relation between twig an leaves partition coefficient.

The state of the two variable: respectively r_s (eq. 70) and H_s (eq. 71) per canopy radius and plant height are obtained thanks the state of the two variable (r_{s-1}; H_{s-1}) at previous time step and the rate of the two variables.

Equation 70

$$r_s = r_{s-1} + r_r$$

Equation 71

$$H_s = H_{s-1} + H_r$$

Also the $SCOV$ is updated (eq. 72).

Equation 72

$$SCOV = \frac{{r_s}^2 \cdot \pi \cdot PN}{10000}$$

Where PN is the plant number in an hectare.

Pruning

The model estimates if it is required the plant pruning. This crop operation is useful to reduce the plant canopy in order to avoid self-shading or shading in general, to have an optimal ratio between vegetative and flowering buds and to avoid yield alternation. It is estimated also a redaction of woody and reserve organs. Pruning is estimated to be just before the restart of the thermal time accumulation (so in late winter or in early spring).

The pruning effects on wood (eq. 73) and storage (eq. 74) are estimated applying a coefficient to the actual state of this two organs.

Equation 73

$$R_s = R_s \cdot WRPC$$

Equation 74

$$Wood_s = Wood_s \cdot WRPC$$

Were R_s and $Wood_s$ are respectively the actual state of reserve and woody organs and $WRPC$ is the wood and reserve pruning coefficient.

For the canopy cover (radius; eq. 76) and plant height (eq. 75) a pruning coefficient (HCP) is applied.

Equation 75

$$H_s = H_s \cdot HCP$$

Equation 76

$$r_s = r_s \cdot HCP$$

For green organs the pruning is estimated differently considering a target of LAI to reach after pruning (LAI_{TP}; eq. 77).

Equation 77

$$GLAI_s = \begin{cases} GLAI_s < LAI_{TP} & GLAI_s \cdot 0.8 \\ else & LAI_{TP} \end{cases}$$

Where $GLAI_s$ is the actual state of green leaves area index and LAI_{TP} is the leaves area index considered the target after pruning.

To transfer the redaction of leaves area index to leaves (eq. 81) and green twig mass (eq. 82), number of leaves (eq. 80) and buds (eq. 79), a coefficient of pruned leaves area index is estimated ($GVPC$; eq. 78)

Equation 78

$$GVPC = \begin{cases} GLAI_s < LAI_{TP} & 0.8 \\ else & 1 - \left(\frac{GLAI_s - LAI_{TP}}{GLAI_s}\right) \end{cases}$$

Where the $GLAI_s$ to consider is before pruning.

Equation 79

$$Bud = Bud \cdot GVPC$$

Equation 80

$$LN = LN \cdot GVPC$$

Equation 81

$$LM_s = LM_s \cdot GVPC$$

Equation 82

$$TM_s = TM_s \cdot GVPC$$

Differently for the number of flowering buds the pruning effect tend to optimize the ratio between flowering and vegetative buds having as target a fixed threshold (eq. 83).

Equation 83

$$FlBud = Min(FlBud, Bud \cdot ORFBP)$$

Where Bud are the buds number after pruning $ORFB$ is the optimum ratio of flowering buds after pruning.

If number of vegetative buds are not available respected the flowering buds are recounted as complementary.

Abiotic damages

The model is able to estimate water stress effect on phenology, growing limitation and damage on plant, temperature (hot, freezing and flower sterility) effects and the damage due to an excess of radiation ($Dam_{rad,exc}$;eq. 86). This damages could be activated or not.

The model estimate also the death of organs or wale plant due to abiotic damages (Sanzani *et al*., 2012). The plants and the woody (and reserve) organs can die in case of extreme freezing or water stress; the twigs can die for freezing, self – shading (for half of the result of eq. 59), water stress and light excess ($Dam_{rad,exc}$;eq. 86); the leaves can die for hot (Dam_{hot}; eq. 87), freezing, self – shading (eq. 59), water stress and light excess ($Dam_{rad,exc}$; eq. 86); the olive fruit can die for hot (Dam_{hot};eq. 86), freezing, water stress and light excess ($Dam_{rad,exc}$; eq. 86).

The damage on twigs and leaves is estimated bigger than the damages on woody (and reserve) organs and death plants (Sanzani *et al*., 2012).

The same impact of twig is reported to bud number, the same for leaf number, leaves area index and leaves biomass and for olive biomass and olive number.

The damage on twigs and leaves are estimated starting for the youngest units.

Sterility

The flower sterility (eq. 84, 85) due to hot and cold temperature is estimate as portion of daily flowered flower that die for an exposition to cold ($Ster_{cold}$) or hot ($Ster_{coldhot}$) temperature and then applied to the rate of number of olive ($N_{olive,r}$)

Cold ($Ster_{cold}$; eq.84):

Equation 84

$$Ster_{cold} = \begin{cases} T_{min} > T_{Ster,cold,crit} & 0 \\ T_{Ster,cold,die} \leq T_{min} \leq T_{Ster,cold,crit} & \frac{T_{min} - T_{Ster,cold,crit}}{T_{Ster,cold,die} - T_{Ster,cold,crit}} \\ T_{min} < T_{Ster,cold,die} & 1 \end{cases}$$

Where T_{min} is the minimum air temperature, $T_{Ster,cold,crit}$ is the critical temperature at which cold sterility starts to act, and $T_{Ster,cold,die}$ is the temperature below which all the flowers that flower in this day die.

hot ($Ster_{hot}$; eq.85):

Equation 85

$$Ster_{hot} = \begin{cases} T_{max} < T_{Ster,hot,crit} & 0 \\ T_{Ster,hot,crit} \leq T_{max} \leq T_{Ster,hot,die} & \frac{T_{max} - T_{Ster,hot,crit}}{T_{Ster,hot,die} - T_{Ster,hot,crit}} \\ T_{max} > T_{Ster,hot,die} & 1 \end{cases}$$

Where T_{max} is the maximum air temperature, $T_{Ster,hot,crit}$ is the critical temperature at which hot sterility starts to act, and $T_{Ster,hot,die}$ is the temperature above which all the flowers that flower in this day die.

Damage due for radiation excess ($Dam_{rad,exc}$;eq. 86)

Equation 86

$$Dam_{rad,exc} = \begin{cases} RAD < 38 & 0 \\ 38 \leq RAD \leq 50 & \frac{PAR - 38}{12} \\ RAD > 50 & 1 \end{cases}$$

This damage lies at same way the leaves, olive fruit and twig organs.

Damage due for extreme hot (Dam_{hot};eq. 87)

Equation 87

$$Dam_{hot} = \begin{cases} T_{max} < T_{hot,crit} & 0 \\ T_{hot,crit} \leq T_{max} \leq T_{hot,die} & \frac{T_{max} - T_{hot,crit}}{T_{hot,die} - T_{hot,crit}} \\ T_{max} > T_{hot,die} & 1 \end{cases}$$

This damage lies at same way the leaves and olive fruit organs. Where $T_{hot,crit}$is the temperature below which there is no damage and $T_{hot,die}$ is the temperature above which all olive fruits and leaves are dropped.

Freezing

Damage due for freezing (Dam_{freeze};eq. 88) this damage change for the various organs and excluding for olive fruit it is sensible to hardening and dehardening phenomenon.

Equation 88

$$Dam_{freeze} = \begin{cases} T_{min} < T_{freeze,crit} & 0 \\ T_{freeze,die} \leq T_{min} \leq T_{freeze,crit} & \frac{T_{min} - T_{freeze,crit}}{T_{freeze,die} - T_{freeze,crit}} \\ T_{min} > T_{freeze,die} & 1 \end{cases}$$

Where $T_{freeze,crit}$ is the air temperature below which the vegetal tissue starts to freeze and $T_{freeze,die}$ is the temperature below which the vegetal tissue dies for freezing. The plant organs have different parameter values (table 3), in order to sensibility olive fruit, leaves, twigs, woody and reserve organs, plant. If the plant are hardened the model subtract 5°C to $T_{freeze,die}$ and $T_{freeze,crit}$ of all organs excluding olive fruits.

Table 3: *Acronym of the freezing parameters for the various organs*

Organs	$T_{freeze,crit}$	$T_{freeze,die}$
Plant	$T_{freeze,pl,crit}$	$T_{freeze,pl,die}$
Woody organs and reserves	$T_{freeze,wo,crit}$	$T_{freeze,wo,die}$
Twigs	$T_{freeze,tw,crit}$	$T_{freeze,tw,die}$
Leaves	$T_{freeze,le,crit}$	$T_{freeze,le,die}$
Olive fruits	$T_{freeze,of,crit}$	$T_{freeze,of,die}$

Hardening ($Hard_d$ - the today hardening coefficient -; $Hard_{d-1}$ – the previous time step hardening coefficient-) approach is organized in two sub-approach one for hardened plant (eq. 89) and the other for not hardened plant (eq.90). $Hard_d$ and $Hard_{d-1}$ values minimum are 0 and maximum are 2, below the minimum and above the maximum are trunked. The value of 1 or above it means that plant is hardened

Equation 89

$$Hard_d \begin{cases} T_{avg} \le 0 \,\&\, T_{min} \le 10 & Hard_{d-1} + 0.833 \\ T_{avg} > 0 \,\&\, T_{min} \le 10 & Hard_{d-1} \\ T_{min} > 10 & Hard_{d-1} + 0.2 - 0.2 \cdot T_{min} \quad \begin{cases} Hard_d \ge 1 & Hard_d + 0.2 - 0.2 \cdot T_{min} \\ else & Hard_d \end{cases} \end{cases}$$

Equation 90

$$Hard_d \begin{cases} -1 \le T_{avg} \le 8 & Hard_{d-1} + 0.0833 \\ -1 \le T_{avg} \le 0 & \begin{cases} Hard_d \ge 1 & Hard_d \dfrac{(T_{avg} - 3.5)^2}{506} \\ else & Hard_d \end{cases} \\ else & Hard_{d-1} \\ T_{min} > 10 & Hard_{d-1} + 0.2 - 0.2 \cdot T_{min} \quad \begin{cases} Hard_d \ge 1 & Hard_d + 0.2 - 0.2 \cdot T_{min} \\ else & Hard_d \end{cases} \end{cases}$$

Water stress

The model is able to estimate water stress effect on phenology, growing limitation and damage on plant.

Equation 91

$$GDD_{r,o} = GDD_{r,o} \cdot \left(1 + W_p\right)$$

The model estimates an increase of growing degree accumulation (eq. 91) according to water stress coefficient on phenology ($W_p$eq. 92)

Equation 92

$$W_p = Max\left(1, \left(\frac{ET_a}{ET_c}\right)^{(1-WS_{tol})}\right)$$

Where ET_c is the water required by atmosphere and canopy (eq. 94), ET_a is the actual evapotranspiration (output of a linked soil model) and WS_{tol} is a water tolerance parameter.

Water deficit damages (Dam_{Wdef}; eq. 93): in similar way to freezing damage there is a unique model with different parameter values for the various organs.

Equation 93

$$Dam_{Wdef} = \begin{cases} Min\left(W_{p,period}\right) < WS_{crit} & 1 - \dfrac{1 - Avg\left(W_{p,period}\right)}{WS_{crit}} \\ else & 0 \end{cases}$$

Where $W_{p,period}$ is the matrix of water stress coefficient (W_p; eq. 92) of period of previous day and WS_{crit} is a critical value of water stress. The length of the period and WS_{crit} are different for the various organs (table 4). The tolerance order is plant, woody and reserve organs, twigs and olive fruit, leaves.

Equation 94

$$W_r = ET0 \cdot K_c \cdot (1 - e^{-k \cdot PAI_{s-1}})$$

Where K_c is the crop evapotranspiration coefficient and $ET0$ is the potential evapotranspiration.

Table 4: *Acronym of the freezing parameters for the various organs*

Organs	$W_{p,period}$	WS_{crit}
Plant	$W_{p,period,pl}$	$WS_{crit,pl}$
Woody organs and reserves	$W_{p,period,wo}$	$WS_{crit,wo}$
Twigs and fruits	$W_{p,period,tf}$	$WS_{crit,tf}$
Leaves	$W_{p,period,le}$	$WS_{crit,le}$

Predators of the olive fruit fly submodel

Predator population ($Pors_n$) is linked to the total olive fruit fly population ($TotPop_{t-x}$; include all the stages) with a delay function that have 3 parameters the number of time step (day) of delay, the theoretical number of flies that eats a predator to survive at each time step ($EFpPor$) and theoretical number of fly for predator at equilibrium ($TFPE$). The heated flies are redistributed according a liking coefficient per phenological phase ($PLik_{c,ph}$) to the actual populations;

The population of predators ($Pors_n$) is estimated as current (eq. 95)

Equation 95

$$Pors_n = TFPE \cdot TotPop_{t-x}$$

Where $t - x$ is the number of day to delay.

The theoretical number of eaten fly ($F_{eat,t}$) is estimated according to equation 96.

Equation 96

$$F_{eat,t} = Pors_n \cdot EFpPor$$

The theoretical coefficient ($cF_{eat,t}$) of eaten olive fruit fly is given by two alternative equations (eq. 97, 98)

Equation 97

$$cF_{eat,t} = \frac{F_{eat,t}}{TotPop_{t-x}}$$

Equation 98

$$cF_{eat,t} = \frac{EFpPor}{TFPE}$$

The actual olive fruit fly population it is changed in number, so the predators could have abundance or shortage of pray, for this reason the number of eaten fly ($F_{eat,att}$; eq. 99) and the percentage of eaten fly ($cF_{eat,att}$; eq. 100) are adjusted.

Equation 99

$$F_{eat,att} = \begin{cases} cF_{eat,att} \cdot TotPop_t > TotPop_t - 2 & TotPop_t - 2 \\ else & Min\left(3 \cdot F_{eat,t}, cF_{eat,att} \cdot TotPop_t\right) \end{cases}$$

Equation 100

$$cF_{eat,att} = \left(cF_{eat,t} \cdot cF_{eat,pot}\right)^{0.5}$$

Where $cF_{eat,pot}$ is the potential coefficient of olive fruit fly eaten (eq.101)

Equation 101

$$cF_{eat,pot} = \frac{F_{eat,t}}{TotPop_t}$$

Than the number of eaten flies is spread in the various phenological phases (egg, larva I, larva II, larva III, pupae, adult) taking in account the various phases population number and liking following the approach below.

For each phenological phases the minimum value of population number (different from 0, in this case the minimum value major than 0) is used as divisor of all the phenological phases population number.

For each phenological phases the minimum value of liking coefficient (different from 0, in this case the minimum value major than 0) is used as divisor of all the phenological phases liking coefficient.

The two list obtained are multiplied obtaining a list of predation score for each fly phenological phases.

For each phenological phases the score is multiplied to $F_{eat,att}$ and divided by the sum of all the score obtaining the phase specific number of eaten fly.

In case of surplus of eaten olive fruit fly in one or more phenogical phase than the phase/s population number, the surplus of eaten fly is applied to the phenological phase with the higher number of population.

The phase specific number of eaten fly obtained as above is divided by the phase population number to obtain fMP specific per phase.

6. Conclusions and remarks

In this PhD Thesis, the importance of simulating the interactions between cultivated and wild species was underlined, for its crucial role in optimising crop management, quantifying the effects of climate change and the identification of adaptation strategies, estimating the quality of production (forage and olive fruits), and evaluating ecosystem services provided by agroecosystems.

In this context, knowledge gaps were identified and prioritised and this provided us with insights for the development of new simulation models. We documented the accuracy of the simulations obtained and the usability of the models in operational contexts. In particular, the crop-weed interaction model was developed and parameterized using experimental data, and then assessed with *in silico* experiments for its capability to support weed management. For olive trees, the olive fruit fly and its predator, the suitability of the model for operational contexts was successfully tested by an insurance company that used the model (and a derived meta-model) to develop new index-based insurance products. A limitation of the use of these models could be the need to simplify the developed models to be easily understood by farmers and insurance personnel (Tartarini et al., 2021; Colbach et al., 2014). The new suitability function (including approaches specific for grazing) implemented in CoSMo demonstrated their usefulness in different grasslands and pastures, extending the CoSMo capability to support management in the short and medium term (including adaptation to climate change).

Looking forward, new models of interactions between cultivated and wild species could be developed by adapting the modelling solutions developed and assessed in this thesis.

7. References

- Abdel-Razik, M.,1989. A model of the productivity of olive trees under optional water and nutrient supply in desert conditions. Ecological Modelling, 45(3), 179-204. https://doi.org/10.1016/0304-3800(89)90081-1
- Addiscott, T.M., Whitmore, A.P., 1987. Computer simulation of changes in soil mineral nitrogen and crop nitrogen during autumn, winter and spring. The Journal of Agricultural Science, 109(1), 141-157. https://doi.org/10.1017/S0021859600081089
- Allen, R.G., Pereira, L.S., Raes D., Smith, M., 1998. Crop evapotranspiration – guidelines for computing crop water requirements. FAO Irrigation and drainage paper 56. Food and Agriculture Organization, Rome, Italy.
- Argenti, G., Bottai, L., Chiesi, M., Maselli, F., Staglianò, N., Targetti, S. 2011. Analisi e valutazione di pascoli montani attraverso l'integrazione di dati multispettrali e ausiliari. Rivista Italiana di Telerilevamento/Italian Journal of Remote Sensing, 43(1), 45-57. (in Italian).
- Argenti, G., Parrini, S., Staglianò, N., Bozzi, R., 2021. Evolution of production and forage quality in sown meadows of a mountain area inside Parmesan cheese consortium. Agronomy Research, 19(2), 344–356, 2021. https://doi.org/10.15159/AR.21.061
- Ascherio, A., Chen, H., Weisskopf, M.G., O'Reilly, E., McCullough, M.L., Calle, E.E., Schwarzschild, M.A., Thun, M.J., 2006. Pesticide exposure and risk for Parkinson's disease. Annals of Neurology, 60, 197-203.
- Bartolucci, F., Peruzzi, L., Galasso, G., Albano, A., Alessandrini, A., Ardenghi, N.M.G., Astuti. G., Bacchetta G., Ballelli, S., Banfi, E., Barberis, G., Bernardo, L., Bouvet, D., Bovio, M., Cecchi, L., Di Pietro, R., Domina, G., Fascetti, S., Fenu, G., Festi,F., Foggi, G., Gallo, L., Gottschlich, G., Gubellini, L., Iamonico, D., Iberite, M., Jiménez-Mejías, P., Lattanzi, E., Marchetti, D., Martinetto, E., Masin, R.R., Medagli, P., Passalacqua, N.G., Peccenini S., Pennesi, R., Pierini, B., Poldini, L., Prosser, F., Raimondo,F.M., Roma-Marzio, F., Rosati, L., Santangelo, A., Scoppola, A., Scortegagna, S., Selvaggi, A., Selvi, F., Soldano, A., Stinca, A., Wagensommer, R.P., Wilhalm, T., Conti, F., 2018. An updated checklist of the vascular flora native to Italy. Plant Biosystems, 152, 179-303.

- Bastiaans, L., Kropff, M.J., Kempuchetty, N., Rajan, A., Migo, T.R., 1997. Can simulation models help design rice cultivars that are more competitive against weeds? Field Crops Research, 51, 101-111.
- Batjes, N.H., 2016. Harmonized soil property values for broad-scale modelling (WISE30sec) with estimates of global soil carbon stocks. Geoderma 269: 61-68.
- Belder, P., Bouman, B.A.M., Spiertz, J.H.J., 2007. Exploring options for water saving in lowland rice using a modeling approach. Agricultural Systems, 92, 91-114.
- Bellocchi, G., Acutis, M., Fila, G., Donatelli, M., 2002. An indicator of solar radiation model performance based on a fuzzy expert system. Agronomy Journal, 94, 1222-1233.
- Bellocchi, G., van Oijen, M., Höglind, M., 2018. Effects of climate change on grassland biodiversity and productivity: the need for a diversity of models. Agronomy, 8, 14.
- Beltran, J.C., Pannell, D.J., Doole, G.J., White, B., 2011. RIMPhil: a bioeconomic model for integrated weed management of annual barnyardgrass (*Echinochloa crus-galli*) in Philippine rice farming systems. Working Paper WP1112, School of Agricultural and Resource Economics, University of Western Australia, 10.22004/ag.econ.104637.
- Ben Touhami, H., Lardy, R., Barra, V., Bellocchi, G., 2013. Screening parameters in the Pasture Simulation model using the Morris method. Ecological Modelling, 266, 42-57. 10.1016/j.ecolmodel.2013.07.005
- Bengtsson, J., Bullock, J.M., Egoh, B., Everson, C., Everson, T., O'Connor, T., O'Farrell, P.J., Smith, H.G., Lindborg, R., 2019. Grasslands−more important for ecosystem services than you might think. Ecosphere, 10(2), e02582. https://doi.org/10.1002/ecs2.2582
- Biondi, E., Blasi, C., Allegrezza, M., Anzellotti, I., Azzella, M.M., Carli, E., Casavecchia, S., Copiz, R., Del Vico, E., Facioni, L., Galdenzi, D., Gasparri, R., Lasen, C., Pesaresi, S., Poldini, L., Sburlino, G., Taffetani, F., Vagge, I., Zitti, S., Zivkovic, L., 2014. Plant communities of Italy: The Vegetation Prodrome, Plant Biosystems, 148,728-814.
- Bohan, D.A., Powers, S.J., Champion, G., Haughton, A.J., Hawes, C., Squire, G., Cussans, J., Mertens, S.K., 2011. Modelling rotations: can crop sequences explain arable weed seedbank abundance? Weed Research, 51, 422-432.

- Bonfante, A., Monaco, E., Manna, P., De Mascellis, R., Basile, A., Buonanno, M., Gantilena, G., Esposito, A., Tedeschi, A., De Michele, C., Belfiore, O., Catapano, I., Ludeno, G., Salinas, K., Brook, A., 2019. LCIS DSS – An irrigation supporting system for water use efficiency improvement in precision agriculture: A maize case study. Agricultural Systems, 176, 102646.
- Boob, M., Truckses, B., Seither, M., Elsäßer, M., Thumm, U. & Lewandowski, I., 2019. Management effects on floristic composition of species-rich meadows within the Natura 2000 network. Biodiversity and Conservation, 28(3), 729−750. https://doi.org/10.1007/s10531-018-01689-1
- Borgy, B., Reboud, X., Peyrard, N., Sabbadin, R., Gaba, S., 2015. Dynamics of weeds in the soil seed bank: a hidden Markov model to estimate life history traits from standing plant time series. PLoS ONE, 10, e0139278.
- Bouman, B.A.M., van Laar, H.H., 2006. Description and evaluation of the rice growth model ORYZA2000 under nitrogen-limited conditions. Agricultural Systems, 87, 249-273.
- Bregaglio, S., Donatelli, M., 2015. A set of software components for the simulation of plant airborne diseases. Environmental Modelling & Software, 72, 426-444.
- Busetto, L., Casteleyn, S., Granell, C., Pepe, M., Barbieri, M., Campos-Taberner, M., Casa, R., Collivignarelli, F., Confalonieri, R., Crema, A., García-Haro, F.J., Gatti, L., Gitas, I.Z., Gonzalez-Pérez, A., Grau-Muedra, G., Guarneri, T., Holecz, F., Katsantonis, D., Minakou, C., Miralles, I., Movedi, E., Nutini, F., Pagani, V., Palombo, A., Di Paola, F., Pascucci, S., Pignatti, S., Rampini, A., Ranghetti, L., Ricciardelli, E., Romano, F., Stavrakoudis, D.G., Stroppiana, D., Viggiano, M., Boschetti, M., 2017. Downstream services for rice crop monitoring in Europe: From regional to local scale. IEEE Journal of Selected Topics in Applied Earth Observations and Remote Sensing, 10, 5423-5441.
- Buxton, D.R., Fales, S.L., 1994. Plant environment and quality. In: Fahey, G.C. Jr (Ed.) Forage quality, evaluation, and utilization. ASA, CSSA, and SSSA Books, Madison, Wisconsin, USA, pp. 155-199.
- Calanca, P., 2016., Modelling the impacts of seasonal drought on herbage growth under climate change. Advances in Animal Biosciences, 7, 231–232.
- Campbell, C.S., Heilman, J.L., McInnes, K.J., Wilson, L.T., Medley, J.C., Wu, G., Cobos, D.R., 2001. Seasonal variation in radiation use

efficiency of irrigated rice. Agricultural and Forest Meteorology, 110, 45-54.

- Cappelli, G., Yamaç, S.S., Stella, T., Francone, C., Paleari, L., Negri, M., Confalonieri, R., 2015. Are advantages from partial replacement of corn with second-generation energy crops undermined by climate change? A case study for giant reed in northern Italy. Biomass and Bioenergy 80, 85-93. https://doi.org/10.1016/j.biombioe.2015.04.038
- Casanova, D., Epema, G.F., Goudriaan, J., 1998. Monitoring rice reflectance at field level for estimating biomass and LAI. Field Crops Research, 55, 83-92.
- Caton, B.P., Foin, T.C., Hill, J.E., 1999. A plant growth model for integrated weed management in direct-seeded rice. III. Interspecific competition for light. Field Crops Research, 63, 47-61.
- Cavanna, S., Bacci, L., Larelle, D., Carone, A., 2004. Penoxsulam (Viper®): nuovo erbicida di post-emergenza per il riso. Atti Giornate Fitopatologiche, 1, 301-308.
- Chung, S.W., Gasman, P.W., Kramer, L.A., Williams, J.R., Gu, R., 1999. Validation of EPIC for two watersheds in Southwest Iowa. Journal of Environmental Quality, 28, 971-979.
- Cola, G., Mariani, L., Maghradze, D., Failla, O., 2020. Changes in thermal resources and limitations for Georgian viticulture. Australian Journal of Grape and Wine Research, 26, 29-40.
- Colbach, N., 2010. Modelling cropping system effects on crop pest dynamics: how to compromise between process analysis and decision aid. Plant Science, 179, 1-13.
- Colbach, N., Biju-Duval, L., Gardarin, A., Granger, S., Guyot, S.H.M., Mézière, D., Munier-Jolain, N.M., Petit, S., 2014. The role of models for multicriteria evaluation and multiobjective design of cropping systems for managing weeds. Weed Research, 54, 541-555.
- Colbach, N., Gardarin, A., Moreau, D., 2019. The response of weed and crop species to shading: Which parameters explain weed impacts on crop production? Field Crops Research, 238, 45-55.
- Collins, W.J., Bellouin N., Doutriaux-Boucher, M., Gedney N., Halloran, P., Hinton, T., Hughes, J., Jones, C.D., Joshi, M., Liddicoat, S., Martin, G., O'Connor, F., Rae, J., Senior, C., Sitch, S., Totterdell, I., Wiltshire, A., Woodward, S., 2011. Development and evaluation of an Earth-system model - HadGEM2. Geoscientific Model Development, 4, 1051-1075.

- Confalonieri, R. and Bechini L., 2004. A preliminary evaluation of the simulation model CropSyst for alfalfa. European Journal of Agronomy, 21(2), 223-237. https://doi.org/10.1016/j.eja.2003.08.003
- Confalonieri, R., 2014. CoSMo: A simple approach for reproducing plant community dynamics using a single instance of generic crop simulators. Ecological Modelling, 286, 1-10.
- Confalonieri, R., Bregaglio, S., Rosenmund, A.S., Acutis, M., Savin, I., 2011. A model for simulating the height of rice plants. European Journal of Agronomy, 34, 20-25.
- Confalonieri, R., Orlando, F., Paleari, L., Stella, T., Gilardelli, C., Movedi, E., Pagani, V., Cappelli, G., Vertemara, A., Alberti, L., Alberti, P., Atanassiu, S., Bonaiti, M., Cappelletti, G., Ceruti, M., Confalonieri, A., Corgatelli, G., Corti, P., Dell'Oro, M., Ghidoni, A., Lamarta, A., Maghini, A., Mambretti, M., Manchia, A., Massoni, G., Mutti, P., Pariani, S., Pasini, D., Pesenti, A., Pizzamiglio, G., Ravasio, A., Rea, A., Santorsola, D., Serafini, G., Slavazza, M., Acutis, M., 2016. Uncertainty in crop model predictions: What is the role of users? Environmental Modelling & Software, 81, 165-173.
- Confalonieri, R., Rosenmund, A.S., Baruth, B., 2009. An improved model to simulate rice yield. Agronomy for Sustainable Development, 29, 463-474.
- Cong, W-F., van Ruijven, J., Mommer, L., De Deyn, G.B., Berendse, F., Hoffland, E., 2014. Plant species richness promotes soil carbon and nitrogen stocks in grasslands without legumes. J. Ecol. 102:1163-1170.
- Connor, D.J., Gómez-del-Campo, M., Comas J., 2012. Yield characteristics of N–S oriented olive hedgerow orchards, cv. Arbequina. Scientia horticulturae, 133, 31-36. https://doi.org/10.1016/j.scienta.2011.10.008
- Coucheney, E., Buis, S., Launay, M., Constantin, J., Mary, B., de Cortázar-Atauri, I.G., Ripoche, D., Beaudoin, N., Ruget, F., Andrianarisoa, K.S., Le Bas, C., Justes, E., Léonard, J., 2015. Accuracy, robustness and behavior of the STICS soil–crop model for plant, water and nitrogen outputs: evaluation over a wide range of agro-environmental conditions in France. Environmental Modelling and Software, 64, 177-190.
- Cowles, J.M., Wragg, P.D., Wright, A.J., Powers, J.S., Tilman, D., 2016. Shifting grassland plant community structure drives positive interactive effects of warming and diversity on aboveground net primary productivity. Global Change Biology, 22, 741–749.

- Craine, J.M., Ocheltree, T.W., Nippert, J.B., Towne, E.G., Skibbe, A.M., Kembel, S.W., Fargione, J.E., 2013. Global diversity of drought tolerance and grassland climate-change resilience. Nature Climate Change, 3, 63–67.
- Criss, R.E., Winston, W.E., 2008. Do Nash values have value? Discussion and alternate proposals. Hydrological Processes, 22, 2723-2725.
- Daget, P., Poissonet, J., 1971. Une méthode d'analyse phytologique des prairies Critères d'application. Annales Agronomiques 22, 5-41.
- Danuso, F., 2002. Climak: a stochastic model for weather data generation. Italian Journal of Agronomy, 6(1), 57–72.
- Dass, A., Shekhawat, K., Kumar Choudhary, A., Sepat, S., Singh, Rathore S., Mahajan, G., Singh Chauhan, B., 2017., Weed management in rice using crop competition-a review. Crop Protection 95, 45-52.
- Debaeke, P., Caussanel, J.P., Kiniry, J.R., Kafiz, B., Mondragon, G., 1997. Modelling crop:weed interactions in wheat with ALMANAC. Weed Research, 37, 325-341.
- Dee, D.P., Uppala, S.M., Simmons, A.J., Berrisford, P., Poli, P., Kobayashi, S., Andrae, U., Balmaseda, M.A., Balsamo, G., Bauer, P., Bechtold, P. et al., 2011. The ERA-Interim reanalysis: Configuration and performance of the data assimilation system. Quarterly Journal of the Royal Meteorological Society, 137, 553-597.
- Deen, W., Cousens, R., Warringa, J., Bastiaans, L., Carberry, P., Rebel, K., Riha, S., Murphy, C., Benjamin, L.R., Cloughley, C., Cussans, J., Forcella, F., Hunt, T., Jamieson, P., Lindquist, J., Wang, E., 2003. An evaluation of four crop: weed competition models using a common data set. Weed Research, 43, 116-29.
- Dellar, M., Topp, C.F.E., Banos, G., Wall, E., 2018. A meta-analysis on the effects of climate change on the yield and quality of European pastures. Agriculture, Ecosystems & Environment, 265, 413-420.
- Di Vaio, C., Marra, F.P., Scaglione, G., La Mantia, M., Caruso, T., 2012. The effect of different vigour olive clones on growth, dry matter partitioning and gas exchange under water deficit. Scientia horticulturae, 134, 72-78. https://doi.org/10.1016/j.scienta.2011.11.001
- Diarra, A., Smith, R.J., Talbert, R.E., 1985. Interference of red rice (Oryza sativa) with rice (O. sativa). Weed Science, 33, 644-649.
- Dibari, C., Costafreda-Aumedes, S., Argenti, G., Bindi, M., Carotenuto, F., Moriondo, M., Padovan, G., Pardini, A., Staglianò, N., Vagnoli, C.,

Brilli, L., 2020. Expected changes to Alpine pastures in extent and composition under future climate conditions. Agronomy 10, 926.
- Dingkuhn, M., Johnson, D.E., Sow, A., Audebert, A.Y., 1999. Relationships between upland rice canopy characteristics and weed competitiveness. Field Crops Research, 61, 79-95.
- Dingkuhn, M., Jones, M.P., Johnson, D.E., Sow, A., 1998. Growth and yield potential of *Oryza sativa* and *O. glaberrima* upland rice cultivars and their interspecific progenies. Field Crops Research, 57, 57-69.
- Fernández, J.E., Perez-Martin, A., Torres-Ruiz, J.M., Cuevas, M.V., Rodriguez-Dominguez, C.M., Elsayed-Farag, S., Morales-Sillero, A., García, J.M., Hernandez-Santana, V., Diaz-Espejo, A., 2013. A regulated deficit irrigation strategy for hedgerow olive orchards with high plant density. Plant and soil, 372(1), 279-295. https://doi.org/10.1007/s11104-013-1704-2
- Fletcher, J.S., Johnson, F.L., McFarlane, J.C., 1988. Database assessment of phytotoxicity data published on terrestrial vascular plants. Environmental Toxicology and Chemistry, 7, 615-622.
- Fontaine, L., Rolland, B., Bernicot, M.H., Poiret, L., 2009. Des variétés rustiques concurrentes des adventices pour l'agriculture durable en particulier l'agriculture biologique. Innovations in Agronomy, 4, 115-124.
- Franke, J.A., Mueller, C., Minoli, S., Elliott, J., Folberth, C., Gardner, C., hank, T., Izaurralde R.C., Jägermeyr, J., Jones, C., D. Liu, W., Olin, S., Pugh, T.A.M., Ruane, A.C., Stephens, H., Zabel., F., Moyer, E.J., 2022. Agricultural breadbaskets shift poleward given adaptive farmer behavior under climate change. Global Change Biology, 28, 167-181. https://doi.org/10.1111/gcb.15868
- Freckleton, R.P., Stephens P.A., 2009. Predictive models of weed population dynamics. Weed Research, 49, 225-232.
- Freckleton, R.P., Sutherland, W.J., Watkinson, A.R., Stephens P.A., 2008. Modelling the effects of management on population dynamics: some lessons from annual weeds. Journal of Applied Ecology, 45, 1050-1058.
- Freemark, K., Boutin, C., 1995. Impacts of agricultural herbicide use on terrestrial wildlife in temperate landscapes: a review with special reference to North America. Agriculture, Ecosystems & Environment, 52, 67-91.

- Gardarin, A., Dürr, C., Colbach, N., 2012. Modeling the dynamics and emergence of a multispecies weed seed bank with species traits. Ecological Modelling, 240, 123-138.
- Genc, H., Nation, J.L., 2008. Survival and development of Bactrocera oleae Gmelin (Diptera:Tephritidae) immature stages at four temperatures in the laboratory. African Journal of Biotechnology, 7(14).
- Giglioli, G., Pasquali, S., 2007. Use of individual-based models for population parameters estimation. Ecological modelling, 200(1-2), 109-118. https://doi.org/10.1016/j.ecolmodel.2006.07.017
- Giustini, L., Acciaioli, A., Argenti, G., 2007. Apparent balance of nitrogen and phosphorus in dairy farms in Mugello (Italy). Italian Journal of Animal Science, 6(2), 175−185. https://doi.org/10.4081/ijas.2007.175
- Glover, F., 1986. Future paths for integer programming and links to artificial intelligence. Computers & operations research, 13 (5), 533-549. https://doi.org/10.1016/0305-0548(86)90048-1
- Godfray, H.C.J., Beddington, J.R., Crute, I.R., Haddad, L., Lawrence, D., Muir, J.F., Pretty, J., Robinson, S., Thomas, S.M., Toulmin, C., 2010. Food Security: The Challenge of Feeding 9 Billion People. Science, 327, 812-818.
- Graf, B., Gutierrez, A.P., Rakotobe, O., Zahner, P., Delucchi, V., 1990. A simulation model for the dynamics of rice growth and development: Part II-The competition with weeds for nitrogen and light. Agricultural Systems, 32, 367-392.
- Grant, S.A., Torvell, L., Sim, E.M., Small, J.L., Armstrong, R.H., 1996. Controlled grazing studies on Nardus grassland: Effects of between-tussock sward height and species of grazer on Nardus utilization and floristic composition in two fields in Scotland. Journal of Applied Ecology, 33, 1053–1064.
- Gutierrez, A.P., Ponti, L., Cossu, Q.A., 2009. Effects of climate warming on olive and olive fruit fly (Bactrocera oleae (Gmelin)) in California and Italy. Climatic Change, 95(1), 195-217. DOI 10.1007/s10584-008-9528-4
- Habel, J.C., Dengler, J., Janišová, M., Török, P., Wellstein, C., Wiezik, M., 2013. European grassland ecosystems: threatened hotspots of biodiversity. Biodiversity and Conservation, 22, 2131-2138.
- Hao, R., Yu, D., Liu, Y., Liu, Y., Qiao, J., Wang, X., Du, J., 2017. Impacts of changes in climate and landscape pattern on ecosystem

services. Science of Total Environment, 579, 718−728. https://doi.org 10.1016/j.scitotenv.2016.11.036

- Hattori, Y., Nagai, K., Furukawa, S., Song, X.J., Kawano, R., Sakakibara, H., Wu, J., Matsumoto, T., Yoshimura, A., Kitano, H., Matsuoka, M., Mori, H., Matsuoka, M., 2009. The ethylene response factors SNORKEL1 and SNORKEL2 allow rice to adapt to deep water. Nature, 460, 1026-1030.
- Hennessy, J., 1986. MARS-The ECMWF Meteorological archive and retrieval system in proceedings. 66th annual meeting of the American Meteorological Society.
- Hernandez-Santana, V., Fernández, J.E., Cuevas, M.V., Perez-Martin, A., Diaz-Espejo, A., 2017. Photosynthetic limitations by water deficit: effect on fruit and olive oil yield, leaf area and trunk diameter and its potential use to control vegetative growth of super-high density olive orchards. Agricultural Water Management, 184, 9-18. https://doi.org/10.1016/j.agwat.2016.12.016
- Höglind, M., Thorsen, S.M., Semenov, M.A., 2013. Assessing uncertainties in impact of climate change on grass production in Northern Europe using ensembles of global climate models. Agricultural and Forest Meteorology, 170, 103-113.
- Homma, T., Saltelli, A., 1996. Importance measures in global sensitivity analysis of nonlinear models. Reliability Engineering & System Safety, 52(1), 1-17. https://doi.org/10.1016/0951-8320(96)00002-6
- Huang, Z., Liu, Y., Cui, Z., Fang, Y., He, H., Liu, B.R., Wu, G.L., 2018. Soil water storage deficit of alfalfa (Medicago sativa) grasslands along ages in arid area (China). Field Crops Research, 221, 1-6. https://doi.org/10.1016/j.fcr.2018.02.013
- IPCC (2013) Summery for Policymakers. In: Stocker, T.F., Qin, D., Plattner, G-K., Tignor, M., Allen, S.K., Boschung, J., Nauels, A., Xia, Y., Bex, V., Midgley, P.M., (Eds.). Climate change 2013: The physical science basis. Contribution of working group I to the fifth assessment report of the Intergovernmental Panel on Climate Change. Cambridge University Press, Cambridge.
- Iraldo, F., Testa, F., Bartolozzi, I., 2013. An application of Life Cycle Assessment (LCA) as a green marketing tool for agricultural products: the case of extra-virgin olive oil in Val di Cornia, Italy Journal of Environmental Planning and Management, 57(1), 78-103. https://doi.org/10.1080/09640568.2012.735991

- Jeangros, B, Scehovic, J., Troxler, J., Bachmann, H.J., Bosset, J.O., 1999. Comparaison de caractéristiques botaniques et chimiques d'herbages paturés en plaine et en montagne. Fourrages, 159, 277-92.
- Jonckheere, I., Fleck, S., Nackaerts, K., Muys, B., Coppin, P.,Weiss, M., Baret, F. 2004. Review of methods for in situ leaf area index determination. Part I. Theories, sensors and hemispherical photography. Agricultural and Forest Meteorology 121: 19–35. https://doi.org/10.1016/j.agrformet.2003.08.027
- Jørgensen, S.E., Kamp-Nielsen, L., Christensen, T., Windolf-Nielsen, J., Westergaard, B., 1986. Validation of a prognosis based upon a eutrophication model. Ecological Modelling, 32: 165-182.
- Jost, L., 2006. Entropy and diversity. Oikos 113, 363-375.
- Jouven, M., Carrère, P., Baumont, R., 2006. Model predicting dynamics of biomass, structure and digestibility of herbage in managed permanent pastures. 1. Model description. Grass Forage Science, 61, 112–124.
- Kadiyala, M.D.M., Nedumaran, S., Singh, P., Chukka, S., Irshad, M.A., Bantilan, M.C.S., 2015. An integrated crop model and GIS decision support system for assisting agronomic decision making under climate change. Sci. Total Environ. 521, 123-134.
- Kasnakoglu, H., 2006. FAOSTAT and CountrySTAT: Integrated Global and National Food and Agriculture Statistical Databases. In: Proceedings of the XLIII Scientific Meeting, Società Italiana di Statistica, Universita di Torino, 2006, 183-194.
- Kic, P., 2019. The course of drying and colour changes of alfalfa under different drying conditions. Agronomy Research, 17(2), 491–498. https://doi.org/10.15159/AR.19.033
- Kirkpatrick, S., Gelatt, C.D., Vecchi, M.P., 1983. Optimization by simulated annealing. Science, 220 (4598), 671-680. https://www.science.org/doi/10.1126/science.220.4598.671
- Kraehmer, H., Jabran, K., Mennan, H., Chauhan, B.S., 2016. Global distribution of rice weeds–A review. Crop protection, 80, 73-86.
- Kropff, M.J., Spitters, C.J.T., 1991. A simple model of crop loss by weed competition from early observations on relative leaf area of the weeds. Weed Research, 31, 97-105.
- Kropff, M.J., Spitters, C.J.T., Schnieders, B.J., Joenje, W., De Groot, W., 1992. An eco-physiological model for interspecific competition, applied to the influence of Chenopodium album L. on sugar beet. II. Model evaluation. Weed Research, 32,451-463.

- Kropff, M.J., Van Laar, H.H., 1993. Modelling crop-weed interactions. (Eds.) International Rice Research Institute.
- Kropff, M.J., Weaver, S.E., Lotz, L.A.P., Lindquist, J.L., Joenje, W., Schnieders, B.J., van Keulen, N.C., Migo, T.R., Fajardo, F.F., 1993. Understanding Crop-Weed Interaction in Field Situations. In: Kropff, M.J., van Laar, H.H. (Eds) Modelling Crop-Weed Interactions. CAB International, Wallingford, UK, pp 105-136.
- Kwon, S.L., Smith, R.J., Talbert, R.E., 1992. Comparative growth and development of red rice (*Oryza sativa*) and rice (*O. sativa*). Weed Science, 40, 57-62.
- Kyriakidis, N.B., Dourou, E.F.I., 2002. Effect of storage and Dacus infection of olive fruits on the quality of the produced virgin olive oil. J. Food Lipids, 9, 47–55.
- Leifeld, J., 2016. Current approaches neglect possible agricultural cutback under large-scale organic farming. A comment to Ponisio et al. Proceedings of the Royal Society B, 283, 20151623.
- Lindquist, J.L., Kropff, M.J., 1997. Improving rice tolerance to barnyardgrass through early crop vigour: simulations with INTERCOM. In: Kropff, M.J., Teng, P.S., Aggarwal, P.K., Bouma, J., Bouman, B.A.M., Jones, J.W., van Laar, H.H. (Eds.) Systems approaches for sustainable agricultural development. Kluwer Academic Publishers, pp. 53-62.
- Liu, H., Mi Z., Lin, L., Wang, Y., Zhang, Z., Zhang, F., Wang, H., Liu, L., Zhu, B., Cao, G., Zhao, X,. Sanders, N.J., Classen, A.T., Reich, P.B., He, J-S., 2018. Shifting plant species composition in response to climate change stabilizes grassland primary production. Proceedings of the National Academy of Sciences, 115, 4051-4056.
- Loague, K., Green, R.E., 1991. Statistical and graphical methods for evaluating solute transport models: overview and application. Journal of Contaminant Hydrology, 7, 51-73.
- Longo, D., Baglivo, A., Cibei, C., Dose, G., Giordana, F., Magni, C., Salvai, G., Servodio, S., Tomasi, D., Zepigli, M., Nicolella, G., 2021. Acta Plantarum, more than a forum: a new national floristic distribution database completes the numerous online IPFI facilities. Biogeographia 36, s004.
- Lopez, O., Hernandez, A.F., Rodrigo, L., Gil, F., Pena, G., Serrano, J.L., Parrón, T., Villanueva, E., Pla, A., 2007. Changes in antioxidant enzymes in humans with long-term exposure to pesticides. Toxicology Letters, 171, 146-153.

- López-Bernal, Á., Morales, A., García-Tejera, O., Testi, L., Orgaz, F., De Melo-Abreu, J.P., Villalobos, F.J., 2018. OliveCan: a process-based model of development, growth and yield of olive orchards. Frontiers in plant science, 9, 632. https://doi.org/10.3389/fpls.2018.00632
- Ma, S., Lardy, R., Graux, A.-I., Ben Touhami, H., Klumpp, K., Martin, R., Bellocchi, G., 2015. Regional-scale analysis of carbon and water cycles on managed grassland systems. Environmental Modelling & Software, 10.1016/j.envsoft.2015.03.007
- Mackie, K.A., Zeiter, M., Bloor, J.M.G., Stampfli, A., 2018. Plant functional groups mediate drought resistance and recovery in a multisite grassland experiment. Journal of Ecology, 107, 937-949.
- Mancini, M.C., Arfini, F., Guareschi, M., 2019. Innovation and typicality in localised agri-food systems: the case of PDO Parmigiano Reggiano. British Food Journal, 121(12), 3043−3061. https://doi.org/10.15159/ar.21.061
- Manousis, T, Moore, N.F., 1987. Control of Dacus oleae, a major pest of olives. International Journal of Tropical Insect Science, 8(1), 1-9. https://doi.org/10.1017/S1742758400006858
- Mariani, L., Cola, G., Ferrante, A., Martinetti, L., Bulgari, R., 2016. Space and time variability of heating requirements for greenhouse tomato production in the Euro-Mediterranean area. Science of the Total Environment, 562, 834-844.
- Mariani, L., Parisi, S.G., Cola, G., Failla, O., 2012. Climate change in Europe and effects on thermal resources for crops. International Journal of Biometeorology, 56, 1123-1134.
- Mariscal, M.J., Orgaz, F., Villalobos, F.J., 2000. Radiation-use efficiency and dry matter partitioning of a young olive (Olea europaea) orchard. Tree Physiology, 20 (1), 65-72. https://doi.org/10.1093/treephys/20.1.65
- Marriott, C., Fothergill, M., Jeangros, B., Scotton, M., Louault, F., 2004. Long term impacts of extensification of grassland management on biodiversity and productivity in upland areas. Agronomy, 24, 447-462.
- Martin, S.G., Van Acker, R.C., Friesen, L.F., 2001. Critical period of weed control in spring canola. Weed Science, 49, 326-333.
- Masin, R., Loddo, D., Benvenuti, S., Zuin, M.C., Macchia, M., Zanin, G., 2010. Temperature and water potential as parameters for modelling weed emergence in central-northern Italy. Weed Science, 58, 216-222.

- Matches, A.G., 1992. Plant response to grazing: a review. Journal of Production Agriculture, 5, 1-7.
- Matsumoto, T., Du, H., Lindsey, J.S., 2002. A parallel simplex search method for use with an automated chemistry workstation. Chemometric Intelligent Laboratory, 62 (2), 129-147. https://doi.org/10.1016/S0169-7439(02)00010-2
- Minson, D.J., McDonald, C.K., 1987. Estimating forage intake from the growth of beef cattle. Tropical Grasslands, 21:116-122.
- Mohammed, B.K., Noori, I.M., 2008. Effect of Irrigation levels on the growth and yield of olive trees (Olea europaea L. cv.Ashrasie). Journal of Kirkuk University–Scientific Studies, 3(1).
- Monsi, M., Saeki, T., 1953. Über den Lichtfaktor in den Pflanzengesellschaften und seine Bedeutung für die Stoffproduktion. Japanese Journal of Botany, 14, 22-52.
- Monteith, J.L., Climate and the efficiency of crop production in Britain. Philosophical Transaction of the Royal Society of London, Series B, 281, 277-294.
- Mooney, H.A., Hobbs, R.J., 2000. Global change and invasive species: where do we go from here. Invasive species in a changing world. Island Press, Washington, DC, 425-434.
- Morales, A., Leffelaar, P.A., Testi, L., Orgaz, F., and Villalobos, F.J., 2016. A dynamic model of potential growth of olive (Olea europaea L.). European Journal of Agronomy, 74, 93-102. https://doi.org/10.1016/j.eja.2015.12.006
- Moriasi, D., Arnold, J., Van Liew, M., Bingner, R., Harmel, R., Veith, T., 2007. Model evaluation guidelines for systematic quantification of accuracy in watershed simulations. Transactions of the ASABE 50, 885-900.
- Moriondo, M., Leolini, L., Brilli, L., Dibari, C., Tognetti, R., Giovannelli, A., Rapi, B., Battista, P., Caruso, G., Gucci, R., Argenti, G., Raschi, A., Centritto, M., Cantini, C., Bindi, M., 2019. A simple model simulating development and growth of an olive grove. European Journal of Agronomy, 105, 129-145. https://doi.org/10.1016/j.eja.2019.02.002
- Moulin, T., Perasso, A., Gillet, F., 2018. Modelling vegetation dynamics in managed grasslands: Responses to drivers depend on species richness. Ecological Modelling, 374, 22–36.
- Movedi, E., Bellocchi, G., Argenti, G., Paleari, L., Vesely, F., Staglianò, N., Dibari, C., Confalonieri, R., 2019. Development of

generic crop models for simulation of multi-species plant communities in mown grasslands. Ecological Modelling, 401, 111–128.

- Movedi, E., Valiante, D., Colosio, A., Corengia, L., Cossa, S., Confalonieri, R., 2022. A new approach for modelling crop-weed interaction targeting management support in operational contexts: a case study on the rice weeds barnyardgrass and red rice. Ecological Modelling, 463, 109797.
- Mucina, L., Bultmann, H., Dierßen, K., Theurillat, J-P., Raus, T., Čarni, A., Šumberová, K., Willner, W., Dengler, J., Gavilán García, R., Chytrý, M., Hájek, M., Di Pietro, R., Iakushenko, D., Pallas, J., Daniëls, F.J.A., Bergmeier, E., Santos Guerra, A., Ermakov, E., Valachovič, M., Schaminée, J.H.J., Lysenko, T., Didukh, Y.P., Pignatti, S., Rodwell, J.S., Capelo, J., Weber, H.E., Solomeshch, A., Dimopoulos, P., Aguiar, C., Hennekens, S.M, Tichý L., 2016. Vegetation of Europe: hierarchical floristic classification system of vascular plant, bryophyte, lichen, and algal communities. Applied Vegetation Science, 19, 3-26.
- Nash, J.E., Sutcliffe, J.V., 1970. River flow forecasting through conceptual models part I - a discussion of principles. Journal of Hydrology, 10, 282-290.
- Neitsch, S.L., Arnold, J.G., Kiniry, J.R., Srinivasan, R., Williams, J.R., 2002. Soil and water assessment tool. User's manual. Grassland, Soil & Water Research Laboratory, Agricultural Research Service 808, East Blackland road, Temple, Texas 76502, 472.
- Nelder, J.A., Mead, R., 1965. A simplex method for function minimization. Computation Journal, 7 (4), 308-313. https://doi.org/10.1093/comjnl/7.4.308
- Nettleton, D.F., Katsantonis, D., Kalaitzidis, A., Sarafijanovic-Djukic, N., Puigdollers, P., Confalonieri, R., 2019. Predicting rice blast disease: machine learning versus process-based models. BMC Bioinformatics, 20, 514.
- Oerke, E.C., Dehne, H.W., 2004. Safeguarding production-losses in major crops and the role of crop protection. Crop Protection, 23, 275-285.
- Oliver, T.H., Heard, M.S., Isaac, N.J., Roy, D.B., Procter, D., Eigenbrod, F., Freckleton, R., Hector, A., Orme, D.L., Petchey, O.L., Proença, V., Raffaelli, D., Suttle, K.B., Mace, G.M., Martín-López, M., Woodcock, B.A., Bullock, J.M, 2015. Biodiversity and resilience of ecosystem functions. Trends Ecology. Evolution, 30, 673-684.

- Otto, S., Zuin, M.C., Chistè, G., Zanin, G., 2007. A modelling approach using seedbank and soil properties to predict the relative weed density inorganic fields of an Italian pre-alpine valley. Weed Research, 47, 311-326.
- Pagani, V., Francone, C., Wang, Z., Qiu, L., Bregaglio, S., Acutis, M., Confalonieri, R.,2014. Evaluation of WARM for different establishment techniques in Jiangsu (China). European Journal of Agronomy, 59, 78-85.
- Pagani, V., Guarneri, T., Busetto, L., Ranghetti, L., Boschetti, M., Movedi, E., Campos-Taberner, M., Garcia-Haro, F.J., Katsantonis, D., Stavrakoudis, D., Ricciardelli, E., Romano, F., Holecz, F., Collivignarelli, F., Granell, C., Casteleyn, S., Confalonieri, R., 2019. A high-resolution, integrated system for rice yield forecasting at district level. Agricultural Systems, 168, 181-190.
- Palese, A.M., Pergola, M., Favia, M., Xiloyannis, C., Celano, G., 2013. A sustainable model for the management of olive orchards located in semi-arid marginal areas: some remarks and indications for policy makers. Environmental science & policy, 27, 81-90. https://doi.org/10.1016/j.envsci.2012.11.001
- Park, S.E., Benjamin, L.R., Watkinson, A.R., 2003. The theory and application of plant competition models: an agronomic perspective. Annals of Botany, 92, 741-748.
- Piseddu, F., Hadj Saadi, D., Movedi, E., Confalonieri, R., Picon-Cochar, C., Seddaiu, S., Roggero, P.P., Bellocchi G., 2019. Modelling plant species composition in permanent grasslands: first results in the massif central of france. Società Italiana di Agronomia, XLVIII Convegno Nazionale, Perugia, 156.
- Press, W.H., Teukolsky, S.A., Vetterling, W.T., Flannery, B.P., 2007. Numerical Recipes 3rd Edition: the art of scientific computing, 2nd edition, Cambridge University Press, Cambridge, UK.
- Pulina, P., Francesconi, A.H.D., Stefanon, B., Sevi, A., Calamari, L., Lacetera, N., Dell'Orto, V., Pilla, F., Ajmone Marsan, P., Mele, M., Rossi, F., Bertoni, G., Crovetto, G.M., Ronchi, B., 2017. Sustainable ruminant production to help feed the planet. Italian Journal of Animal Science, 16(1), 140−17. https://doi.org/10.1080/1828051X.2016.1260500
- Ren, H., Schönbach, P., Wan, H., Gierus, M., Taube, F., 2012. Effects of grazing intensity and environmental factors on species composition

and diversity in typical steppe of Inner Mongolia, China. PLOS ONE, 7, e52180.

- Ren, S., Yi, S., Peichl, M., Wang, X., 2018. Diverse responses of vegetation phenology to climate change in different grasslands in Inner Mongolia during 2000–2016. Remote Sensing, 10:17.
- Renton, M., 2013. Shifting focus from the population to the individual as a way forward in understanding, predicting and managing the complexities of evolution of resistance to pesticides. Pest Management Science, 69, 171-175.
- Riedo, M., Gyalistras, D., Fuhrer, J., 2000. Net primary production and carbon stocks in differently managed grasslands: simulation of site-specific sensitivity to an increase in atmospheric CO_2 and to climate change. Ecological Modelling, 134, 207-277.
- Rojnić, I.D., Bažok, R., Barčić, J.I., 2015. Reduction of olive fruit fly damage by early harvesting and impact on oil quality parameters. European Journal of Lipid Science and Technology, 117(1), 103-111.
- Saaroni, H., Ziv, B., 2000. Summer rain episodes in a Mediterranean climate, the case of Israel: climatological–dynamical analysis. International Journal of Climatology 20, 191-209. https://doi.org/10.1002/(SICI)1097-0088(200002)20:2<191::AID-JOC464>3.0.CO;2-E
- Saier, M.H., 2007. Climate change, 2007. Water Air Soil Pollution, 181(1), 1-2. https://doi.org/10.1007/s11270-007-9372-6
- Saltelli, A., Tarantola, S., Chan, K.P.S., 1999. A quantitative model-independent method for global sensitivity analysis of model output. Technometrics, 41(1), 39-56. https://doi.org/10.1080/00401706.1999.10485594
- Sàndor, R., Picon-Cochard, C., Martin, R., Louault, F., Klumpp, K., Borras, D., Bellocchi, G., 2018. Plant acclimation to temperature: Developments in the Pasture Simulation model. Field Crops Research, 222, 238-255.
- Sanzani, S.M., Schena, L., Nigro, F., Sergeeva, V., Ippolito, A., Salerno, M.G., 2012. Abiotic diseases of olive. Journal of Plant Pathology, 469-491.
- Schmidt, G.A., Ruedy, R., Hansen, J.E., Aleinov, I., Bell, N., Bauer, M., Bauer, M., Cairns, B., Canuto, V., Cheng, Y., Del Genio, A., Faluvegi, G., Friend, A.D., Hall, T.M., Hu, Y.A., Kelley, M., Kiang, N.Y., Koch, D., Lacis, A.A., Lerner, J., Lo, K.K., Miller, R.L., Nazarenko, L., Oinas, V., Perlwitz, J., Perlwitz, J., Rind, D., Romanou,

A., Russell, G.L., Sato, M., Shindell, D.T., Stone, P.H., Sun, S., Tausnev, N., Thresher, D., Yaob, M-S., 2006. Present-day atmospheric simulations using GISS Model E: Comparison to in situ, satellite, and reanalysis data. Journal of Climate, 19, 153-192.

- Schulze, E.D., Luyssaert, S., Ciais, P., Freibauer, A., Janssen, I.A., Soussana, J.F., Smith, P., Grace, J., Levin, I., Thiruchittampalam, B., Heimann, M., Dolman, A.J., Valentini, R., Bousquet, P., Peylin, P., Peters, W., Rödenbeck, C., Etiope, G., Vuichard, N., Wattenbach, M., Nabuurs, G.J., Poussi, Z., Nieschulze, J., Gash, J.H., and the CarboEurope Team, 2009. Importance of methane and nitrous oxide for Europe's terrestrial greenhouse-gas balance. Nature Geoscience, 2, 842-850.
- Schwartz, M.D, Ahas, R., Aasa, A., 2006. Onset of spring starting earlier across the Northern Hemisphere. Global Change Biology, 12, 343-351.
- Semenov, M.A., Barrow, E.M., 1997 Use of a stochastic weather generator in the development of climate change scenarios. Climatic Change, 35, 397-414.
- Seufert, V., Ramankutty, N., Foley, J.A., 2012. Comparing the yields of organic and conventional agriculture. Nature, 485, 229-232.
- Simpson, E.H., 1949. Measurement of diversity. Nature, 16,: 688-688.
- Soussana, J.-F., Maire, V., Gross, N., Bachelet, B., Pagès, L., Martin, R., Hill, D., Wirth, C., 2012. Gemini: A grassland model simulating the role of plant traits for community dynamics and ecosystem functioning. Parameterization and evaluation. Ecological Modelling, 231, 134–145.
- Soussana, J-F., Graux A-I., Tubiello F.N., 2010. Improving the use of modelling for projections of climate change impacts on crops and pastures. Journal of Experimental Botany, 61, 2217-2228.
- Stella, T., Frasso, N., Negrini, G., Bergaglio, S., Cappelli, G., Acutis, M., Confalonieri, C., 2014. Model simplification and development via reuse, sensitivity analysis and composition: A case study in crop modelling. Environmental Modelling & Software, 59, 44-58. https://www.sciencedirect.com/science/article/pii/S1364815214001388?via%3Dihub
- Stöckle, C.O., Donatelli, M., Nelson, R. 2003. CropSyst, a cropping systems simulation model. European Journal of Agronomy, 18, 289-307.

- Suttie, J.M., Reynolds, S.G., Batello, C., 2005. Grasslands of the world. FAO Plant Production and Protection Series, 34, Food and Agriculture Organization of the United Nations, Rome (Italy), 538 pp.
- Swinehart, D.F., 1962. The beer-lambert law. Journal of chemical education, 39(7), 333.
- Tabacco, E., Comino, L., Borreani, G., 2018. Production efficiency, costs and environmental impacts of conventional and dynamic forage systems for dairy farms in Italy. European Journal of Agronomy, 99, 1−12. https://doi.org/10.1016/j.eja.2018.06.004
- Tang, L., Cai, H., Zhai, H., Luo, X., Wang, Z., Cui, L., Bai, X., 2014. Overexpression of Glycine soja WRKY20 enhances both drought and salt tolerance in transgenic alfalfa (Medicago sativa L.). Plant Cell, Tissue and Organ Culture (PCTOC), 118(1), 77-86. https://doi.org/10.1007/s11240-014-0463-y
- Tartarini, S., Paleari, L., Movedi, E., Sacchi, G.A., Nocito, F.F., Confalonieri, R., 2019. Analysis and modeling of processes involved with salt tolerance and rice. Crop Science, 59, 1155-1164.
- Tartarini, S., Vesely, F., Movedi, E., Radegonda, L., Pietrasanta, A., Recchi, G., Confalonieri, R., 2021. Biophysical models and meta-modelling to reduce the basis risk in index-based insurance: A case study on winter cereals in Italy. Agricultural and Forest Meteorology, 300, 108320.
- Thorp, K.R., DeJonge, K.C., Kaleita, A.L., Batchelor, W.D., Paz, J.O., 2008. Methodology for the use of DSSAT models for precision agriculture decision support. Computers and Electronics in Agriculture, 64, 276-285.
- Tribot, A.-S., Deter, J., Mouquet, N., 2018. Integrating the aesthetic value of landscapes and biological diversity. Proceedings of the Royal Society B: Biological Sciences, 285(1886), 20180971.
- Tubiello, F.N., Soussanna, J.F., Howden, S.M., 2007. Crop and pasture response to climate change. Proceedings of the National Academy of Sciences, 104, 19686-19690.
- Turtureanu, P.D., Barros, C., Bec, S., Hurdu, B.I., Saillard, A., Šibík, J., Balázs, Z.R., Novikov, A., Renaud, J., Podar, D., Thuiller, W., Puşcaş, M., Choler, P., 2020. Biogeography of intraspecific trait variability in matgrass (Nardus stricta): High phenotypic variation at the local scale exceeds large scale variability patterns. Perspectives in Plant Ecology, Evolution and Systematics. 46, 125555.

- Tzanakakis, M.E., 2003. Seasonal development and dormancy of insects and mites feeding on olive: a review. Netherlands Journal of Zoology, 52(2/4), 87-224
- Tzanakakis, M.E., 2006. Insects and Mites Feeding on Olive: Distribution, Importance, Habits, Seasonal Developmentand Dormancy. Brill, 182.
- van Genuchten, M.T., Nielsen, D.R., 1985. On describing and predicting the hydraulic properties of unsaturated soils. Annals of Geophysics, 3, 615-28.
- Van Oijen, M., Barcza, Z., Confalonieri, R., Korhonen, P., Kröel-Dulay, G., Lellei-Kovács, E., Louarn, G., Louault, F., Martin, R., Moulin, T., Movedi, E., Picon-Cochard, C., Rolinski, S., Viovy, N., Björn Wirth S., Bellocchi, G., 2020. Incorporating Biodiversity into Biogeochemistry Models to Improve Prediction of Ecosystem Services in Temperate Grasslands: Review and Roadmap. Agronomy, 2020, 10(2), 259. https://doi.org/10.3390/agronomy10020259
- Van Oijen, M., Bellocchi, G., Höglind, M., 2018. Effects of climate change on grassland biodiversity and productivity: The need for a diversity of models. Agronomy, 8, 14.
- Vesely, F.M., Paleari, L, Movedi, E., Bellocchi, G., Confalonieri, R., 2019. Quantifying uncertainty due to stochastic weather generators in climate change impact studies. Scientific Reports, 9, 1-8.
- Viira, A.H., Ariva, J., Kall, K., Oper, L., Jürgenson, E., Maasikamäe, S., Põldaru, R., 2020. Restricting the eligible maintenance practices of permanent grassland – a realistic way towards more active farming? Agronomy Research, 18(S2), 1556–1572. https://doi.org/10.15159/AR.20.018
- Villalobos, F.J., Testi, L., Hidalgo, J., Pastor, M., and Orgaz, F., 2006. Modelling potential growth and yield of olive (Olea europaea L.) canopies. European Journal of Agronomy, 24(4), 296-303. https://doi.org/10.1016/j.eja.2005.10.008
- Vossen, P., 2007. Olive oil: History, production, and characteristics of the world's classic oils. Hortscience, 42(5), 1093-1100. https://doi.org/10.21273/HORTSCI.42.5.1093
- Wang, B., Zhang, G. H., 2017. Quantifying the binding and bonding effects of plant roots on soil detachment by overland flow in 10 typical grasslands on the Loess Plateau. Soil Science Society of America Journal, 81(6), 1567-1576. https://doi.org/10.2136/sssaj2017.07.0249

- Wang, X., Li, L., Ding, Y., Xu, J., Wang, Y., Zhu, Y., Wang, X., Cai, H., 2021. Adaptation of winter wheat varieties and irrigation patterns under future climate change conditions in Northern China. Agricultural Water Management, 243, 106409. https://doi.org/10.1016/j.agwat.2020.106409
- Weber, H.E., Moravec, J., Theurillat, J-P., 2000. International Code of Phytosociological Nomenclature. 3rd ed., J. Journal of Vegetation Science, 11, 739-768.
- Yang, Y., Tilman, D., Furey, G., Lehman, C., 2019. Soil carbon sequestration accelerated by restoration of grassland biodiversity. Nature Communications, 10, 1–7.
- Yu, Q., Saseendran, S.A., Ma, L., Flerchinger, G.N., Green, T.R., Ahuja, L.R., 2006. Modeling a wheat–maize double cropping system in China using two plant growth modules in RZWQM. Agricultural Systems, 89, 457-477.
- Zabel, F., Muller, C., Elliott, J., Minoli, S., Jagermeyr, J., Schneider, J. M., Franke, J. A., Moyer, E., Folberth, C., Francois, M. D. L., Liu, W., Pugh, T. A. M., Olin, S., Rabin, S. S., Mauser, W., Hank, T., Ruane, A. C. (2021). Large potential for crop production adaptation depends on available future varieties. Global Change Biology, 27(16), 3870-3882. https://doi.org/10.1111/gcb.15649
- Zeng, Q., Liu, B., Gilna, B., Zhang, Y., Zhu, C., Ma, H., Pang, J., Chen, G., Zhu, J., 2011. Elevated CO2 effects on nutrient competition between a C3 crop (*Oryza sativa* L.) and a C4 weed (*Echinochloa crusgalli* L.). Nutrient Cycling in Agroecosystems, 89, 93-104.
- Zhang B., Chenu, K., Dreccer, F., Chapman, S., 2012. Breeding for the future: what are the potential impacts of future frost and heat events on sowing and flowering time requirements for Australian bred wheat (Triticum aestivum) varieties? Global Change Biology, 18(9), 2899-2914. https://doi.org/10.1111/j.1365-2486.2012.02724.x.
- Zhang, Z., Gu, T., Zhao, B., Yang, X., Peng, Q., Li, Y., Bai, L., 2017. Effects of common Echinochloa varieties on grain yield and grain quality of rice. Field Crops Research, 203, 163-172.
- Ziliotto, U., Andrich, O., Lasen, C., Ramanzin, M., 2004. Tratti essenziali della tipologia veneta dei pascoli di monte e dintorni. Regione Veneto, Accademia Italiana di Scienze forestali, Venezia 1-2